ADSORPTION OF GASES ON ZINC OXIDE SURFACES

by

TRACEY JANE GIDDINGS

A thesis submitted in partial fulfilment of the requirements for the degree of Doctor of Philosophy in the University of London Imperial College.

1985

Department of Electrical Engineering

ACKNOWLEDGEMENTS

I would like to thank Professor Mino Green, in his capacity as Supervisor of this project. His guidance throughout the course of this work is appreciated. I would also like to thank Dr. K.C. Waugh and Dr. M. Bowker at I.C.I. New Science Group for their collaboration and help generally.

I am indebted to the Department of Electrical Engineering and I.C.I. for the provision of laboratory facilities and for financial support I am grateful to : the SERC (3 years), I.C.I. PLC (4 years), Professor M. Green and the Department of Electrical Engineering (6 months) and also my parents.

I would like to thank David Morris who kindly assisted building the BET apparatus, Len Borov for glass blowing, Jim Wright for furnace winding and also Ken White.

Finally I would like to thank my mother for typing this thesis and my father for preparing the final copies of the diagrams.

ABSTRACT

Methanol is synthesised industrially from a $H_2/CO/CO_2$ mixture over a zinc oxide - copper catalyst. As yet, the detailed mechanism of its action is unknown. The thesis to be presented describes a research programme on just one component of the catalyst, designed to contribute towards identifying the active species and thus further general understanding of the process.

Temperature programmed desorption experiments were carried out on two samples of zinc oxide : one, a polycrystalline powder and the other, long thin needles which expose mainly the prism plane. The effective surface area of the powder consists of both polar and prism planes. Thus, by comparing the adsorptive properties of these samples crystal plane specificity can be detected.

It is found that carbon dioxide adsorbs on the polar planes to large fractional coverage, but not at all on the prism plane. Methanol however, adsorbs undissociatively on special sites on the prism plane, which are not oxygen vacancies or polar planes, but probably step sites. Decomposition products are also observed.

Hydrogen and carbon monoxide, in the feed gas, are both reducing agents, and hence the zinc oxide component is certainly oxygen deficient. Point defects have long been associated with catalytic activity. The prism plane of zinc

oxide is stoichiometric, but oxygen vacancies can be generated (to a maximum of 4% concentration) by heating the needles to 800°C in vacuum. Stoichiometry is restored by subsequent treatment in oxygen at ca. 615°C. By comparing the behaviour of both defected and stoichiometric surfaces, the role, if any, of oxygen vacancies could be determined.

In fact, the presence of oxygen vacancies makes no difference at all, not only in the adsorption of methanol, but also for the adsorption of oxygen, carbon dioxide and nitrous oxide. No strong binding states (> 0.5eV) could be detected. This has significant implications for charge transfer adsorption models.

CONTENTS

LIST OF FIGURES

LIST OF TABLES

INTRODUCTION

There have been two objectives in this research work:

1. To ascertain whether charge transfer adsorption can be shown to occur over zinc oxide surfaces.
2. To determine any crystal plane/defect specificity for methanol decomposition over zinc oxide.

Charge transfer adsorption theory states that an electron (or hole) is completely transferred from the solid to the adsorbate. Calculations to be presented in Chapter 6 show that on an ideal stoichiometric $(10\bar{1}0)$ surface this is energetically unlikely. With oxygen vacancies present, however, the likelihood of adsorption may increase.

Using long thin needles of zinc oxide, which exhibit essentially the $(10\bar{1}0)$ prism plane, it has been possible to carry out temperature programmed desorption studies on both stoichiometric and defected surfaces, in order to determine the role, if any, of oxygen vacancies on adsorption.

Similar studies on powdered samples which have almost equal proportions of polar and prism planes, should enable any differences in adsorption properties to be attributed to the polar plane. However, as will be seen, the steps or active sites seem to dictate the adsorption properties of both.

The thesis to be presented describes temperature programmed

desorption (TPD) experiments on several samples of zinc oxide. The TPD technique yields valuable information concerning the quantities and binding energies of adsorbed species.

Chapters 1 and 2 give general background on the material and TPD technique, Chapters 3 and 4 are concerned with specific experimental arrangements and procedure, and Chapters 5 and 6 contain the results and discussion of the adsorption studies of methanol, oxygen, carbon dioxide and nitrous oxide on zinc oxide.

CHAPTER 1

MATERIAL PROPERTIES

1.1 The Structure of Zinc Oxide

Zinc Oxide crystallises into an hexagonal Wurtzite lattice, of unit cell dimensions[1] a = 3.2495 $\pm$ 0.005 Å, c = 5.2069 $\pm$ 0.005 Å and α = 120° (see Fig. 1.1 and Table 1.1).

Each ion is tetrahedrally bonded to four of the opposite sign. Three of the Zn-O bond lengths are equal (1.973Å), but the fourth is slightly longer (1.992Å). The Wurtzite lattice is noncentrosymmetric and has a polar c-axis. A series of double layers extend along the c-axis, and only every alternate layer is identical. It is possible to cleave the zinc oxide crystal to obtain a surface consisting entirely of zinc or oxygen ions. These are the polar planes and are designated (0001) and $(000\bar{1})$ respectively. The zinc or oxygen ions are hexagonally close packed, giving 1.09×10^{19} ions/m^2. By cleaving the crystal parallel to the c-axis, the stoichiometric prism faces are exposed. The $(10\bar{1}0)$ prism plane is most frequently studied because of its ease of preparation, and its atomic arrangement is shown in Fig. 1.2, along with $(11\bar{2}0)$ prism plane, for comparison.

The imbalance of charge at the surface of the crystal suggests that the surface atomic configuration may become distorted from the bulk structure of zinc oxide. For many years, research workers have calculated, and tried to

FIG. 1.1 : HEXAGONAL WURTZITE LATTICE OF ZINC OXIDE

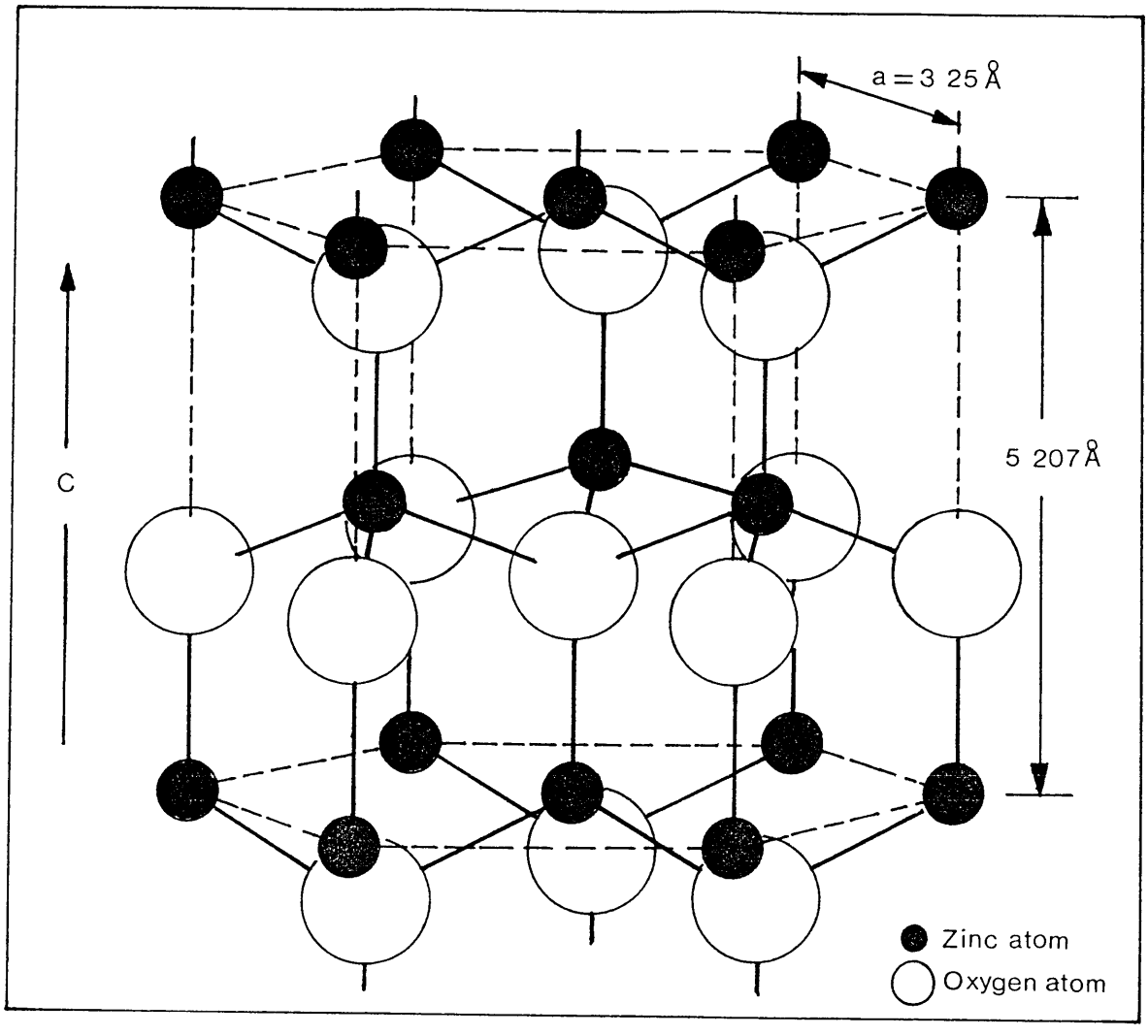

TABLE 1.1

INTERATOMIC BOND DISTANCES AND ANGLES (from Ref. 1)

Zn-O	1.992Å	(1)
Zn-O	1.973Å	(3)
Zn-Zn	3.209Å	(3)
Zn-Zn	3.250Å	(4)
O-$\widehat{\text{Zn}}$-O	108.1°	(3)
O-$\widehat{\text{Zn}}$-O	110.8°	(3)

(The numbers in brackets indicate the number of distances or angles per tetrahedron.)

FIG. 1.2 : ATOMIC ARRANGEMENT ON $(10\bar{1}0)$ AND $(11\bar{2}0)$ PRISM PLANES

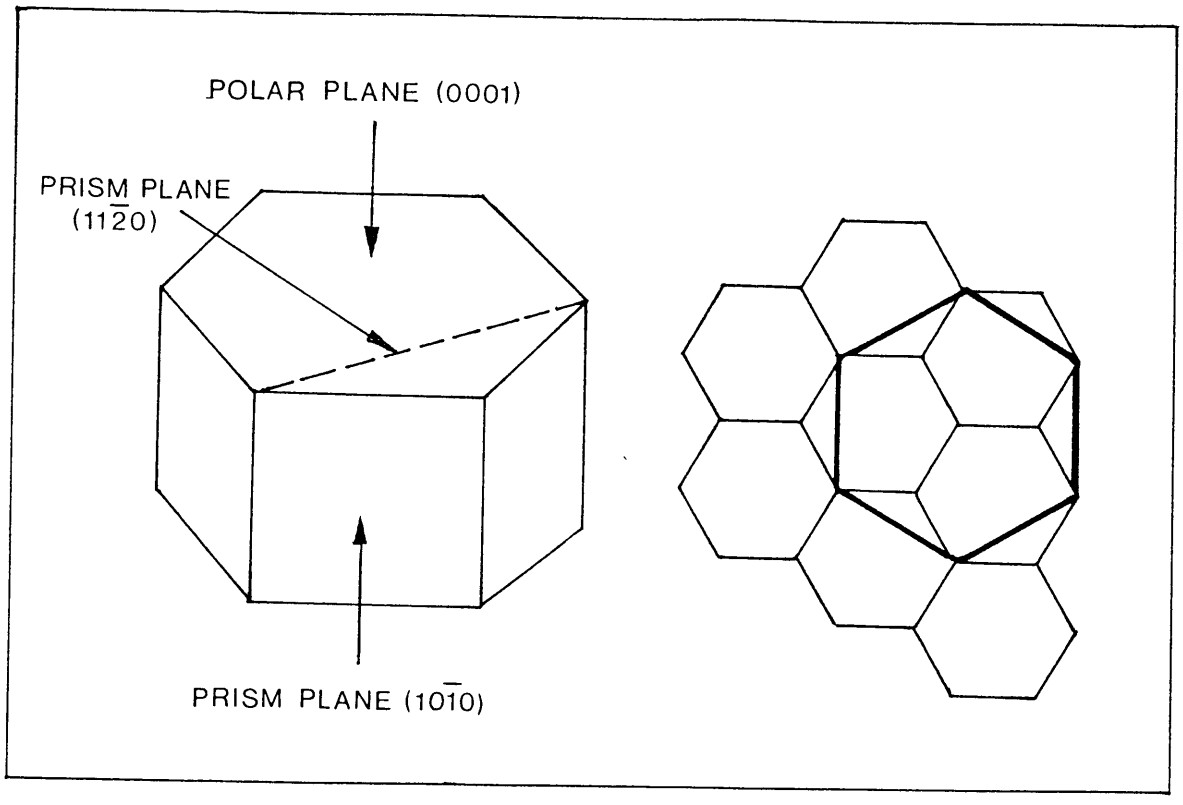

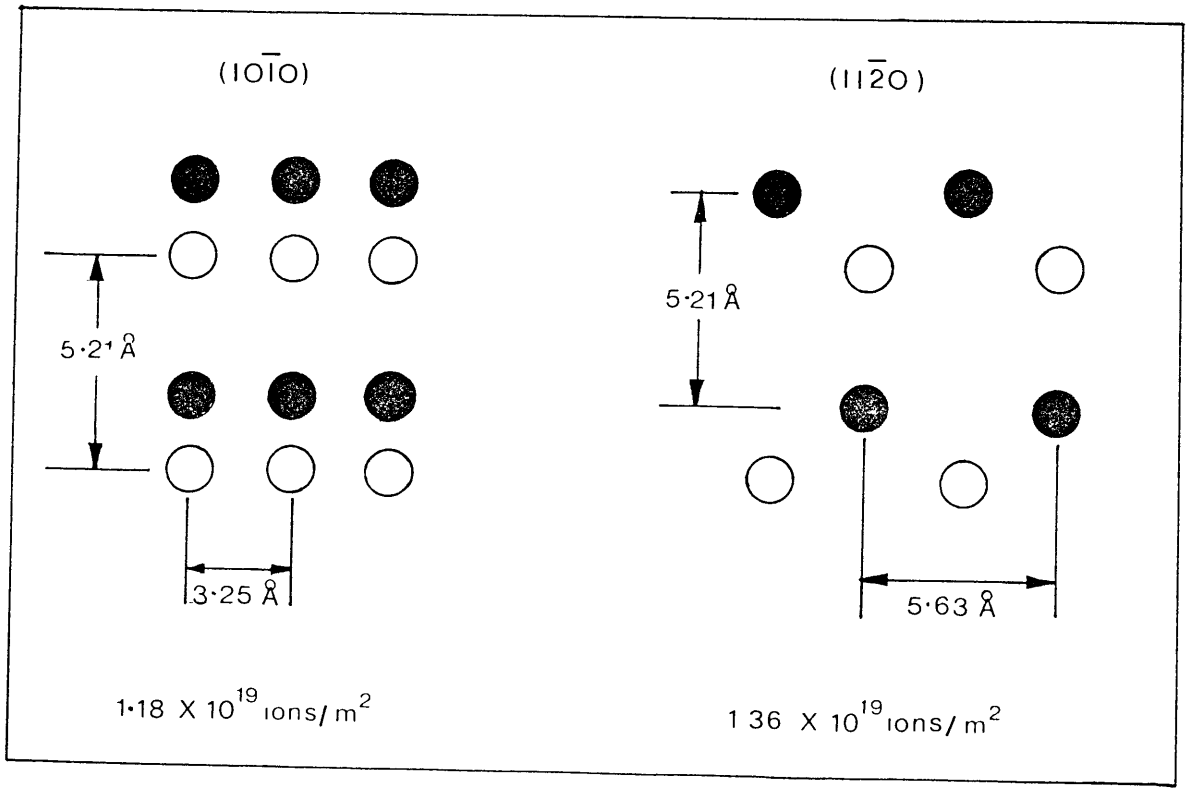

measure experimentally, the surface reconstructions on both polar and prism planes.

The most recent experimental work to date[2], using angle resolved photoemission spectroscopy, detects no significant surface atom reconstruction or charge transfer between surface and sub-surface atoms for either polar or non-polar planes. The calculated density of states for ideal zinc oxide surfaces are obtained[3]. The results do suggest however, that the zinc atoms on the $(10\bar{1}0)$ prism plane do relax slightly inwards by 0.4 ± 0.05Å. This is in agreement with Duke et al[4], who, using low energy electron diffraction reported values of 0.3 ± 0.1Å and 0.1 ± 0.05Å for the zinc and oxygen sub-lattice relaxations respectively. Almost immediately the calculations were modified[5] and extended. The bulk parameters were changed to those obtained by Abrahams and Bernstein[1] and computational methods were improved. This led to the currently accepted[6] surface structure of ZnO $(10\bar{1}0)$ to be one in which the oxygen ions in the upper layer relaxed vertically by 0.05 ± 0.1Å and the zinc ions by 0.45 ± 0.1Å with no lateral displacements within the top or second layer.

Low energy electron diffraction has been less successful for the polar planes[9]. To begin with, a six fold symmetric LEED pattern is observed[7,8] instead of the expected three fold pattern[11]. The six fold symmetry could not be explained in terms of any type of reconstruction and so was

attributed to domains of unknown composition. Solomon et al[10] pointed out that if there are steps on the surface, only one double layer high, the atomic configuration on each terrace would be related by a 60°rotation about the c-axis. Each terrace would give the expected three fold symmetric LEED pattern, but the combination of the two would produce the experimental result: and this "pro tem" is the accepted explanation.

There is now no evidence for surface reconstruction or relaxation on the zinc or oxygen polar planes. The earlier reported value of 0.2Å[8,9] contraction in the zinc layer, no longer applies if the more modern crystal structure determination data of Abrahams and Bernstein[1] are used instead of those of Wyckoff[11].

1.2 Defect Nature of Zinc Oxide

Pure zinc oxide is an intrinsic semiconductor with a band gap of ca.3.1eV. Under usual preparative conditions it accommodates slight deviations in stoichiometry in the form of metal excess $Zn_{1+x}O$ ($x \leq$ ca.10^{-3}). Whether this is manifested as zinc interstitials or oxygen vacancies is a subject of continuing debate[12,13] - both have donor properties. The existence of acceptor type defects in the lattice has also been clearly established[15,16]. A detailed discussion of the defect structure of zinc oxide can be found in Refs. 14-16, and the general concensus of opinion[15,16] is that zinc oxide contains zinc vacancies as the acceptor state and oxygen vacancies as the donor state.

Obviously the latter predominate, to give the observed material properties.

The experimental methods used to elucidate the nature of nonstoichiometry are described fully in the excellent review by Hirschwald et al[14].

The concentration of defects in the bulk of the crystal is governed by the conditions of preparation (1300-1600K). Below ca.1000K bulk diffusion is negligible. At the surface however, as will be explained more fully in Chapter 4, the concentration of defects can be adjusted (to a concentration of ca.4%) on heating in vacuo above 700K.

1. S.C. ABRAHAMS AND J.L. BERNSTEIN
Acta. Cryst. B25, 1233, 1969

2. W. GOPEL, J. POLLMANN, I. IVANOV AND B. REIHL
Phys. Rev. B 26(6), 3144, 1982

3. I. IVANOV AND J. POLLMANN
Phys. Rev. B 24(12), 7275, 1981

4. C.B. DUKE, R.J. MEYER, A. PATON, P. MARK AND B.W. LEE
Phys. Rev. B 15, 4865, 1977

5. C.B. DUKE, R.J. MEYER, A. PATON AND P. MARK
Phys. Rev. B 18(8), 4225, 1978

6. C.B. DUKE, R.J. MEYER AND P. MARK
J. Vac. Sci. Tech. 17, 971, 1980

7. C.B. DUKE AND A.R. LUBINSKY
Surface Science 50, 605, 1975

8. S.C. CHANG, B.W. LEE AND P. MARK
J. Vac. Sci. Tech. 13(1), 189, 1976

9. C.B. DUKE
CRC Crit. Rev. Sol. St. Mat. Sci. December 1978, p.69

10. V.E. HENRICH, H.J. ZEIGER, E.I. SOLOMON AND R.R. GAY
Surface Science 74, 683, 1978

11. R.W. WYCKOFF
Crystal Structures Vol. 1 (2nd Ed.) (1963)
John Wiley p.112

12. G. NEWMANN
Phys. Stat. Sol. (b) 105, 605, 1981

13. E. ZEIGLER, A. HEINRICH, H. OPPERMANN AND G. STOVER
Phys. Stat. Sol. (a) 66, 635, 1981

14. W. HIRSCHWALD et al

Current Topics in Materials Science 7, 143, 1981

Ed. E. Kaldis, North Holland

15. W. GOPEL AND U. LAMPE

Phys. Rev. B 22(12), 6447, 1980

16. G.D. MAHAN

J. Appl. Phys. 54(7), 3825, 1983

CHAPTER 2

GENERAL REVIEW OF TEMPERATURE PROGRAMMED DESORPTION SPECTROSCOPY.

The technique of temperature programmed desorption spectroscopy (TPD) was first described in the literature by Smith and Aranoff[1], in 1958.

Basic equations were presented to describe thermal desorption from an energetically homogeneous surface, using a linear heating schedule. As models for adsorption/desorption have evolved, Smith and Aranoff's theory has been subsequently extended by many research workers, not only to accommodate different heating programmes, but also to take account of surface heterogeneity, lateral interactions between adsorbed species and precursor states.

This Chapter will be concerned with outlining the fundamental principles of temperature programmed desorption with regard to both experimental procedure and theoretical analysis. Further details can be found in three excellent review articles by King[2], Péterman[3], and Dawson and Anderson[4]. Interpretation of the data is a subject of continuing debate in the literature[5,6], and hence, for completeness, several methods for extracting the kinetic parameters from the thermal desorption spectrum will be discussed.

2.1 Experimental Criteria

After completing the adsorption of gas on the substrate, the reaction chamber is evacuated for 3-5 minutes. At room temperature, this removes any species from the surface, of binding energy less than ca. 88 kJ mol^{-1}. The temperature programmed desorption experiment can then commence. The sample is heated in this work, at a steady linear rate, which can be expressed as $T = T_o+Bt$ where T = Temperature(K), T_o = Initial Temperature(K), B = Heating Rate (Ks^{-1}), t = time(s). The desorbed species is monitored using a mass spectrometer and the resulting pressure vs. time (temperature) curve is the thermal desorption spectrum. The rate of change of pressure, dP/dt, represents a balance between the desorption rate and the pumping rate, as shown in Eqn. (2.1) below.

$$\frac{dP}{dt} = -\frac{dN}{dt} \times A \times \frac{1}{V} \times \frac{1}{3.24 \times 10^{19}} - \frac{SP}{V} \qquad (2.1)$$

where N = Surface coverage of desorbing species per unit area (molecs cm^{-2})

A = Area of sample (cm^2)

S = Pump speed (ls^{-1})

V = Volume of system (l)

P = Pressure (torr)

1 torr litre = 3.24×10^{19} molecules at 298 K

Introducing the characteristic pumping time, $\tau = V/S$, it can be seen that for high pumping speeds ($\tau \rightarrow 0$) the final

term in Eqn. (2.1) dominates, and hence the desorption rate, $^{dN}/_{dt}$ is proportional to P; and in our case P is proportional to the mass spectrometer signal.
Chan and Weinberg[7] have shown that for this latter condition to be satisfied the reciprocal of the product of the heating rate and pumping time constant must be greater than ca. 0.5. A typical value in this research work is 3.3 (see later for values of V, S, and B).

2.2 Basic Theory of Temperature Programmed Desorption Spectroscopy

The rate of desorption can be described by the Arrhenius Equation :

$$-\frac{dN}{dt} = kN^m = \nu \exp\left(\frac{-E}{RT}\right) \times N^m \qquad (2.2)$$

where, k = rate constant [s^{-1} for m = 1, s^{-1}(molecs cm^{-2})$^{-1}$ for m = 2]

ν = pre-exponential (or frequency) factor [s^{-1} for m =1, s^{-1}(molecs cm^{-2})$^{-1}$ for m = 2]

E = activation energy for desorption (J mol^{-1})

m = order of the reaction

R = 8.314 JK^{-1} mol^{-1}

As the temperature increases, so the exponential term increases, but this is counteracted by the decrease in surface coverage. Consequently the desorption rate rises to a maximum then decreases. From the desorption peak, information about surface coverage, the activation energy for desorption, the pre-exponential factor and reaction order can be obtained.

2.2.1 Determination of Surface Coverage

The amount of material adsorbed on the surface before commencing a TPD experiment is represented by the area under the TPD curve. Thus $N_o = \int_o^t \left(\frac{-dN}{dt}\right) dt$ (2.3)

Provided t ranges over the entire curve, N_o is the initial surface coverage.

2.2.2 Classical Determination of the Activation Energy for Desorption

Redhead[8] introduced a method for determining the activation energy for desorption using only the temperature of the peak maximum (T_p) from the TPD curve. The condition for a maximum $d^2N/dt^2 = 0$, can be satisfied by differentiating Eqn. (2.2) with respect to t and equating to zero. The following relationships arise:

$$\frac{E}{RT_p^2} = \frac{\nu}{B} \exp\left(\frac{-E}{RT_p}\right) \quad \text{for m = 1} \qquad (2.4a)$$

$$\frac{E}{RT_p^2} = \frac{2N_p\nu}{B} \exp\left(\frac{-E}{RT_p}\right) \quad \text{for m = 2} \qquad (2.4b)$$

where, N_p = surface coverage at $T = T_p$

It will be shown later that $2N_p = N_o$ for second order desorption.

These equations can be solved for E using Newton's Approximation method. The computer program to do this is listed in Appendix A. Obviously this method enables a quick determination of E, once a value has been assigned to ν.

This is usually ca. 10^{13} s^{-1} (for m = 1), the molecular vibration frequency.

2.2.3 Other Methods for Determining the Activation Energy and Pre-exponential Factor

(a) Using T_p and Peak Width

It is possible to determine E quite independently, using T_p and the width of the TPD peak at half the maximum height $\Delta W_{\frac{1}{2}} = T_2 - T_1$ or the low temperature half width $\delta = T_p - T_1$ (see Fig. 2.1.) The equations were originally derived for thermoluminescence peaks[9] using empirical computational analysis. Equations analogous to (2.4a), (2.4b) and (2.2) were solved using Newton's Approximation and/or Series Expansion to obtain values for T_p, maximum rate and T_1 and T_2. The expressions below, relating E to ΔW or δ could then be obtained using the integral form of Eqn. (2.2), the condition for a peak maximum and by approximating the area under the curve (or part curve) to a triangle. The pre-exponential factor, ν , can then be obtained by substituting back for E in Eqn. (2.4a) or (2.4b).

$$\left.\begin{array}{l} E = 2.52 \left(\dfrac{RT_p^2}{\Delta W}\right) - 2RT_p \\ \text{or} \quad E = 1.52 \left(\dfrac{RT_p^2}{\delta}\right) - 3.16\ RT_p \end{array}\right\} \text{for m = 1}$$

$$\left.\begin{array}{l} E = 3.54 \left(\dfrac{RT_p^2}{\Delta W}\right) - 2RT_p \\ \text{or} \quad E = 1.813 \left(\dfrac{RT_p^2}{\delta}\right) - 4RT_p \end{array}\right\} \text{for m = 2} \qquad (2.5).$$

FIG. 2.1

Shape of First and Second Order Desorption Peaks

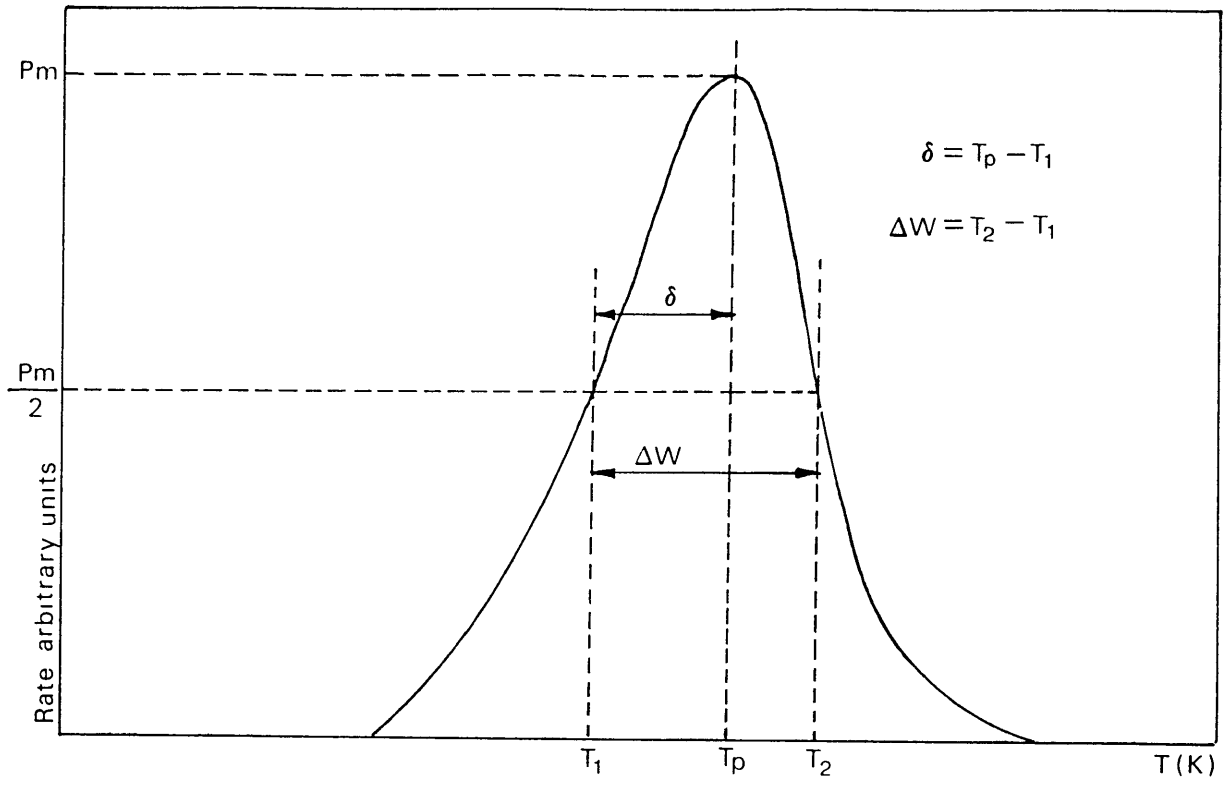

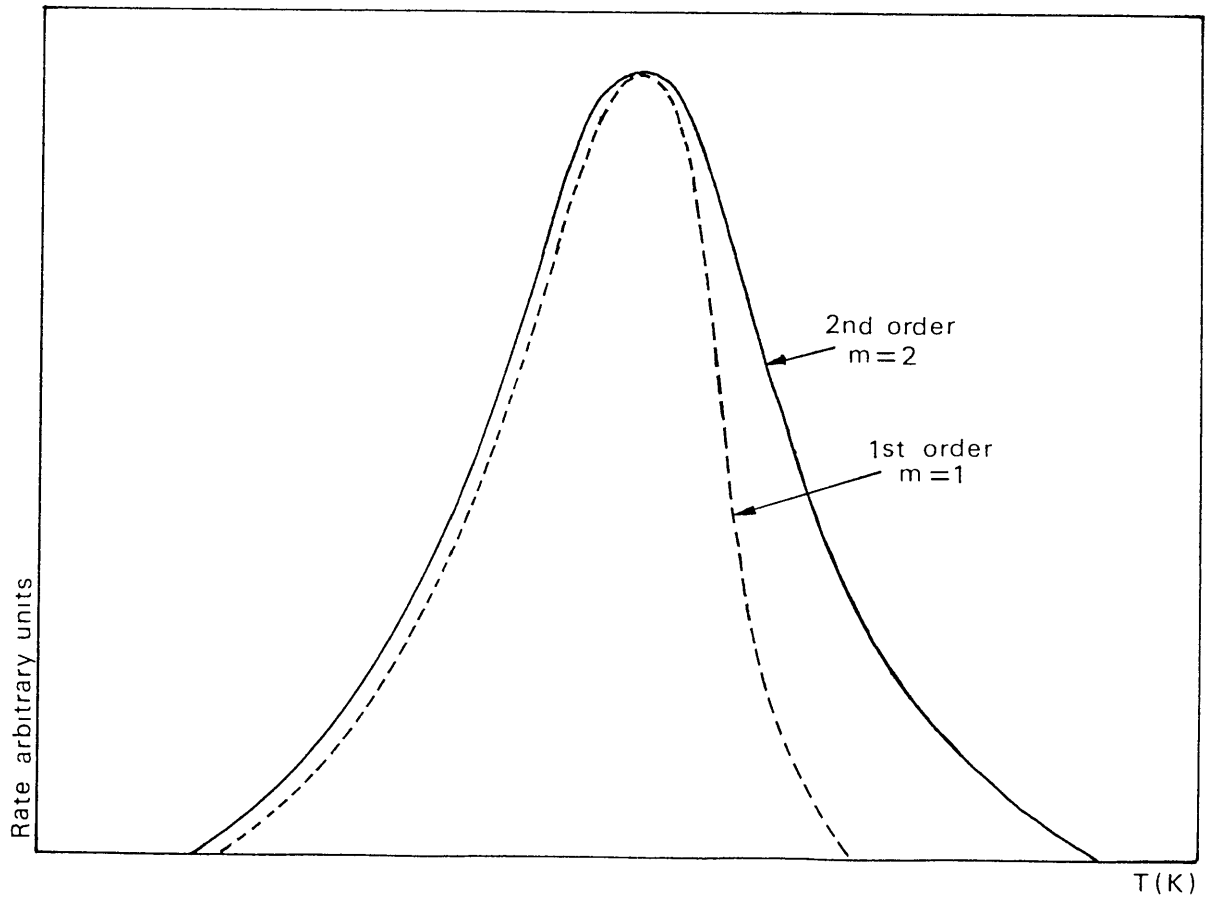

ΔW is an easier parameter to measure, as T_p is not always precise. This method should only be applied to well resolved peaks.

(b) Using a Set of TPD Curves

Several other methods have been devised for determining both E and ν without any assumptions about reaction order, but they require a set of thermal desorption spectra[2-4,10,11]

(i) Variation of T_p With B, Keeping N_o Constant

Rearranging Eqn. (2.4a) gives:

$$\ln\left(\frac{E}{R\nu}\right) + \frac{E}{RT_p} = \ln\left(\frac{T_p^2}{B}\right) \qquad (2.6a)$$

Hence, if T_p is determined for different values of B, a plot of $\ln(T_p^2/B)$ vs. $1/T_p$ yields a straight line of slope E/R.

Second order desorption reactions can also be analysed in this way provided N_o is constant. Alternatively Eqn. (2.2) gives:

$$\ln\left(\frac{-dN}{dt}\right)_p = \ln\left(\nu N_p^m\right) - \frac{E}{RT_p} \qquad (2.6b)$$

where $(dN/dt)_p$ is the maximum peak amplitude.
Hence, a plot of $\ln(dN/dt)_p$ vs. $1/T_p$, obtained at different heating rates and constant N_o, yields a straight line of slope -E/R.

The heating rate has to be varied over at least two orders of magnitude for accurate values of E to be obtained, which is not always feasible.

(ii) Variation of T_p with N_o

Inspection of Eqns. (2.4a) and (2.4b) indicate that for first order desorption T_p is independent of coverage, but for second order T_p decreases as N_o increases (see Fig. 2.2). Thus by obtaining a set of TPD curves taken at different initial coverages, one can tell whether m = 1 or 2, provided E is independent of coverage (see later).

For second order desorption, from Eqn. (2.4b)

$$\ln\left(\frac{EB}{\nu R}\right) + \frac{E}{RT_p} = \ln(N_o T_p^2) \qquad (2.7)$$

A plot of $\ln(N_o T_p^2)$ vs. $1/T_p$ yields a straight line of slope E/R.

(iii) Desorption Isotherm Method

Falconer and Madix[10] used the same set of curves as in (ii) but use several points on each TPD spectrum to generate desorption rate isotherms. These are plots of ln(-dN/dt) vs.ln(N), at constant temperature. From Eqn. (2.2) it is apparent that provided E is independent of coverage the slope of these lines gives the order of the desorption process (m). Then, at constant coverage, a plot of ln(-dN/dt) vs. 1/T yields the activation energy (from Eqn. (2.2) again).

(c) Single Lineshape Analysis

This method was the forerunner of (iii) above but requires only one TPD experiment[12]. Several points are taken along the curve to generate values of -dN/dt and N. After assuming a value for m (see Sec. 2.2.4) a plot of

$\ln\left[\left(dN/dt\right)/N^m\right]$ vs. $1/T$ gives a straight line (if ν and E are independent of coverage) of slope -E/R and intercept $\ln \nu$ (see Fig. 2.3).

FIG. 2.2

First and Second Order Desorption Profiles - Variation with Coverage

FIRST ORDER

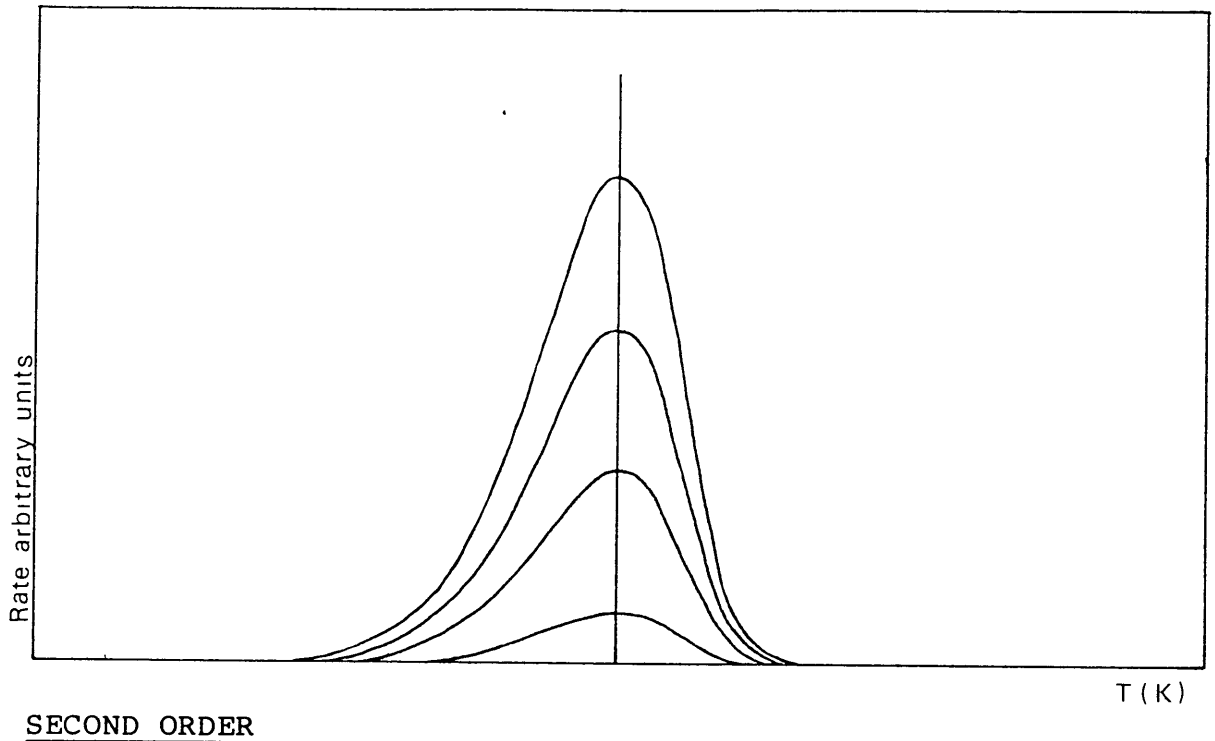

SECOND ORDER

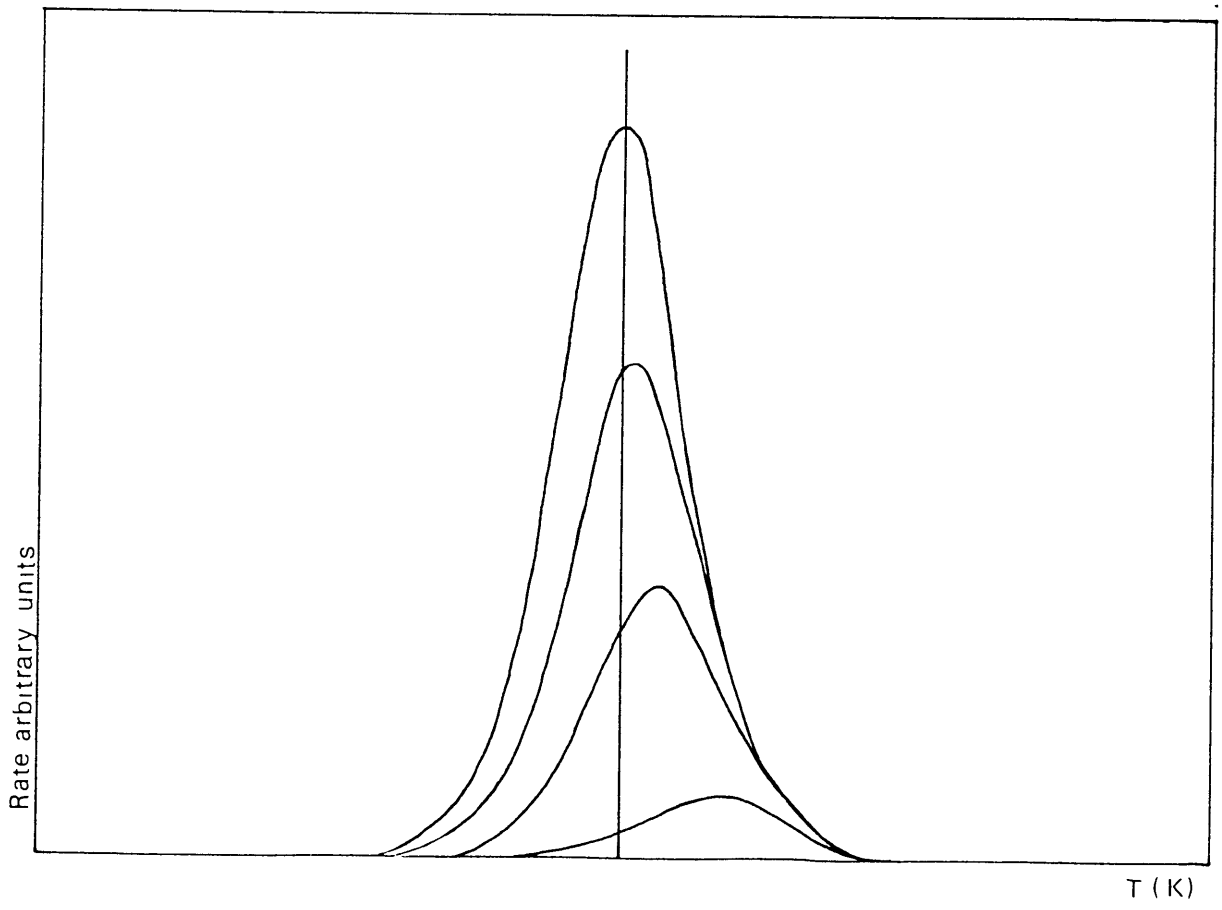

FIG. 2.3

Single Lineshape Analysis

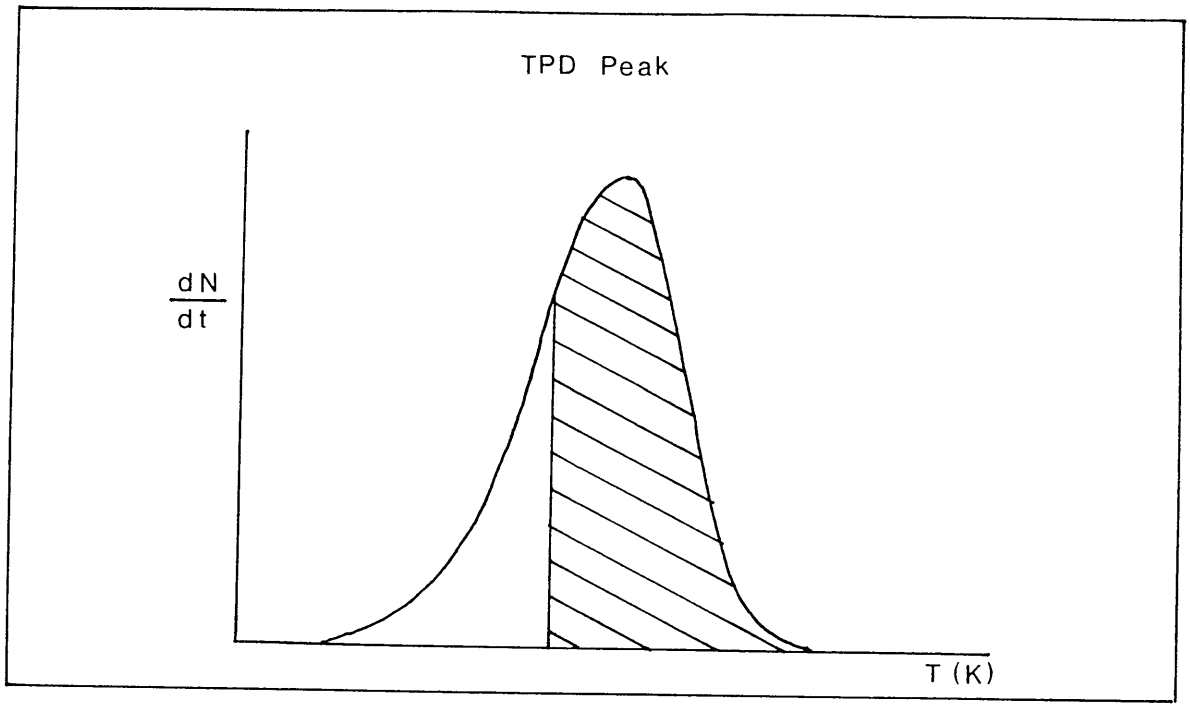

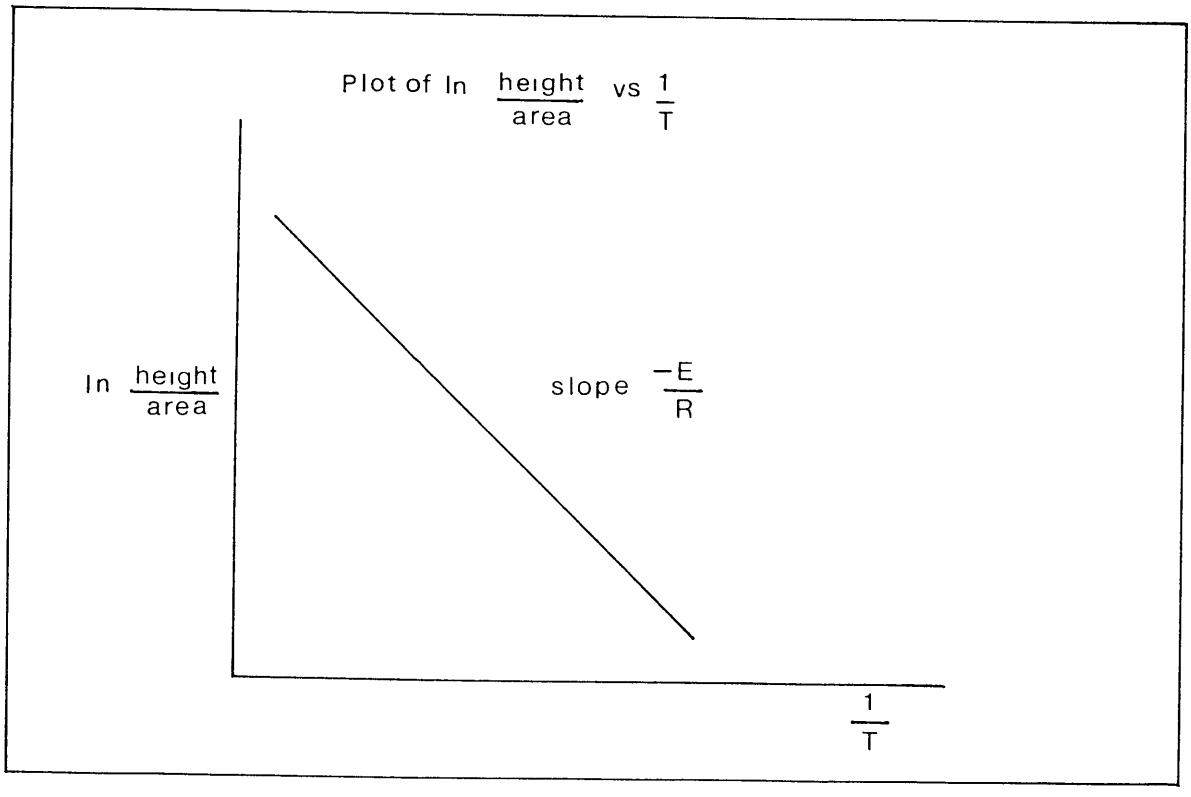

dN/dt = peak height

N = area under curve (material remaining on surface.)

2.2.4 Determination of the Order of the Desorption Process

If a set of spectra is available the order of the desorption process may be inferred as in Section 2.2.3 (b) (ii) and (iii). Otherwise the peak shape itself can be used to discern the order. From Eqn. (2.2)

$$-\int_{N_o}^{N_p}\frac{dN}{N^m} = \frac{\nu}{B}\int_{T_o}^{T_p}\exp\left(\frac{-E}{RT}\right)dT$$

$$\simeq \frac{\nu}{B}\cdot\frac{RT_p^2}{E}\cdot(1-\Delta)\exp\left(\frac{-E}{RT_p}\right) \qquad (2.8)$$

where $\Delta = \frac{2RT_p}{E}$ (see Ref. 4)

using (2.4a) and (2.4b)

for m = 1, $\ln\left(\frac{N_o}{N_p}\right) = (1-\Delta)$

$$\frac{N_o}{N_p} = e^{1-\Delta} \simeq e^1$$

$$N_p \simeq \frac{N_o}{2.718}$$

Thus, for first order desorption, an asymmetrical curve results where almost 2/3 of the amount originally adsorbed has desorbed before the peak maximum.

for m = 2, $\frac{1}{N_p} - \frac{1}{N_o} = \frac{(1-\Delta)}{2N_p}$

$$2(N_o-N_p) = (1-\Delta)N_o \simeq N_o$$

$$N_o \simeq 2N_p$$

A peak which is symmetrical about the peak maximum, indicates second order desorption.

2.3 Variations from the Ideal Case

The discussion so far has been concerned with ideal cases where only one adsorption state is involved and E and ν are independent of coverage. Unfortunately for simple analysis, experimental results usually deviate considerably from these ideals, so necessitating modifications to the theory.

2.3.1 Multiple Binding States

Different adsorbed species will obviously have quite individual binding energies, and therefore results in a multi-peak spectrum. A single species, adsorbed at different types of site would also give a similar result. On an atomic scale, few surfaces could be considered perfectly homogeneous. Some sites for adsorption are particularly stronger than others - for example at a step in the surface. If the difference in binding energy at these sites is sufficiently large, quite distinct well resolved TPD peaks will arise. Usually however, the peaks overlap resulting in one rather broad peak, or a shoulder appearing on one peak. The individual binding states cannot be unequivocally resolved[13], in this instance.

2.3.2 Lateral Interactions Between Adsorbed Species

Lateral interactions between adsorbed species can be of attraction or repulsion. A single adsorbate however, experiences Van de Waal's interactions which, although quite small have a significant effect on the TPD spectrum.

Grunze et al[14] have computed TPD curves to illustrate the effect of attractive lateral interactions on first and second order desorption, with and without a precursor state (see also Sec. 2.3.3). They have used E in the form $E = E_o - W\theta$ in the desorption expressions, where,

E_o = activation energy with no interactions ($Jmol^{-1}$)

W = interation energy ($Jmol^{-1}$)

θ = coverage = $\frac{\text{number of occupied sites}}{\text{total number of available sites}} = \frac{N}{N_s}$

(see also Sec. 2.3.4)

It is immediately apparent that attractive interactions (negative) reduce the peak width, and shift the peak maximum to higher temperatures as θ increases. Conversely, repulsive interactions broaden the peaks and shift the peak maximum to lower temperatures as θ increases[15] (Compare Sec. 2.3.3). In extreme cases peak splitting occurs.

Lateral interactions therefore, can lead to misinterpretation of thermal desorption data - particularly if the variation of T_p with N_o is being studied (Sec. 2.2.3(b)(ii)).

2.3.3 The Effect of a Precursor State on the TPD Spectrum

The concept of adsorption, initially into a weakly bound, mobile precursor state was introduced in the 1950's quite independently by Kisliuk[16] and Ehrlich[20]. Kisliuk used a successive site statistical model which was later modified by King and Wells[17] to take account of lateral

interactions between adsorbed species.

It is reasonable to suppose that the reverse process of desorption occurs via a precursor state. King[18] developed this idea, and computed TPD curves for first order desorption which show that the existence of a precursor state broadens the peaks dramatically, and for a particular coverage, as the tendency for migration increases so T_p increases. The variation of T_p with N_o however, in the precursor state model is the opposite - as N_o increases T_p decreases.

Gorte and Schmidt[19] used Ehrlich's[20] reaction kinetics model to predict similar effects of a precursor state on thermal desorption spectra, which are more pronounced for second order desorption. It is clear that precursor states could simply lead to more ambiguities for data interpretation. However, if additional information about the variation of the sticking co-efficient with coverage is available, one can decide whether the precursor state has a significant effect in the particular desorption reaction. Only when the sticking co-efficient is independent of coverage, has the precursor state to be considered in the analysis.

2.3.4 Variation of Activation Energy with Coverage

This has basically been covered in the preceding sections because any variation of E with coverage is only due to surface heterogeneity or lateral interactions. It has been

shown[4] that desorption from several types of site, distributed evenly within an energy range, results in a broad flat topped peak (fairly constant desorption rate).

If however, E is assumed to be a linear function of θ (as could arise due to lateral interactions or a precursor state), the resulting spectrum is broad, but no longer flat topped.

More complex distribution profiles of $E(\theta)$ have been used[21] to simulate TPD spectra. Sharp peaks correspond to regions of constant E, and where $E(\theta)$ changes rapidly broad peaks result.

2.3.5 Complete Analysis and Desorption Isotherm Method

Falconer and Madix[10] and King[13] have devised similar methods for determining the kinetic parameters and their coverage dependence, using a set of TPD curves, obtained at different values of N_o.

Desorption rate isotherms are constructed at several temperatures (see Sec. 2.2.3(b)(iii)). Then, for a particular coverage, a plot of ln(rate) vs. 1/T gives a straight line of slope -E/R. The coverage dependence of E can be observed by repeating this plot for different values of θ. The intercept on the ln(rate) axis is equivalent to $\ln\nu(N) + m\ln N$. A plot of this intercept versus ln N, if linear, indicates that ν is independent of coverage, and is given by the new intercept. The order of the desorption

process can then be obtained from the gradient of the line. If non-linear plots of [lnν(N) + mlnN] vs. ln N arise, different values of m have to be tried, to determine ν(N), which does lead to ambiguities.

2.4 Distortions to the Peak Shape Due to Vacuum System Parameters

It should also be mentioned that TPD peaks can be distorted due to particular experimental arrangements. The basic theory, already outlined, has been derived for single crystal/filament samples in vacuum systems where desorption and detection occur in the same chamber, and the pump speed is very large (τ --> 0). Re-adsorption on, or desorption from, the sample, and also the walls of the vacuum chamber, have been disregarded, although they can have a profound effect on the spectrum: reducing the peak amplitude, generally broadening the curve and shifting T_p to higher temperatures. For rapid pumping speeds this assumption is acceptable, but if the desorption reaction and subsequent analysis occur in different chambers, separated by a finite conductance (K_2), it may not be correct to ignore these re-adsorption effects. Powdered samples in particular are likely to give broad TPD spectra, not only due to re-adsorption effects but also if the desorption process is diffusion controlled[22].

For a single chamber vacuum system, the TPD curve is expected to lag slightly behind the actual desorption curve, due to the pumping time constant (τ). The intervening

conductance (K_2) however, prohibits characterising the vacuum system by a single time constant, particularly if K_2 is small compared to the pump speed.

In the analysis chamber, V_A, the difference in flow rate in and out is given by:

$$V_A.\frac{dP_A}{dt} = F_{LV2} - SP_A \qquad (2.9)$$

where, F_{LV2} = flow through leak valve 2

This, in turn, is governed by the conductance of the valve and the pressure gradient across it :

$$F_{LV2} = K_2(P_R - P_A) \qquad (2.10)$$

Similarly, in the reaction chamber (V_R) the difference in flow rate is given by :

$$V_R.\frac{dP_R}{dt} = -\frac{dN}{dt} - K_2(P_R - P_A) \qquad (2.11)$$

Substituting Eqn. (2.10) in Eqn. (2.9) gives :

$$V_A.\frac{dP_A}{dt} = K_2P_R - P_A(S + K_2) \qquad (2.12)$$

The rate of change of flow rate can be obtained by differentiating Eqn. (2.12) :

$$V_A.\frac{d^2P_A}{dt^2} = K_2\frac{dP_R}{dt} - \frac{dP_A}{dt}(S + K_2) \qquad (2.13)$$

Substituting Eqn. (2.11) and Eqn. (2.12) in Eqn. (2.13) gives :

$$V_A.\frac{d^2P_A}{dt^2} + \frac{dP_A}{dt}\left(\frac{K_2V_A}{V_R} + K_2 + S\right) + \frac{K_2.SP_A}{V_R} = \frac{-K_2.dN}{V_R\,dt} \qquad (2.14)$$

Donnelly et al[23] used an approximate solution of Eqn. (2.2), and imposed the conditions of Eqn. (2.14) to investigate the effect of K_2, S, V_A and V_R on the TPD curve, obtained from

such an experimental arrangement. The most significant distortions seem to occur to the high temperature edge of the TPD spectrum. This is known as "tailing" and it occurs even for comparatively optimal values of K_2, S, V_A and V_R. Reduction in peak amplitude and increase in T_p occur when K_2 and/or S are considerably small compared to V_A and/or V_R (ratio K_2/V_R(or V_A) $\leq 1/4$, for an effect on the amplitude, and $\leq 1/25$ for an effect on T_p). The effect of heating rate however, was not discussed. An increase in heating rate increases the peak amplitude and shifts T_p to higher temperatures[12].

Edwards[24], by contrast, expresses the temperature shift $\Delta T = T_m - T_p$ as a function of $B\tau / \Delta W$ and α where, T_m is the maximum in P(t) profile, T_p is the maximum in -dN/dt profile, and α equals E/kT_p
He has shown that for $B\tau / \Delta W \leq 0.1$ the instrumental distortion to the TPD curve is low, and hence B can be selected to achieve this condition.

Two other effects : temperature gradients across the sample[25], and chemical reactions occurring during the desorption process[26] also cause "tailing" in the high temperature part of the TPD curve. The former is discounted here because the differential winding of the furnace provided a constant temperature profile in the central region, and the sample was contained in small diameter glass tubing. The latter could be a factor for consideration particularly for methanol decomposition/desorption.

2.5 Resumé

The technique of temperature programmed desorption can be used for monitoring the nature of species desorbed from the surface. Provided the mass spectrometer is calibrated against a total pressure gauge, the amount adsorbed/desorbed can be determined unequivocally, from the area under the TPD curve. Difficulties arise however in determining the kinetic parameters (E and ν), because this requires detailed analysis of the peak shape.

Single lineshape analysis only yields sensible values for the kinetic parameters in idealised cases. Similarly for methods using just the peak width at half maximum ($\Delta W_{\frac{1}{2}}$ or δ)

Even small variations of E and ν with coverage have a profound effect on the shape of the TPD curve, but are indistinguishable by computer fitting[6]. Another method of analysis, the variation of T_p with N_o (Sec. 2.2.3(b)(ii)) also leads to many ambiguities if lateral interactions and precursor states are taken into consideration. Table 2.1 illustrates this point.

The variation of heating rate method is still favoured by some workers[5] but it is not always experimentally realistic. Low heating rates give small signals, whilst a high value for B could mean that dN/dt is no longer proportional to P.

It is more acceptable therefore to assume a value for ν and then determine $E(\theta)$. Sometimes other experiments can be performed (e.g., measuring the isosteric heat) to determine whether E is independent of θ. Temperature programmed desorption alone, is not usually enough to determine kinetic parameters accurately. Additional experimental techniques are required. Consequently temperature programmed desorption has been used in this research work mainly as an analytical tool to determine the nature and amount of species adsorbed, with only a general consideration of kinetics.

TABLE 2.1

Summary of T_p Variation with Coverage for Different Desorption Processes

T_p Independent of Coverage
1st order, E independent of coverage
2nd order, attractive lateral interactions
1st or 2nd order, precursor state and attractive lateral interactions
T_p Decreases as Coverage Increases
2nd order, E independent of coverage
1st order, E decreases as coverage increases, repulsive lateral interactions
1st and 2nd order, E independent of coverage with precursor state
T_p Increases as Coverage Increases
1st and 2nd order, attractive lateral interactions

1. A.W. SMITH AND S. ARANOFF
J.Phys. Chem. 62, 684, 1958

2. D.A. KING
CRC Crit. Revs. Sol. St. Mat. Sci. 7(1), 194, 1978

3. L.A. PÉTERMANN
Prog. Surface Science 3(1), 1, 1972

4. P.F. DAWSON AND R.B. ANDERSON
Experimental Methods in Catalytic Research Vol.3
(1976) Chapter 6

5. M. ALNOT AND A. CASSUTO
Surface Science 112, 325, 1981

6. J.M. SOLER AND N. GARCIA
Surface Science 124, 563, 1983

7. C.M. CHAN AND W.H. WEINBERG
Appl. of Surf. Sci. 1, 377, 1978

8. P.A. REDHEAD
Vacuum 12,. 203, 1962

9. R. CHEN
J.Appl.Phys. 40(2), 570, 1969

10. J.L. FALCONER AND R.J. MADIX
J. Catal. 48, 262, 1977

11. J.L. FALCONER AND R.J. MADIX
Surface Science 48, 393, 1975

12. G. EHRLICH
Adv. in Catal. 14, 255, 1983

13. D.A. KING
Surface Science 47, 384, 1975

14. M. GOLZE, M. GRUNZE, AND W. HIRSCHWALD
Vacuum 31(10-12), 697, 1981

15. V.P. ZHDANOV

Surface Science 133, 469, 1983

16. P. KISLIUK

J. Phys. Chem. Solids 3, 95, 1957

J. Phys. Chem. Solids 5, 78, 1958

17. D.A. KING AND M.G. WELLS

Proc. Roy. Soc. A339, 245, 1974

18. D.A. KING

Surface Science 64, 43, 1977

19. R. GORTE AND L.D. SCHMIDT

Surface Science 76, 559, 1978

20. G. EHRLICH

J. Phys. Chem. 59, 473, 1955

21. Y. TOKORO, T. UCHIJIMA AND Y. YONEDA

J. Catal. 56, 110, 1979

22. B.J. CVETANOVIC AND Y. AMENOMIYA

Adv. Catal. 17, 103, 1967

23. R.P. WEBB, S.E. DONNELLY AND D.G. ARMOUR

Vacuum 27(9), 559, 1977

24. D. EDWARDS

Vacuum 26(3), 91, 1976

25. T.Y. KURENYOVA, M.E. RYSKIN AND B.R. SHUB

Surface Science 109, 482, 1981

26. R. GORTE AND L.D. SCHMIDT

Appl. of Surf. Sci. 3, 381, 1979

CHAPTER 3

EXPERIMENTAL PROCEDURES I

Most of the experimental work was carried out at Imperial College using a bakeable UHV system, capable of achieving a base pressure of ca. 2×10^{-9} torr. This is to be described in detail below. The equipment used at I.C.I. for similar thermal desorption experiments is detailed in Ref.1 and Appendix B.

3.1 Vacuum System

The apparatus built in this laboratory consisted of three chambers each of known volume: a gas admission chamber (V_S), a reaction chamber (V_R) and an analysis chamber (V_A) (see Fig. 3.1). These were separated from each other by MD6 leak valves (Vacuum Generators). Both the analysis and gas admission chambers were comprised of standard UHV fittings and were of approximately the same volume (1.53 and 1.33 litres respectively). They were evacuated independently, using molecular sieve sorption pumps for roughing followed by sputter ion pumps. The analysis chamber housed the QX200 quadrupole mass spectrometer and also an ionisation gauge.

The gas admission chamber had valves leading to the flasks of research grade gases/vacuum distilled methanol and also a "Baratron" gauge (or capacitance manometer) for measuring absolute pressure in the 10^{-3} to 10 torr range.

FIG. 3.1a SCHEMATIC DIAGRAM OF APPARATUS

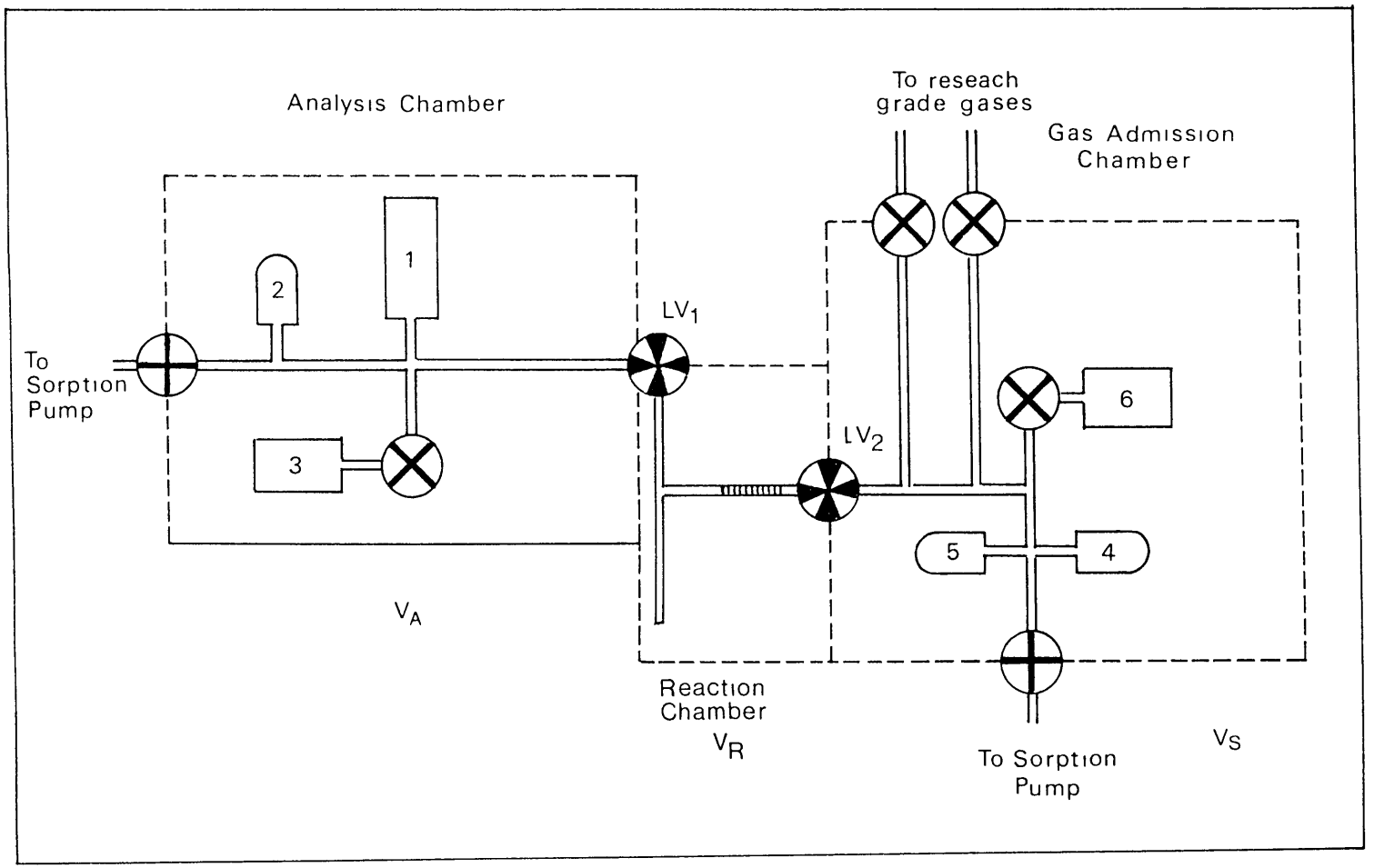

MD6 Leak Valves (VG)

UHV Valves (Leisk VG)

VRD Viton Valves (VG)

1. QX200 Quadrupole Mass Spectrometer (VG)
2. Ionisation Gauge (Mullard IOG 12)
3. 15 ls^{-1} Ion Pump (A.E.I.)
4. MKS "Baratron" Gauge, Type 222A
5. Ionisation Gauge (ITL)
6. 8 ls^{-1} Ion Pump (Ferranti)

FIG. 3.1b.

PHOTOGRAPH OF APPARATUS

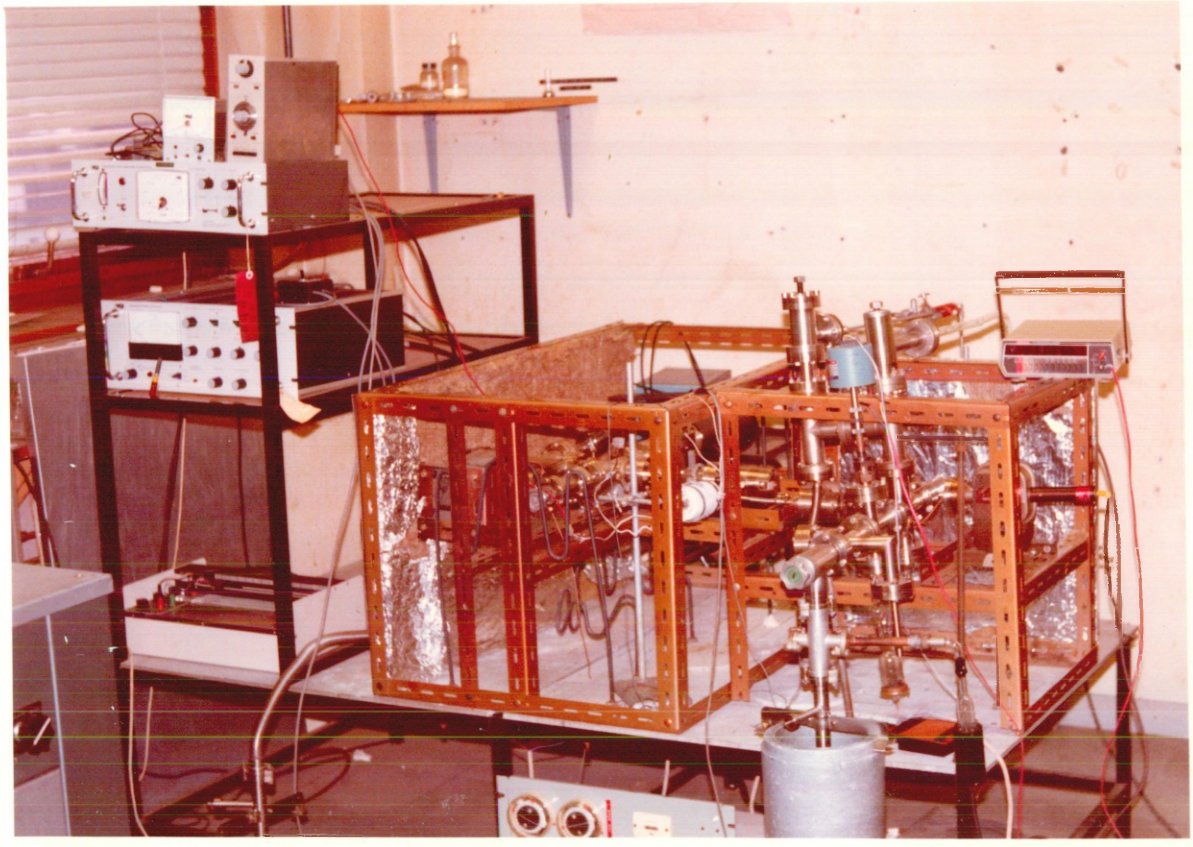

3.1.1. The Reaction Chamber

The reaction chamber (V_R) is shown in Fig. 3.2. It was made of silica glass, and connected to the stainless steel-pyrex transition tubes via graded glass seals. A small metal bellows gave some flexibility and the total volume between the leak valves was 32.06 cm^3.

The zinc oxide was placed in the inner tube and its temperature was monitored externally on a "Comark" electronic thermometer by placing a chromel/alumel thermocouple in the "well".

3.1.2 Furnace and Temperature Programmer

A tube furnace was used, with a differential winding, to heat the sample during the TPD experiments. 32 SWG Kanthal A was wound around a 1" diameter quartz tube with 18 turns per inch (tpi) at the centre and 22 tpi at the ends. This helped to reduce heat loss at the ends of the coil and maintain a constant temperature profile along the length of the sample. The coils were cemented to the quartz tube using a thin layer of alumina which was made into a paste with sodium silicate solution (50% v/v). This was also used, to secure the thermocouple sensor for the temperature programmer, close to the coils. The furnace was insulated with "Triton Kaowool Wetfelt" (an alumino-silicate material, which can be moulded into shape and then hardened by drying out).

FIG. 3.2

DIAGRAM OF SAMPLE HOLDER

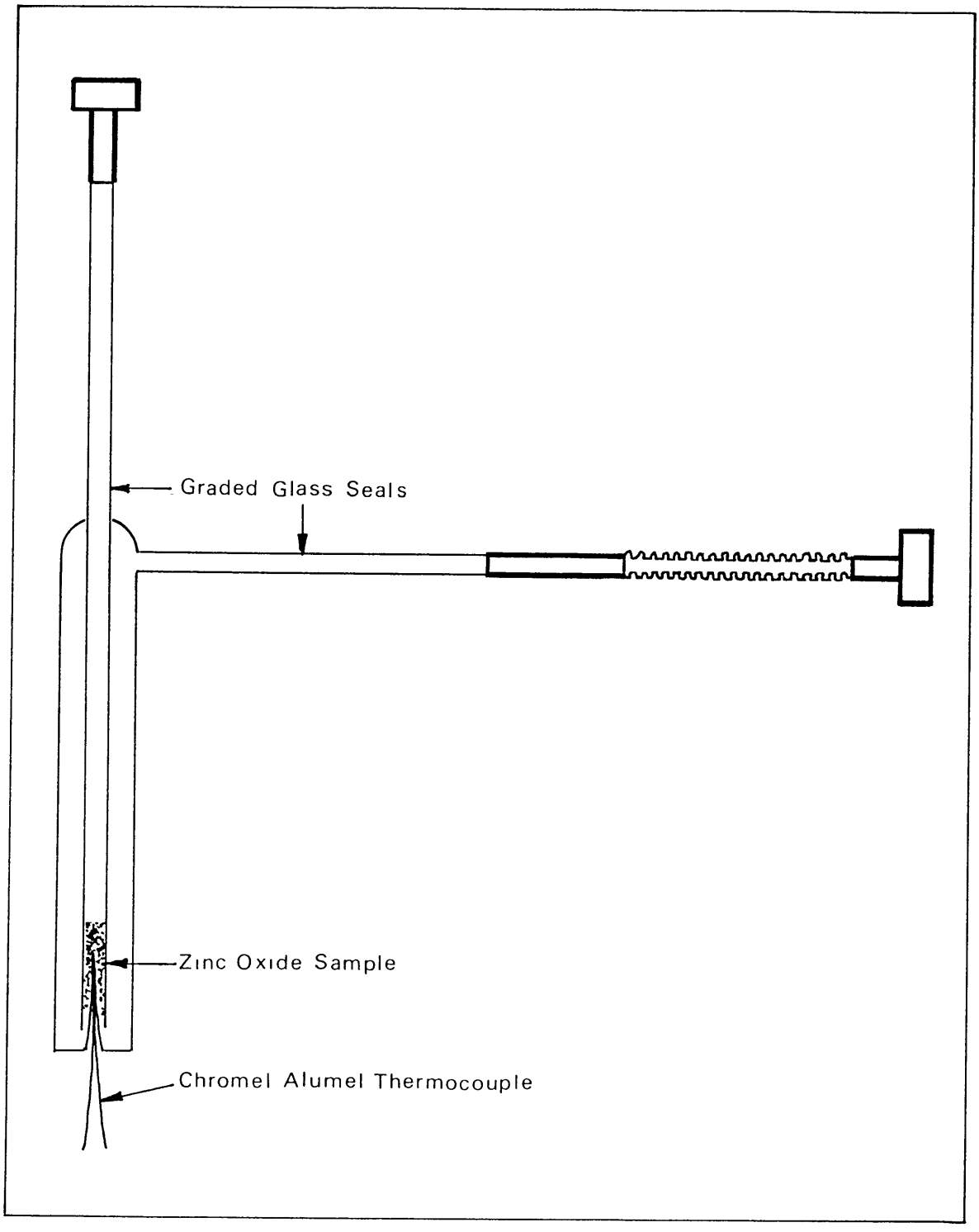

The temperature programmer (Stanton Redcroft) for chromel/alumel thermocouples, operated over a temperature range 0-1000°C and for heating rates of 1-100°C min^{-1}. By inserting another "reference" thermocouple, held at (l)N_2 temperature, between the control unit and furnace's thermocouple sensor it was possible to use the same programmer at sub zero temperatures (°C).

The low temperature work was carried out using a simple aluminium box, filled with solid carbon dioxide to surround and cool the reaction chamber. Pouring (l)N_2 over this, enabled temperatures as low as -140°C to be reached. The horizontal orientation of the reaction chamber, coupled with the external heating assembly precluded direct immersion in (l)N_2.

3.1.3 Mass Spectrometer

The mass spectrometer uses a hot filament for the initial electron emission to ionise the gas, and this is typically made of tungsten. Chemically active gases however (such as H_2, O_2, CO and H_2O) interact with any hot filament (a subject reviewed in depth by Redhead et al[2]), thus altering the composition of the gas to be analysed. This occurred to a quite unsatisfactory level and hence the filament was changed to one of thoria coated iridium. This material, having a lower work function, operates at a lower temperature and is therefore less efficient at decomposing stable molecules. Oxygen disociates at a hot filament and interacts with any carbon present to form carbon monoxide

and (to a lesser extent) carbon dioxide. This still occurs using a thoriated iridium filament but only to ca.10% at 10^{-6} torr. The problem is more acute at lower pressures (ca.10^{-8} torr).

3.2 Adsorbents : Zinc Oxide Samples

Three different kinds of zinc oxide samples were used in these experiments.

(a) A polycrystalline powder of high surface area ($36.5 m^2 g^{-1}$), which is prepared from the nitrate by precipitation using sodium carbonate, then calcined in air at 570K for 6 hours. Transmission electron microscopy (see Fig. 3.3) suggests a particle size of 105-300 Å, axial ratio ca.1 and hence the ratio polar: prism plane is ca.1:2.

(b) Another polycrystalline powder, manufactured by Johnson-Matthey Chemicals Ltd, "Puratronic grade" zinc oxide. The surface area, determined by BET analysis at Coulter Electronics Ltd., was 809 ± 3 $cm^2 g^{-1}$. Scanning electron microscopy indicates a particle size of a few microns (see Fig.3.4). From this it is not possible to discern any details regarding crystallographic orientation.

(c) Long thin single crystal needles of zinc oxide, kindly supplied by Professor G. Heiland (Aachen) (See Fig. 3.5). These crystals were grown by the oxidation of zinc vapour[3], and were ca.10μ diameter and a few mm long. The c axis lies parallel to the length of the crystal and hence it is the prism plane of zinc oxide which is predominantly exposed in this sample. For a typical crystal, (diameter 10μ, length 5mm) the ratio of polar : prism planes is ca.1 : 1000. It has been shown by X-ray oscillation photographs[4] that it is the $(10\bar{1}0)$ prism plane and not the $(11\bar{2}0)$ plane which

occurs, and so, the adsorption studies on this sample, where coverages of 1% and greater are involved, are effectively on the $(10\bar{1}0)$ prism plane alone.

3.3 Adsorbates

All of the gases used in this work were supplied by the British Oxygen Company in 1 litre flasks of research grade quality. The flasks were attached to the gas admission line and the seals were broken only after evacuating and baking the lines.

Methanol (Aristar 99.8% pure), was supplied by BDH Chemicals Ltd. This has a vapour pressure of ca.100mm Hg at room temperature, and so once the line had been evacuated and the methanol vacuum distilled, no further assistance in vaporisation was required.

FIG. 3.3

Transmission Electron Micrograph of Sample (a)

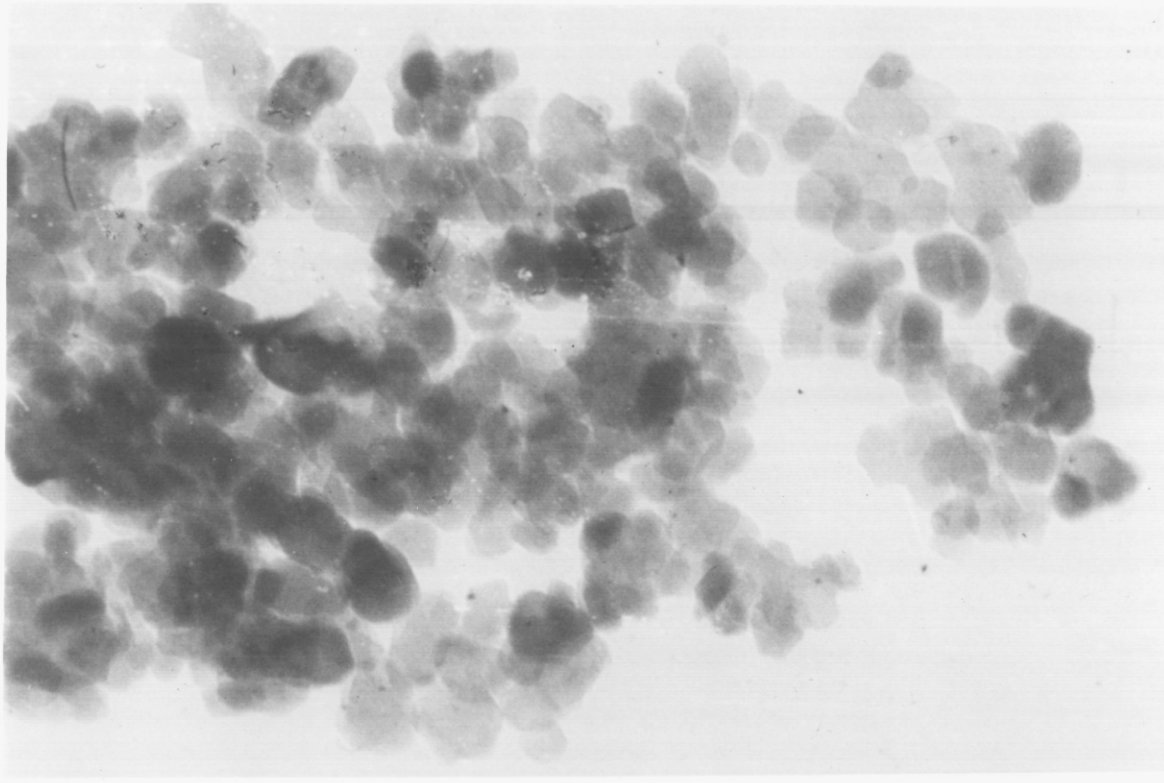

FIG. 3.4

Scanning Electron Micrograph of Sample (b)

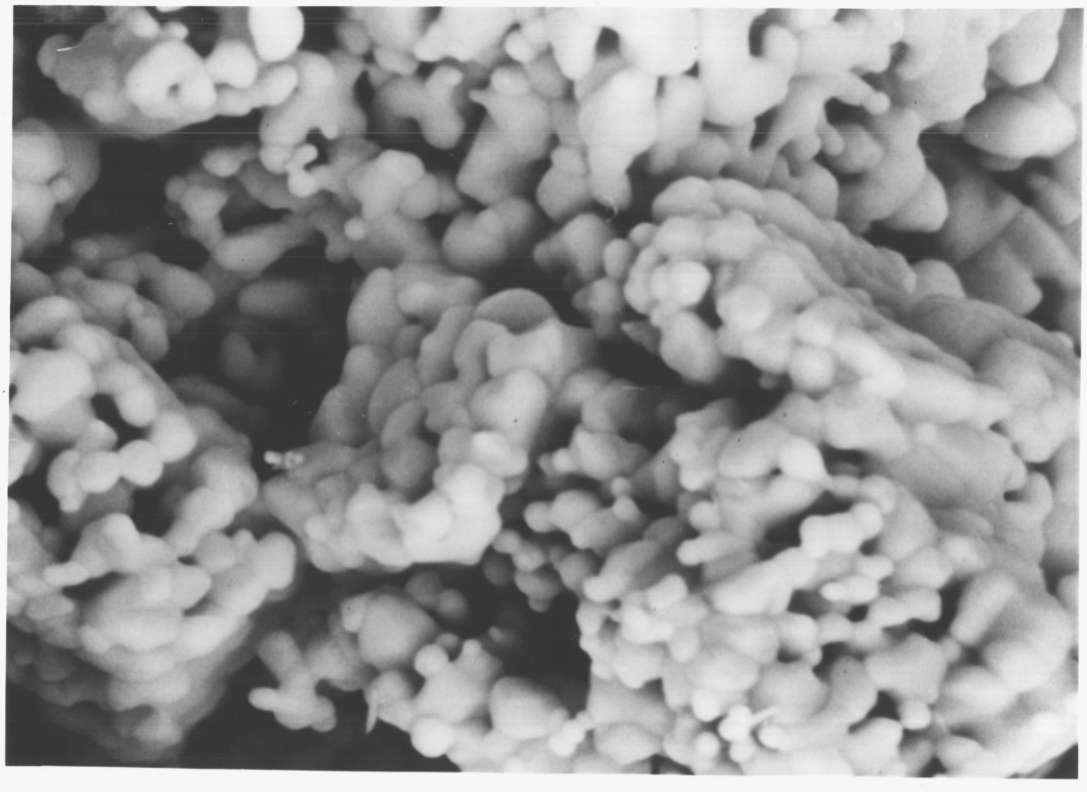

FIG. 3.5

Optical Photograph of Sample (c)

3.4 Calibration Procedure

The thermal desorption experiment requires knowledge of the mass spectrometer sensitivity and the pump speed for each gas studied if a quantitative analysis is to be made. This is immediately apparent from the expression given below which is used to calculate the amount of gas adsorbed on the surface, from the area under the desorption curve.

$$N = y \times C \times \frac{G}{\sigma} \times S \times \frac{3.24 \times 10^{19}}{A} \qquad (3.1)$$

where N = number of molecules adsorbed per unit surface area (molecs cm^{-2})

y = number of squares under the curve

C = size of square (volts deflection vs. time in secs)

G = gain factor setting on mass spectrometer, to convert volts into amps (A/V)

σ = sensitivity of mass spectrometer (A/torr)

S = pump speed (l/s)

A = surface area of sample (cm^2)

1 torr litre = 3.24×10^{19} molecules at 298K

A, y, C and G are easily obtained, but the sensitivity of the mass spectrometer and the pump speed have to be carefully calibrated for each gas.

It was necessary to calibrate the ionisation gauge against an absolute pressure gauge (in this case the "Baratron" gauge) in order to use it in subsequent calibration of the mass spectrometer.

3.4.1. Ionisation Gauge

There are mnay articles in the literature discussing errors in pressure measurement with ionisation gauges[5] and most books on vacuum practice give the problem good coverage. Briefly, factors arising from the gauge itself, such as gauge pumping, reactions at the hot filament and desorption from the grid are important, but so is the position of the gauge within the system. It is therefore essential to calibrate the ion gauge against an absolute total pressure gauge.

Such a calibration was carried out "in situ" against the absolute "Baratron" gauge, using a pressure expansion technique[6]. In this technique the reaction chamber was filled with nitrogen to an accurately known pressure (ca.0.2 $\pm$ 0.001 torr). The nitrogen was then allowed to expand back into the evacuated gas admission chamber, with the pump valved off. Leak valve 1 was then closed and leak valve 2 opened, to allow the nitrogen to expand into the evacuated analysis chamber, also with the ion pump valved off. In each case after valving off the pump the pressure in V_A was allowed to reach 10^{-7} torr before LV_2 was opened. The expansion ratio in each step was ca.50, thus giving final pressure readings 2500 times lower, in the 10^{-5} to 10^{-4} torr range. This final pressure is sufficiently above the outgassing level of an unpumped system, namely ca. 10^{-7} torr, for adsorption, desorption and outgassing effects to be negligible.

In all, ten calibration points were taken (two of which required a second back expansion into V_S). These are tabulated below.

TABLE 3.1

Ion Gauge Calibration

P_o	$P_{calc(true)}$	P_{gauge}	P_{gauge}/P_{calc}
0.192	9.237×10^{-5}	2.739×10^{-5}	0.296
0.2236	1.076×10^{-4}	3.089×10^{-5}	0.287
0.161	7.745×10^{-5}	2.188×10^{-5}	0.2825
0.1464	7.043×10^{-5}	2.145×10^{-5}	0.3045
0.2406	1.157×10^{-4}	3.698×10^{-5}	0.3195
0.2029	9.761×10^{-5}	2.699×10^{-5}	0.2765
0.3017	1.451×10^{-4}	4.585×10^{-5}	0.328
0.4323	2.080×10^{-4}	6.221×10^{-5}	0.299
1.6689	1.882×10^{-5}	5.005×10^{-6}	0.266
2.37	2.672×10^{-5}	6.757×10^{-6}	0.253

The average value for $P_{gauge}/P_{calc} = 0.29 \pm 0.02$ in the pressure range 1.882×10^{-5} to 2.08×10^{-4} torr. Hence, for the standard gas nitrogen $P_{calc} = P_{gauge} \times 3.448$.

The ion gauge pressure was monitored on a DVM from the mV output on the pirani-ion gauge control unit (Vacuum Generators) as this gave a clearer indication of the pressure changes. An initial rapid rise (seconds) in pressure occurred, as expected, which then levelled off for ca.10 secs. before the effects of the ion gauge acting

as a pump could be observed, gradually reducing the pressure (over a substantial fraction of an hour). It was the value of the maximum which was used in the calculations.

The sensitivity of an ion gauge (X) is defined as

$$X = \frac{I_p}{I_e} \times \frac{1}{P}, \text{ and since } I_p = QI_e nL, \quad X = \frac{QL}{kT}$$

where I_p = current of positive ions

I_e = current of electrons

Q = total ionisation cross section

n = P/kT = density of molecules

L = total electron path length

P = pressure

Each type of atom/molecule has an individual ionisation cross section, and hence the sensitivity of the ion gauge varies for different gases.

Absolute sensitivities however, are very dependent upon minor fluctuations in the geometry of the gauge and control circuitry[7] so a more useful parameter is the relative sensitivity ($X_{gas}/X_{nitrogen}$). The relative sensitivity can also be obtained from the relative ionisation cross section[8]. Table 3.2 gives experimental values collated from the literature by Nakao[8] for both relative sensitivity and relative ionisation cross section. Methanol was the exception as no value for relative sensitivity is recorded, but the relative ionisation cross section was found in Ref.9.

TABLE 3.2

Relative Sensitivity and Relative Ionisation Cross Section for Several Gases

Gas	Relative Sensitivity	Relative Ionisation Cross Section*
N_2	1	1
O_2	0.87	0.96
CO_2	1.36	1.39
CO	1.02	1.06
H_2	0.44	0.38
N_2O	1.66	1.30
MeOH	-	1.27

* at 75eV electron energy

Thus all pressure readings taken, are first corrected for the gauge calibration and then for the relative sensitivity of the gas.

$$P_{gas} = P_{gauge} \times 3.448/\text{Relative sensitivity of gas}$$

3.4.2 Mass Spectrometer

The sensitivity of the mass spectrometer (in amps per torr) was obtained by correlating the most prominent or characteristic peak of the spectrum with the total pressure (as read on the ionisation gauge). Both mass spectrometer and ion gauge were initially degassed. The pressure readings and mass spectra were recorded in a steady state, continuous flow mode, controlled by LV_2. Each sensitivity

determination was an average of three or four values, taken in the 10^{-7} to 10^{-6} torr range.

Regular determinations of the sensitivity were essential as some gases such as oxygen, can impair the performance of the channel electron multiplier, apart from the general degradation with time. For this reason, values of relative sensitivity should be treated with caution, unless both sensitivities are determined within a short time scale (which was not necessarily the case here).

Some typical values of the sensitivity are tabulated below.

TABLE 3.3

Typical Values of Mass Spectrometer Sensitivity

Gas (mass used)	Sensitivity (A $torr^{-1}$) *
N_2(28)	1.206×10^{-3}
O_2(32)	7.588×10^{-4}
CH_3OH(31)	3.860×10^{-4}
CO_2(44)	1.53×10^{-3}
N_2O(44)	7.65×10^{-4}

* These values have been calculated using total pressure readings which have been corrected for absolute calibration and relative sensitivity as described in Section 3.4.1.

It can be seen that the sensitivity of the mass spectrometer genuinely varies for different gases. This is due to the

fact that, as in the ionisation gauge, the initial positive ion production occurs, by electrons emitted from a hot filament, bombarding the gas molecules, which is a process dependent on the ionisation cross section. The sensitivity of the instrument is also governed by the gain of the electron multiplier and the quadrupole transmission, which in turn are dependent upon the mass of the species detected.

Further variation in the sensitivity will arise if anomolous cracking patterns occur due to successive electron impacts[2]. Madix et al[16] consider all of these factors, and also the yield, for each mass fragment in the cracking pattern, when evaluating correction factors for their desorption spectra. Subsequent calibration against a known standard is then essential for quantitative results. Such analysis is circumvened here, by calibrating the mass spectrometer against the ion gauge for each gas.

3.4.3. Pump Speed

The pump speed was determined using a variation of the "pipette exhaust" technique[10]. A known amount of gas was put into the reaction chamber (P_RV_R) at room temperature, then with LV_1 firmly closed the gas was passed slowly through LV_2 into the analysis chamber, monitored by the mass spectrometer, as in a thermal desorption experiment. The ion gauge was off throughout the experiment. From the area under the curve, the amount of gas (N) could be determined in terms of the pump speed (S), from Eqn. (3.1) viz:

$$N = y \times C \times \frac{G}{\sigma} \times S \times \frac{3.24 \times 10^{19}}{A}$$

This was equated to the amount put into V_R, and hence S evaluated:

$$S = P_R V_R \times \frac{\sigma}{G} \times \frac{A}{y} \times \frac{1}{3.24 \times 10^{19}}$$

At least three determinations were made of each pump speed, and the average values are tabulated below.

TABLE 3.4

Some Experimental Values of Pump Speed

Gas (mass used)	Pump Speed (ls^{-1})
N_2 (28)	1.80 ± 0.2
O_2 (32)	2.00 ± 0.4
CH_3OH (31)	0.96 ± 0.08

On comparison with the literature values of relative pump speeds[11,12] the value obtained here for oxygen seems high. The different experimental methods used therefore, were carefully scrutinised. Bance and Craig[11] adopted the two gauge method[13]: the flow rate of gas (Q), is determined by measuring the pressure drop ($P_1 - P_2$) across a known conductance (C). Now, $Q = C(P_1 - P_2)$ and the throughput of the pump, also Q, is equal to SP_2. Therefore, $S = C[(P_1/P_2) - 1]$. Obviously this does not require absolute pressure measurement and has immediate appeal.

The method used in this research however, was carried out "in situ", quite conveniently, and is believed to give a

true result for this vacuum system. The foundation of this assertion rests on the fact that because oxygen molecules are decomposed at the the hot filament in the mass spectrometer, subsequently forming carbon monoxide and carbon dioxide, the value for y (number of squares under the curve) in Eqn. 3.1 would be reduced because the mass spectrometer only monitors mass 32, and hence S would increase. The mass spectrometer essentially acts as a second chemical pump - and because the mass spectrometer is used in the TPD experiments it will be operating then as well.

No literature value exists for the relative pump speed of methanol or nitrous oxide specifically, but low molecular weight hydrocarbons (acetylene in Ref. 11) are reported to have pump speeds 90-160% of the nitrogen value[12]. Kelly and Vanderslice[14] observed that a carbonaceous layer gradually forms near the gas entrance port and over the cathodes of the ion pump, when pumping benzene or toluene at pressures even below 10^{-5}torr. This carbon is difficult to sputter, and thus reduces the pumping action. (Momentary large increases in pressure could completely cover the cathodes with carbon, and thus pumping would cease). Similarly, the decomposition of methanol in the ion pump discharge could also affect its pumping action.

The pump speed for carbon dioxide and nitrous oxide were not measured by this method but were taken to be $1{\cdot}8\ ls^{-1}$ (the same as the nitrogen value[12]). They had been measured

previously however, using the rate of rise method[15], which for completeness is outlined below.

A steady flow rate of gas was established via LV_2, into V_A, and the equilibrium base pressure (P_A) noted from the mass spectrometer. The ion pump was then valved off, and the increase in pressure with time was monitored. Using the equation $V_A \times dP/dt = SP_A$, S was evaluated. This method is reportedly rather inaccurate because the equilibrium base pressure should ideally be at least ten times the background pressure, so that desorption from the chamber walls would be negligible. In these experiments P_A was three to five times greater than the background, at the most, due to limitations on monitoring dP/dt. This method was also used for nitrogen and oxygen before suspicions were finally aroused over the methanol (mass 31) value of 0.1 ls^{-1}. (The values for nitrogen, oxygen, carbon dioxide and nitrous oxide by this method were 3.66 ls^{-1}, 3.84 ls^{-1}, 3.69 ls^{-1} and 4.7 ls^{-1} respectively). Monitoring a different mass in the cracking pattern, did not give the same result. This indicates that the cracking pattern changes as the pressure is increased, which should not happen, and can only mean that the background spectrum is interfering with the initial measurement of P_A or that chemical reactions are occurring at the hot filament. The latter is most probably the answer, particularly for oxygen, nitrous oxide and methanol, as the system is not pumping during the experiment. Thoria coated filaments do produce carbon dioxide to a large extent[15] (28 being one of the mass fragments) which could

explain why even nitrogen (an inert gas) gives such a high value for the pump speed by this method. This method was therefore abandoned and the following values used:

TABLE 3.5

Pump Speeds Used.

Gas	Speed (ls^{-1})
N_2	1.8
O_2	2.0
CH_3OH	0.96
CO_2	1.8
CO	1.8
N_2O	1.8
H_2	4.8

The pump speed for nitrogen, oxygen and methanol in Table 3.5 were measured experimentally. The values for hydrogen, carbon monoxide and carbon dioxide were calculated, using tabulated values[12] of the relative pump speed (compared to nitrogen). Nitrous oxide and carbon dioxide are isoelectronic, and therefore, assigned the same speed.

1. M. BOWKER, H. HOUGHTON AND K.C. WAUGH
J.C.S. Far.Trans.I 77(12), 3023, 1981

2. P.A. REDHEAD, J.P. HOBSON AND E.V. KORNELSON
The Physical Basis of Ultra High Vacuum (1968)
Chapman and Hall

3. G. HEILAND, E MOLLWO AND F. STOCKMANN
Solid State Physics 8, 191, 1959

4. I.R. LAUKS
PhD.Thesis, University of London 1977

5. P.A. REDHEAD
Trans. Natl. Vac. Symp. 7, 108, 1960

6. F.R. SELLENGER
Vacuum 18, 645, 1969

7. T.A. FLAIM AND P.D. OWENBY
J.Vac. Sci. Tech. 8(5), 661, 1971

8. F. NAKAO
Vacuum 25(9-10), 431, 1975

9. R.D. KLEEMAN
Proc. Roy. Soc. Lond. 79A, 220, 1907

10. D.R. DENISON AND E.S. McKEE
J.Vac. Sci., Tech. 11(1), 337, 1974

11. U.R. BANCE AND R.D. CRAIG
Vacuum 18, 391, 1968
Vacuum 16, 647, 1966

12. V.G. and Ferranti Technical Data

13. D. ANDREW
Vacuum 16, 653, 1966

14. J.E. KELLY AND T.A. VANDERSLICE
Vacuum 11, 205, 1961

15. J.F. O'HANLON

A User's Guide to Vacuum Technology (1980), John Wiley

16. E.I. KO, J.B. BENZIGER AND R.J. MADIX

J.Catal. 62, 264, 1980

CHAPTER 4

EXPERIMENTAL PROCEDURES II

Before any temperature programmed desorption experiments could commence the zinc oxide samples had to be cleaned thoroughly to remove surface contaminants. Then in order to establish a reproducible, well characterised starting state, the samples were "treated" prior to each experiment to yield stoichiometric or defected surfaces as required (see below).

The cleaning procedures adopted for the different types of sample used in these experiments, have many similarities. They all consisted of heat treatment in oxygen/hydrogen/ vacuum in order to oxidise/reduce/volatise any impurities present on the surface. Diffusion of impurities from the bulk of the crystal to the surface obviously has a more pronounced effect on samples with a low surface area/volume ratio (large single crystals) compared to those with a high surface area/volume ratio (powdered samples). Consequently, the cleaning procedure for the latter is less critical, because the percentage impurity concentration at the surface is fairly small. The needle crystals used in these experiments would have correspondingly less percentage contamination than a large single crystal. Green and Lauks[11] discuss this more fully in their paper.

4.1 Polycrystalline Powdered Zinc Oxide

For the polycrystalline powdered samples, a fairly standard cleaning procedure, similar to that of Boccuzzi et al[1], was adopted. This involved heating the sample in oxygen (ca.0.4 torr) to 723K (450°C), and maintaining these conditions for ca.1 hr., in order to burn off oxidisable impurities such as carbon. Subsequent heating in vacuo at 723K for 15 mins. to outgas the sample, concluded the experimental preliminaries. Care was taken not to exceed 773K as several reports of sample decomposition and conductivity changes at this temperature have appeared in the literature[2,3]. This is probably due to sublimation from the zinc polar planes[4].

For experiments carried out at I.C.I. New Science Group, the sample was cleaned by heating in vacuo to 723K and then pre-treated in hydrogen, ostensibly to simulate conditions during methanol synthesis. The sample was heated in 1 torr hydrogen at 555K for 15 minutes, then on evacuation of the chamber the temperature was raised further to 700K to desorb any hydrogen species. It is questionable whether hydrogen actually reduces the zinc oxide at these temperatures[1,5]. Infra red spectra recorded during various stages of oxidation/reduction cycles implied that heating zinc oxide in vacuo or in hydrogen at 433K produced the same effect, namely, removal of hydroxyl and carbonate species. Only by subsequent cooling of the sample in hydrogen to room temperature was a less stoichiometric surface obtained[1]. A detailed review of hydrogen adsorption on zinc oxide can

be found in ref. 6. Quite recently however, Braid et al[7] have published conflicting assignments for some of the infra red bands.

4.2 Thin Needle Crystals of Zinc Oxide

The prism plane of zinc oxide is stable to heat in vacuo up to ca.700K. Above this temperature both zinc and oxygen sublime[8,9], but at different rates, thus giving overall deficiency in oxygen. This can be represented quantitatively as a concentration of oxygen vacancies, and is dependent only upon the temperature of sublimation and the pressure of oxygen above the zinc oxide sample.

Green and Lauks[10] conducted a rigorous investigation of this system, and have established, quite precisely, the temperature and pressure ranges required to generate a particular concentration of oxygen vacancies. Their results are summarised in Fig. 4.1. Clearly, in the temperature range 888-993K and 0-0.45 torr oxygen, the vacancy concentration can be adjusted between 0-4%. It is the two extreme cases which are of particular interest here. The former will be referred to as a stoichiometric surface, and the latter as a defected surface.

Several corroborative experiments were considered necessary, in order to establish precise pre-treatment conditions. These will be outlined below as the work by Green and Lauks forms the starting point for the adsorption experiments on

FIG. 4.1

Fractional Surface Oxygen Vacancy Concentration, θ, as a Function of Oxygen Pre-treatment Pressure at Various Temperatures.

(Taken from I.R. Lauks, Ph.D. Thesis, London University 1977.)

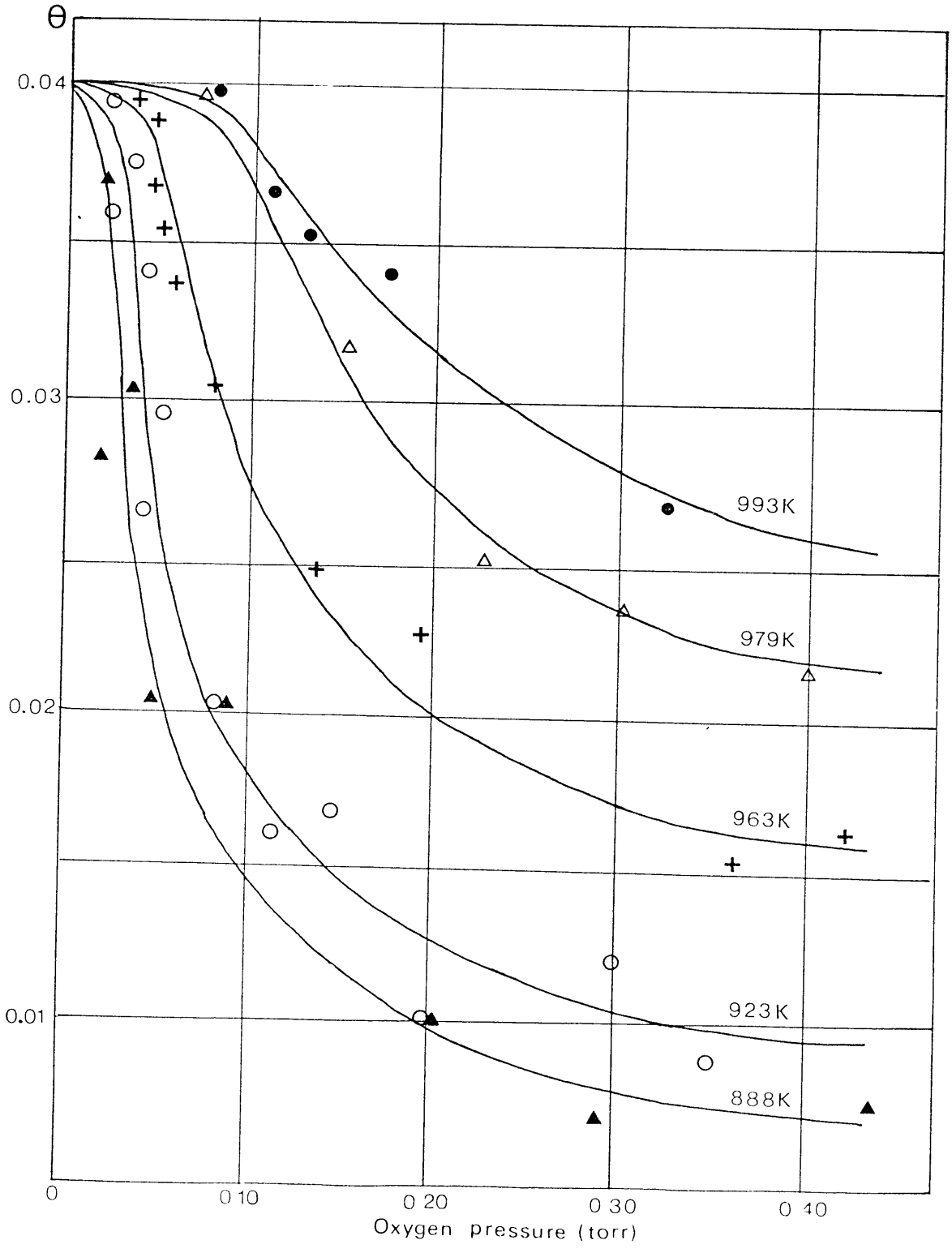

stoichiometric/defected surfaces to be presented here.

The zinc oxide needle crystals were initially cleaned by heating them in ca.0.11 torr flowing oxygen to ca.1073K, and maintaining these conditions for several hours. It has been shown that this type of sample can be cleaned by heat treatment alone[11] provided the diameter/surface area ratio is sufficiently small. Chemical etching, and argon ion bombardment were not employed. As a precautionary measure, the temperature was not taken above 1073K, because irreversible changes in surface structure[12] have been reported at 1100K.

Before each experiment, the sample was heated to ca.1050K in vacuo for 15 minutes to remove any surface contaminants and also to produce a defected surface. If a stoichiometric surface was required (or a surface with an intermediate concentration of vacancies, in the range 0-4%) the sample was then cooled to a specified temperature, LV_2 was closed and LV_1 opened, to expose the zinc oxide to a prescribed pressure of oxygen for ca. 20 minutes. After evacuating the reaction chamber (through the gas admission chamber), LV_1 was closed and LV_2 opened while the sample cooled to the required adsorption temperature. In order to generate a stoichiometric surface, the conditions used were as follows: cooling to 880K and exposing to > 0.5 torr oxygen for 20 minutes, then cooling in the gas to ca.773K before evacuation.

It is apparent that having generated a stoichiometric surface, a subsequent TPD experiment, to 1050K, monitoring oxygen should yield a peak which ultimately represents 4% of the surface area. Consequently, this method was used to determine the total surface area of the zinc oxide "fur", when the conventional BET method was proclaimed not sensitive enough (see Appendix C). As a bonus this "in situ" measurement, enabled regular monitoring of the sample and any degradation with time.

Green and Lauks used this procedure of temperature programmed desorption to derive their "map" of pre-treatment conditions.

1. F. BOCCUZZI, C. MORTIERRA, R. SCALA, and A. ZECCHINA,
J.C.S Far. Trans. II 77, 259, 1981
2. J.O. COPE and I.D. CAMPBELL,
J.C.S Far. Trans. I 69, 1, 1973
3. B.M. ARGHIROPOULOS and S.J. TEICHNER,
J.Catal. 3, 47, 1964
4. D. KOHL, M. HENZLER and G. HEILAND,
Surface Science 41, 403, 1974
5. P.S. WEHNER, P.N. MERCER and G. APAI,
J.Catal. 84, 244, 1983
6. C.S. JOHN
Chem.Soc.Spec.Per.Rep.(1980) Catalysis Vol.III p.169
7. J. HOWARD and I.J. BRAID
J.C.S Far. Trans. I 80, 225, 1984
8. W. GOPEL
Z.Phys. Chem.Neue.Folge 106, 211, 1977
9. W. GOPEL
Ber.Bunsen.Phys.Chem. 82, 744, 1978
10. M. GREEN and I.R. LAUKS
J.C.S Far. Trans. II 74, 2724, 1978
11. I.R. LAUKS and M. GREEN
Surface Science 71, 735, 1978
12. W. GOPEL and G. NEUENFELDT
Surface Science 55, 362, 1976

CHAPTER 5

ADSORPTION OF METHANOL ON ZINC OXIDE SURFACES

5.1 General Review

Methanol is an important commodity in the chemical industry. It is one of the starting materials for the synthesis of many organic chemicals, viz., olefins, carboxylic acids, esters, ketones and higher alcohols. Hence, a cheap and efficient manufacturing process is highly desirable.

In the 1920's, methanol was produced by destructive distillation of wood wastes. This is very inefficient and was soon replaced by a high pressure (100-500 atm), high temperature (300-450°C) synthesis from CO and H_2, over a mixed catalyst containing ZnO/Cr_2O_3. During the next sixty years, many catalysts were developed to synthesize methanol, almost all comprised of zinc, copper and aluminium/chromium oxides in various proportions. Different catalysts require different reactant mixtures/ratios, and it was discovered early on that the addition of small quantities of CO_2 in the feed gas, enhanced the methanol yield. The most economical process used nowadays, was developed by I.C.I. PLC., in 1965. This operates at a lower temperature (250°C) and lower pressure (50-100 atm) than previous methods. The catalyst consists of $Cu/ZnO/Al_2O_3$ in the approximate metal atomic ratio 60/30/10 and the gaseous reactant mixture (feed stock) contains 10% CO, a few percent CO_2 and the rest H_2. These catalysts are usually prepared in three stages: the

carbonates are precipitated from a solution of the nitrates, by addition of sodium carbonate solution; this is followed by calcination in air at 350°C; and finally, reduction, using 2% H_2 in N_2 at 250°C, 1 atm, yields phases of metallic copper and zinc oxide. The role of alumina appears to be structural promotion, although one catalyst is reported to contain zinc aluminate[3,15].

The review by Natta[1] in 1955, concerning the evolution of a methanol synthesis catalyst, and the more recent accounts by Kung[2], Klier[3], Bowker[4] and Poels and Ponec[5] are all worthy of note. It is apparent that despite the wealth of research which has been conducted over the years, in this area, the precise nature of the catalytic process (more especially the reaction mechanism and active sites) has yet to be established definitively.

The literature contains innumerable references to adsorption/co-adsorption studies of the reactants on mainly powdered samples of catalysts/single component, using the techniques of infra red spectroscopy and/or temperature programmed desorption. Similar experiments to study the adsorption/decomposition reaction of methanol and possible intermediates are also providing useful information.

As a result, some progress has been made in elucidating the reaction mechanism. From TPD studies on zinc oxide powder[6] and on copper[7], methanol synthesis is believed to occur via formate, formaldehyde and methoxy

intermediates. Corroborative evidence for the existence of formate species on zinc oxide is available from infra red studies[8,9]. However, co-adsorption of CO_2 and H_2 at 200°C results in the same spectrum as formic acid but not if CO and H_2 are used. It has been suggested[4] that CO_2 and H_2 are the major reactants, with CO simply maintaining the catalyst in a reduced state. Indeed, in the reverse process, copper and zinc oxide are both reported to have high selectivity for dehydrogenating the formate to CO_2 and H_2 at ca.200°C - instead of the dehydration reaction to CO and H_2O[10]. The fact that Bowker et al failed to detect CO adsorption on zinc oxide[6] at room temperature or above, was offered as further evidence to support this idea. However, there are reports to the contrary. Solomon et al[19,20] observed CO adsorption on several planes of zinc oxide at 80K. The CO molecule is bound to the surface zinc ion via its carbon atom.

There are conflicting results in co-adsorption studies as well. Deluzarche et al[11] isolated both formate and methoxy intermediates, after CO/H_2 co-adsorption on a ZnO/Cr_2O_3 catalyst at pressures up to 50 atm. and at a temperature of 250°C. The formyl species has also been detected[12,14], using infra red spectroscopy, after CO/H_2 co-adsorption on ZnO and Cu/ZnO catalysts at 270K. More recently, Lavalley et al[32] have detected formyl and methoxy intermediates by chemical trapping and transmission infra red spectroscopy after CO/H_2 co-adsorption on ZnO at ca. 490K and 260K respectively. Edwards and Schrader[33]

have observed methoxy and formate species after adsorption of methanol on Cu/ZnO and Cu/ZnO/Cr_2O_3 catalysts at 130-200°C. (Gaseous CO_2 and adsorbed carbonate were also detected as the methoxy species decomposed.)

Klier et al[3,13] envisage competitive adsorption between CO_2 and CO or H_2, to explain the profound effect of a small percent of CO_2 in the feed gas on the synthesis rate of methanol. In Reference 14, Lavalley et al confirm that H_2 and CO_2 are adsorbed on the same sites. The idea that the CO_2/CO ratio governs the extent to which the catalyst exists in its oxidised/reduced form, was developed by Klier et al[13], and kinetic expressions were derived which reflect the experimental results well: maximum performance with ca.2% CO_2 in the feed gas.

It is well known that copper (oxide) enhances the catalyst's activity considerably but its precise role has not been established. Both hydrogen and carbon monoxide are reported to adsorb on copper[30], whilst carbon dioxide adsorption has not been reported. (Compare zinc oxide, where hydrogen and carbon dioxide are both strongly adsorbed, hydrogen dissociatively, but carbon monoxide adsorption is weak.) On copper oxide (cupric or cuprous), both hydrogen and carbon monoxide would reduce the adsorbate. In the activated catalyst, copper is believed to exist in the + 1 oxidation state[15,16,17,18], which is a stronger adsorption site for carbon monoxide[5] than Cu^o.

It has been postulated that further activation of the CO molecule, by an adjacent oxygen vacancy(2), could be the first step in the synthesis reaction. A more complete discussion of the role of oxygen vacancies will be made later in this Chapter.

Clearly a lot of research still has to be done before the reaction mechanism is completely understood. It is still not certain whether CO is simply hydrogenated in stages to methanol (via a formyl intermediate, or whether CO insertion into an OH group occurs, to give the formate, then, subsequent hydrogenation and dehydration to methanol (see Fig. 5.1). The nature of the "active sites" has also to be determined unequivocally. With this objective, attention has been turning towards single crystal studies, where activity of specific crystal planes and lattice defects can be investigated. It is in this sphere of interest, that the research to be presented in this Chapter has been directed. Experiments to monitor the decomposition of methanol on both defected and stoichiometric $(10\bar{1}0)$ surfaces of zinc oxide will be described, and subsequently compared with similar experiments performed on polycrystalline zinc oxide powder, in an endeavour to identify the "active sites"/planes.

FIG. 5.1

Proposed Reaction Mechanisms for Methanol Synthesis

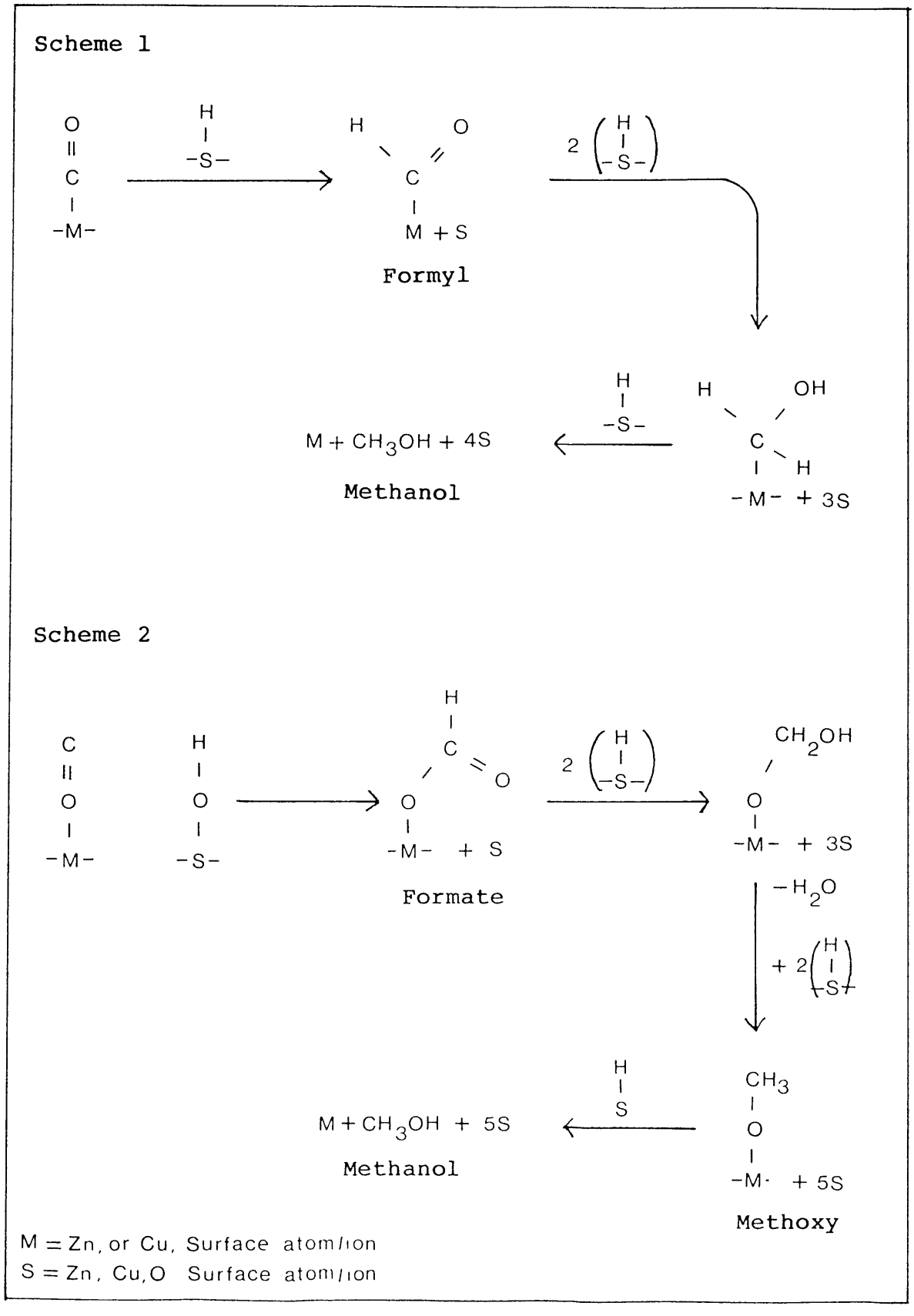

5.2.1 Adsorption of Methanol on the $(10\bar{1}0)$ Prism Plane of Zinc Oxide at Room Temperature

Adsorption experiments were carried out in this laboratory on stoichiometric and defected $(10\bar{1}0)$ surfaces, prepared as described in Chapter 4 Secion 4.2. The sample is then cooled in vacuo to room temperature. Leak valve 2 was closed and leak valve 1 opened (see Chapter 3, Fig.3.1) to expose the sample to 0.763 torr methanol for half an hour. Subsequent evacuation for 200-300 seconds removed any adsorbed species of binding energy less than ca.88kJ mol^{-1} (assuming a pre-exponential factor of $10^{13}s^{-1}$ in the rate equation) thus enabling only fairly strong binding states to be detected.

Leak valve 1 was then closed and leak valve 2 opened ready to commence the TPD experiment. For both stoichiometric and defected surfaces, the experiment was repeated several times, in order to monitor the following masses individually: 2 (hydrogen), 28 (carbon monoxide), 31 (methanol), and 44 (carbon dioxide). The facility to monitor several masses simultaneously was not available but the dosing procedure was straight forward and accurate enough for errors to be minimal. The heating rate was $0.4Ks^{-1}$

The resulting TPD spectra are shown in Fig. 5.2 and are identical for both stoichiometric and defected surfaces. These TPD curves offer substantial support for the conclusions drawn in Chapter 2, namely that detailed line

FIG. 5.2

TPD Spectra of Methanol and its Decomposition Products after Adsorption on the $(10\bar{1}0)$ Prism Plane of Zinc Oxide at Room Temperature

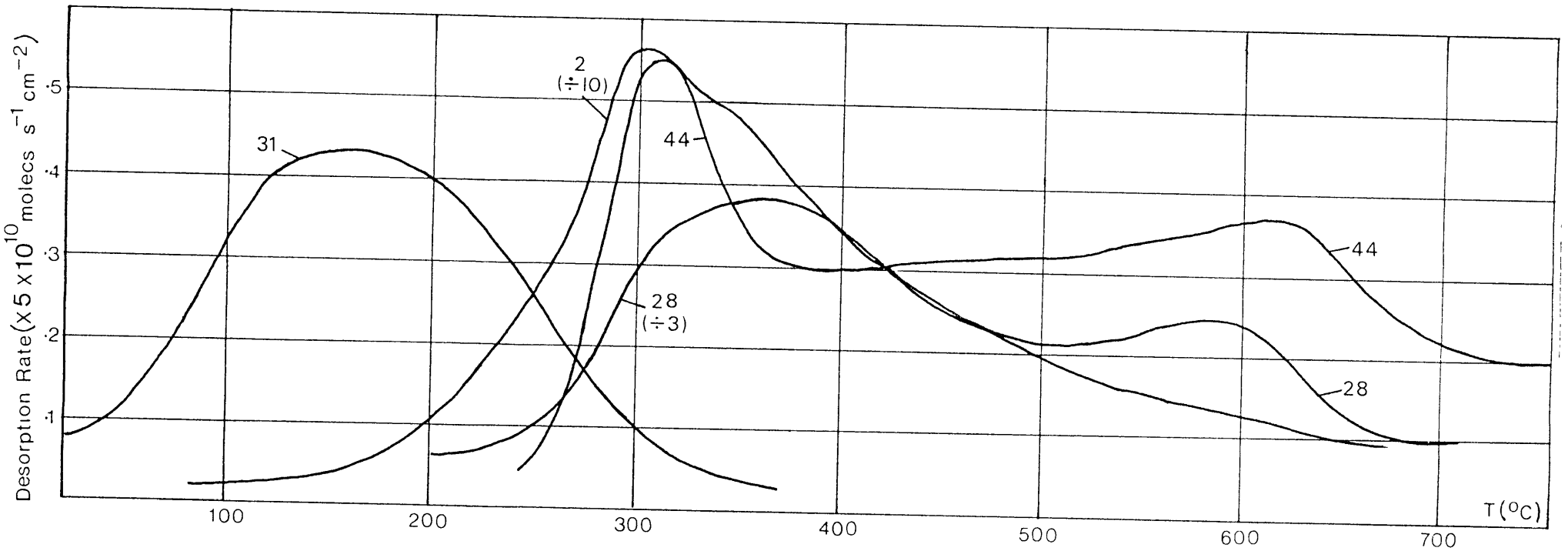

shape analysis is rarely practicable, despite every endeavour to eliminate temperature gradients and provide sufficient pumping capability. Consequently the analysis to be presented later is restricted. The activation energies for desorption were determined by substituting the peak maximum temperatures into the Redhead equation (see Chapter 2 Section 2.2.2) and the results are tabulated in Table 5.1. These results will be discussed more fully in Section 5.3.

TABLE 5.1

Activation Energies of Desorption for Methanol and its Decomposition Products from the $(10\bar{1}0)$ Prism Plane

Desorbed Species	Temperature of Peak Maximum (K)	Activation Energy of Desorption (kJ/mol)
CH_3O-	433	120
CO	633	176.9
CO_2	583	162.5
H-	573	159.6
H-	623	174

NOTE: The values for the activation energies have been evaluated using the Redhead equation (see Chapter 2 Section 2.2.2) assuming a pre-exponential factor of $10^{13}s^{-1}$ in the rate equation.

The coverage of each species was determined from the area under the curve as described in Chapter 3. Where a direct/ recent determination of the mass spectrometer sensitivity was not available for a particular species, the methanol

value was adopted, and corrected accordingly, using the appropriate relative ionisation cross section (compared to methanol), and also the relative gain factor for the quadrupole filter $(31/M.Wt.)^{\frac{1}{2}}$. The results are shown in Table 5.2 and are expressed in molecules/cm^{-2}. The surface area of the sample was 1809 cm^2, determined as described in Chapter 4.

In calculating the coverage values shown in Table 5.2, contributions from other species, also exhibiting a peak at a particular mass have been carefully accounted for. For example, the mass 28 peak, was not only derived from carbon monoxide but also from methanol and carbon dioxide. Consequently their contributions to the mass 28 signal had to be evaluated and subtracted, to give the true coverage value. Using the mass spectral cracking patterns (tabulated in Appendix D) for methanol and carbon dioxide, the relative peak heights of mass 28 to mass 31 and 44 respectively are 1.148 and 0.314. Hence, 1.148 multiplied by the coverage of methanol (mass 31), represents the contribution of methanol to the mass 28 signal. Similarly 0.314 multiplied by the coverage of carbon dioxide (mass 44) represents the contribution of carbon dioxide to the mass 28 signal.

TABLE 5.2

Coverage of Methanol and its Decomposition Products on Stoichiometric and Defected $(10\bar{1}0)$ Prism Planes of Zinc Oxide, after Adsorption of Methanol at Room Temperature

Desorbed Species	Defected Surface (molecs/cm^2)	Stoichiometric Surface (molecs/cm^2)
CH_3O-	9.78×10^{12} (0.016)	8.96×10^{12} (0.015)
CO	5.13×10^{13} (0.085)	3.03×10^{13} (0.051
CO_2	4.26×10^{13} (0.07)	3.21×10^{13} (0.05
[H-	5.79×10^{14} (0.97)	5.52×10^{14} (0.92)]

NOTES: 1. The number in brackets () represents the coverage of the adsorbed species, as a function of the number of sites available (5.97×10^{14} ZnO sites per cm^2). The defected surface has an oxygen vacancy concentration of 4% which corresponds to 2.39×10^{13} vacancies per cm^2.

2. In evaluating these data, the mass spectrometer sensitivity for methanol has been used throughout. Where necessary, corrections for relative ionisation cross section and relative gain of the quadrupole filter, have been applied, as described in Section 5.2.1. The hydrogen data has been enclosed in parentheses [] because the relative gain of the quadrupole filter, for this gas is unknown (see Section 5.4)

3. The error associated with each value is ca. $\pm$ 7 - 14%.

From Chapter 3 (Section 3.4.1), it is clear that even after calibration with a "Baratron" gauge, the ionisation gauge reading is only accurate to ca. $\pm$ 7%. This will be reflected in the value for the mass spectrometer sensitivity. Compared to this, errors associated with determining the number of squares (by weighing) are negligible. The reproducibility of these coverage values was usually within $\pm$ 7%. However, for particularly small peaks or after some time delay, this did rise to a maximum of 14%. (This applies to all results presented in this thesis.)

It was possible to calculate the coverage expected, using the dose pressure, measured on the "Baratron" gauge. For example, in an adsorption experiment over defected zinc oxide, when the pressure of methanol in V_S was 0.7628 torr before leak valve 1 was opened, and the final pressure reading was 0.7399 torr (in $V_S + V_R$) - see chapter 3 - using Boyle's Law one can determine the amount of methanol adsorbed (1.206×10^{14} molecs/cm^2). Comparing this value with Table 5.2 is quite encouraging. The total coverage of carbon containing compounds is 1.04×10^{14} molecs/cm^2, and this gives further credence for this method of analysis.

That these values represent saturation coverage was verified by repeating the adsorption experiment at different dose pressures and monitoring mass 31. The results are shown in Fig. 5.3 and Table 5.3.

FIG. 5.3

Plot of Methanol Coverage vs. Pressure of Adsorption

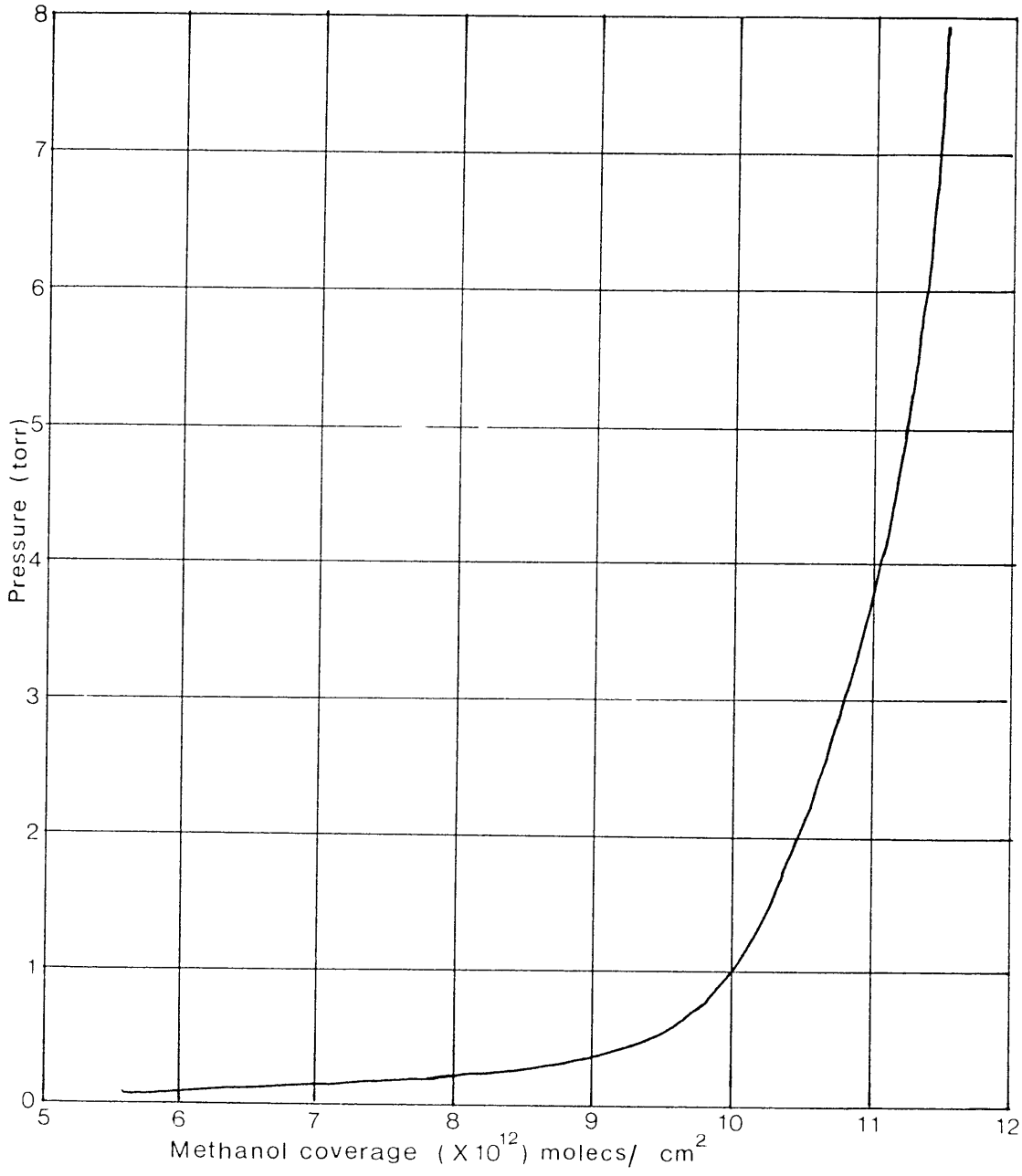

TABLE 5.3

Coverage of Methanol on a Defected $(10\bar{1}0)$ Surface of Zinc Oxide after Adsorption at Room Temperature at Different Pressures.

Pressure of Adsorption (torr)	Coverage of Methanol (molecs/cm^2)
7.67	1.15×10^{13}
1.6	1.03×10^{13}
0.736	9.78×10^{12}
0.1	6.10×10^{12}

The average of the first three values in this table is 1.05×10^{13} (standard deviation 7.2×10^{11})

A final point which must be made is that throughout this series of experiments reduction of the zinc oxide occurred, manifested by the formation of a metallic film of zinc which condensed on the cooler part of the sample holder. This could be caused when oxygen is abstracted by adsorbed CO going to CO_2. A 1/7 monolayer of zinc, from the 1800 cm^2 of adsorbate, would give a layer of zinc, about 250Å thick, over 1 cm^2 area of the sample holder, and hence easily seen.

5.2.2 Adsorption of Methanol on the $(10\bar{1}0)$ Prism Plane of Zinc Oxide at Low Temperature

The adsorption experiment was repeated at lower temperatures in an attempt to identify any weakly adsorbed species. The additional experimental arrangements necessary for temperature control in this region have been detailed in Chapter 3 Section 3.1.2.

Because the vapour pressure of methanol is quite low (ca.2.75 x 10^{-2} torr) at solid CO_2 temperature (195K), it was necessary to modify the dosing procedure, to prevent condensation occurring to such an extent that the subsequent TPD signal was too high for the mass spectrometer to be used. Consequently, the zinc oxide was initially exposed to a fairly low pressure of methanol (ca.0.2 torr) at room temperature for ca.120 secs.. Then, after isolating the reaction chamber, the sample was cooled and allowed to equilibrate before temperature programming commenced. Ostensibly it should have been possible to cool the sample first, and then to control the flow of methanol on to the sample through leak valve 2 (see Chapter 3). However, because previous attempts to calibrate the conductance of the leak valve were unsatisfactory, this was not done. As explained in Section 5.2.1, if the dosing procedure is rigorously monitored it is possible to run internal checks on the coverage values reported.

The subsequent temperature programmed desorption experiment revealed a peak in the mass 31 spectrum at ca.218K, for both

stoichiometric and defected surfaces (equivalent to a binding energy of ca.59kJ/mol). This represents a coverage of methanol molecules of ca.1.20 x 10^{14} molecs/cm^2 (or 2.17 x 10^{17} molecules total). This is in fair agreement with the value calculated from the final "Baratron" gauge reading (ca. 0.1994 torr) and the volume of the reaction chamber - namely 1.14 x 10^{14} molecs/cm^2. The results for both types of surface are tabulated below.

TABLE 5.4

Coverage of Methanol on Stoichiometric and Defected $(10\bar{1}0)$ Prism Planes of Zinc Oxide at Low Temperatures

	Defected Surface	Stoichiometric Surface
Baratron gauge readings P_1, P_2 (torr)	0.2074, 0.1994	0.2076, 0.2005
Amount Adsorbed (from Peak Area) Molecs/cm^2	1.20 x 10^{14}	1.27 x 10^{14}
Amount Adsorbed (calculated using P_2) Molecs/cm^2	1.14 x 10^{14}	1.15 x 10^{14}

NOTE: P_1 = Pressure of methanol in V_S before exposure to zinc oxide

P_2 = Pressure of methanol in $(V_S + V_R)$, once leak valve 1 has been opened and the methanol and zinc oxide have been equilibrating for ca.120 secs. at room temperature.

The error associated with each value is ca.$\pm$ 7 - 14%.

No decomposition products were detected (although in this pressure region it would have been difficult to distinguish them from the methanol cracking pattern) - and this has recently been confirmed by Hirschwald and Hofmann(26).

On continuing the temperature programme, peaks characteristic of room temperature adsorption (see Table 5.2) were observed at 433K, 583K, 633K and 573K/623K due to CH_3O-, CO_2, CO and H-. They were all of lower coverage, however, as expected. In order to discern them at all, it was necessary to hold the sample at room temperature for several minutes to allow the background level to decay to ca.10^{-7} torr, after the comparatively large low temperature peak.

5.2.3. Adsorption of Methanol on Polycrystalline Zinc Oxide Powder at Room Temperature

These experiments were carried out at I.C.I. New Science Group on the polycrystalline powdered sample described in Chapter 3 Section 3.2a. The sample was cleaned and pre-treated in hydrogen as described in Chapter 4, before cooling in vacuo to room temperature. Methanol was admitted to the chamber to a pressure of ca.10^{-3}torr for 15 minutes, before the ambient gas was evacuated and temperature programmed desorption begun (ca.15 mins. later). The spectra are shown in Fig. 5.4 and the approximate coverages and peak maximum temperatures in Table 5.5.

TABLE 5.5

Adsorption of Methanol on Polycrystalline Zinc Oxide Powder at Room Temperature

Desorbed Species	Temperature of Peak Maximum (K)	Activation Energy of Desorption (kJ/mol)	Coverage (molecs/cm^2)
CH_3O-	423	117	4.4×10^{11}
CO	550	153	3.3×10^{11}
CO_2	555	155	3.4×10^{10}
[H-	535	149	4.0×10^{11}]

NOTE: 1. The activation energies were calculated using the Redhead equation (Chapter 2 Section 2.2.2) assuming a pre-exponential factor of $10^{13}s^{-1}$.

2. The mass spectrometer sensitivity was determined for each gas individually and used to evaluate the respective coverages (although the ion gauge was not calibrated against a total pressure gauge, in this laboratory).
3. Uncertainty due to the unknown relative gain of the quadrupole filter, for hydrogen, applies in these experiments also. These values are included in parenthese [].

In view of the extremely low coverages, the sample was cleaned in oxygen at 300°C for several hours before the experiment was repeated (see Table 5.6).

TABLE 5.6

Coverage of Methanol on Polycrystalline Zinc Oxide Powders

(from Ref.25)

Desorbed Species	Amount Adsorbed Sample A (molecs/cm^2)	Amount Adsorbed Sample B (molecs/cm^2)
CO	2×10^{14}	1×10^{14}
H_2	2×10^{14}	1×10^{14}

NOTE: 1. Sample A - I.C.I. ZnO with ca. 33% surface area polar planes.
Sample B - Analar ZnO with ca. 14-20% surface area polar planes.
2. Notes 2 and 3 of Table 5.5 apply here also.

FIG. 5.4

TPD Spectra of Methanol and its Decomposition Products after Adsorption on Polycrystalline Zinc Oxide Powder at Room Temperature

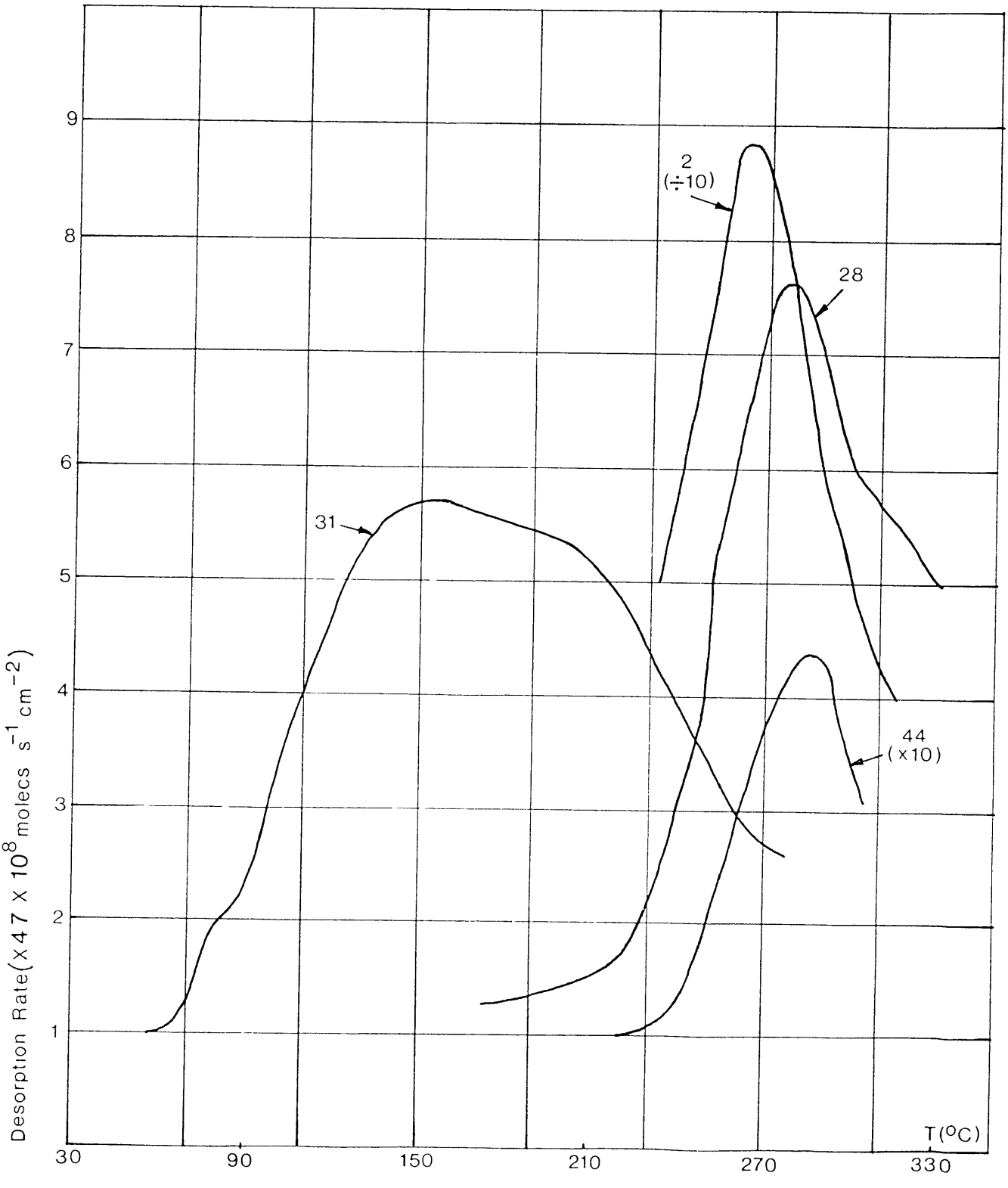

These results have already been presented and compared[25] with data collected from identical experiments[6] on Analar zinc oxide. The samples were characterised by transmission electron microscopy which indicated that the polar plane comprised 33% total surface area of the sample used here, and 14-20% of the Analar zinc oxide. The adsorbate coverages were comparable for CO_2 amd H_2 adsorption individually, but for methanol, formaldehyde and CO_2/H_2 co-adsorption, the sample with the higher percentage of polar planes adsorbed approximately twice as much as the other.

Experiments were also conducted in the I.C.I. laboratory on the prism plane of zinc oxide[25]. The pre-treatment, however, was identical to that of the powdered samples (see Chapter 4 Section 4.1) and not as described in Section 4.2 for the needle crystals.

In this instance, no adsorption was detected on the prism plane, and it was therefore concluded that the polar planes are entirely responsible for the adsorptive properties and catalytic activity of zinc oxide. The studies on the two powdered samples seem to support this hypothesis. Subsequent experiments carried out at Imperial College, and reported in Section 5.2.1 clearly refute this planar specificity. Re-inspection of Table 5.2 indicates substantial adsorption/decomposition of methanol on the prism plane. The failure to detect any adsorption on the prism plane using the apparatus at I.C.I.[25], can be

attributed to insufficient sensitivity. The background pressure (ca.10^{-7} torr) was probably too high to monitor adsorption on such a low surface area.

5.3 Discussion

The purpose of this work has been to help identify the active planes or sites in the methanol synthesis catalyst. It is in this context that the results presented in Section 5.2, will be discussed below. The conclusions drawn from these experiments will be incorporated into a synopsis of the recent research endeavours to resolve this specific issue.

5.3.1 Adsorption of Methanol on the $(10\bar{1}0)$ Prism Plane of Zinc Oxide at Room Temperature

On inspection of the TPD curves shown Fig 5.2 and the respective amounts adsorbed (see Table 5.2), it is clear that methanol adsorbs and decomposes on both stoichiometric and defected $(10\bar{1}0)$ prism planes of zinc oxide.

On the defected surface the ratio of CO plus CO_2 to methanol is 9.6 to 1, giving a percentage decomposition of 90.56%. The correspoding figures for the stoichiometric surface are 7:1 (that is, 87.5% decomposition). It is tempting to infer from this that the introduction of a small concentration of oxygen vacancies (ca.4%) did enhance the decomposition reaction (and hence synthesis) of methanol, by a proportionate amount. It is widely accepted[27,28] that defects in the crystal lattice on a varying scale (including point defects, steps and dislocations) are particularly likely to be adsorption and reaction centres. Oxygen vacancies, however, are clearly not the sole or predominant reaction centre - as one would expect significatly different

results for these two surfaces, if they were - in fact, both surfaces were of comparable activity.

As explained in Chapter 3, mass 31 was used to monitor methanol, because it is a characteristic and distinctive peak in the mass spectrum. It seems likely however, that methanol dissociates on the surface to give CH_3O- or -CH_2OH, which on desorption at 433K, recombines with hydrogen, to form methanol molecules. (The bond strengths CH_3O-H, H-CH_2OH and H-H are 436.8, 393 and 436 kJ/mol respectively - see Ref.29). It is not possible to state whether CH_3O- or -CH_2OH are present, from this experiment alone, but corroborative evidence for the existence of the methoxy intermediate has been obtained by Deluzarche et al[11].

The broad nature of the desorption profile probably arises due to surface heterogeneity (see Chapter 2 Sections 2.3.1 and 2.3.4). The combination of TPD spectra from several sites in an energy range would yeild such a result. Imperfections of the crystals such as jagged edges and steps, both of which expose different crystal sites, are likely candidates. Lateral interactions are discounted, in view of the low concentration (except perhaps along an edge), and precursor states would not have a significant effect at this temperature.

The unusually low concentration also indicates the

possibility of adsorption on "special sites" or "surface irregularities".

The desorption spectra of the decomposition products, H_2, CO and CO_2 have less well defined peak shapes, and all appear at 573 to 633K. The spectrum for hydrogen appears to consist of two peaks at 573K and 623K which cannot be fully resolved. The largest error is associated with the hydrogen coverage value because of wide instrumental variation for this low mass species. In the analysis of the results, the transmission of the quadrupole filter was considered to be unity for all masses. However, this only applies over a fairly small range, usually 20-50 amu, and decays by a decade with an increase of 150 amu. Hydrogen, therefore, would give an anomolously high reading and should be scaled down. Unfortunately data for the instrument used, is not available, so accurate corrections cannot be made.

Carbon dioxide has the lowest coverage of the three products. In view of the fact that little CO_2 adsorption was found on the prism plane (see Chapter 6), this peak is attributed to reduction of the surface by CO and/or decomposition of a formate intermediate (see later). The reason for the levelling of the spectrum at 673K and apparent peak at 893K is uncertain - possibly imperfections in the crystals expose particularly strong binding sites.

The spectrum for carbon monoxide is comparatively broad. it is clearly distorted on the low temperature side, due to

mass 28 being a fragment in the CO_2 cracking pattern, and it follows mass 44 to give a second peak at 863K. The main peak at ca.633K is probably derived from the decomposition of a formyl species (see later). The only other possible explanation for the CO and CO_2 peaks at the high temperature could be evolution of oxygen, and subsequent conversion to CO and CO_2, to restore surface equilibrium after the reduction of the surface on methanol adsorption.

In the industrial synthesis of methanol, hydrogen is the major constituent of the feed gas (ca.87%) - presumably to keep the water - gas - shift equilibria :

$$CO + H_2O = CO_2 + H_2$$

well to the left.

In this experiment however, one would expect stoichiometric decomposition according to the equation: $CH_3OH \rightarrow CO + 2H_2$ giving a ratio of H_2 to CO of 2 : 1 (or more realistically a ratio of H_2 to CO plus CO_2 of 2 : 1). The ratio here is 6.17, but as outlined previously, the hydrogen value is circumspect.

The carbon dioxide could be produced by the reaction :

$$CO + \text{"O"} \rightarrow CO_2 + V_o$$

where "O" is from the zinc oxide lattice and V_o is a surface oxygen vacancy.

This is a standard procedure for generating oxygen vacancies[23] and can be observed at temperatures as low as 330K[24]. Alternatively, CO_2 could be derived from a formate species. Coincident desorption peaks indicate a common intermediate. The fact that H_2, CO and CO_2 all have corresponding peak maximum temperatures suggests that methanol decomposition occurs via formate and formyl species.

It is possible that the formation of the formate species is responsible for the reduction of zinc oxide. Ueno et al have noted this in their experiments on adsorption/ decomposition of methanol on zinc oxide[9]. They also found that at 473K the formate ion (resulting from methanol adsorption) decomposes to carbon monoxide plus hydrogen, which is contrary to the findings of a previous publication stating that at 473K it was carbon dioxide and hydrogen (not carbon monoxide and hydrogen) which were required to produce the formate species[8]. The authors did state however, that at 573K the formate species was dehydrated to carbon monoxide[8]. It was suggested[9] that the discrepancy could arise because reduction of the surface occurred to produce the formate from the methoxy species, but not from $CO_2 + H_2$ synthesis, and decomposition of the formate could occur by different routes on different types of surface.

5.3.2 Adsorption of Methanol on the $(10\bar{1}0)$ Prism Plane of Zinc Oxide at Low Temperatures

From these experiments, it is clear that oxygen vacancies do not have a significant effect on the adsorption of methanol at low temperature either. Both stoichiometric and defected surfaces adsorb methanol equally well, with a binding energy of ca.59 kJ/mol (calculated using a pre-exponential factor of $10^{13}s^{-1}$ in the Redhead equation - see Chapter 2 Section 2.2.2). At this temperature (218K) methanol is adsorbed molecularly - confirmed by the fairly close agreement between the results in Table 5.4, obtained using the peak area, and those using the "Baratron" gauge pressure.

5.3.3 Adsorption of Methanol on Polycrystalline Zinc Oxide Powder at Room Temperature

The results for the polycrystalline powdered sample have similarities with those for the $(10\bar{1}0)$ prism plane. Inspection of Tables 5.1 and 5.5 show that the peak at ca.433K, due to CH_3O- is common to both samples. The decomposition products, however, are produced at slightly lower temperatures on the powdered sample. Comparisons between the respective coverages is not feasible, due to incomplete data on the powdered sample and ambiguities in the calibration procedure at I.C.I.

5.3.4. Studies of Methanol Adsorption on Zinc Oxide by other Research Groups

Because of the substantial interest of the chemical industry to understand catalytic processes, many research workers are currently engaged in similar projects. The work of one group will be summarised below because it is particularly relevant to this work. Cheng et al[21,22] have conducted experiments on several planes of zinc oxide: stoichiometric and reduced (defected) $(10\bar{1}0)$ prism planes, stoichiometric and defected $(40\bar{4}1)$ and $(50\bar{5}1)$ stepped surfaces, and also on the polar planes. Single crystals of zinc oxide were used ($6mm \times 6mm^2$), oriented by X-ray Laue back scattering to within 0.5°.

The stepped surfaces, comprised of $(10\bar{1}0)$ terraces and (0001) steps, were prepared by cutting the crystal at 7.7° or 6.2° with respect to the $(10\bar{1}0)$ plane in order to generate a $(40\bar{4}1)$ or $(50\bar{5}1)$ surface respectively. These surfaces were cleaned and ordered by cycles of sputtering and annealing : $(10\bar{1}0)$ and (0001) surfaces were annealed at 773K and $(40\bar{4}1)$ and $(50\bar{5}1)$ surfaces at 923K then 773K.

Methanol was adsorbed at room temperature on all of the surfaces. The product distributions from each experiment are shown in Table 5.7, and the temperatures of the peak maxima and amounts of methanol adsorbed in Tables 5.8 and 5.9.

TABLE 5.7

Product Distribution in CD_3OD Decomposition over Zinc Oxide Surfaces

(taken from Tables 1, 2 and 3 in Ref.21)

Surface	CD_3OD	CO	CO_2	CD_4	D_2	CD_2O
Stoichiometric $(10\bar{1}0)$	Decomposition products barely detected					
Defected $(10\bar{1}0)$	1	0.07	0.04	0.036	0.14	-
Defected $(50\bar{5}1)$	1	0.27	0.15	0.12	0.66	-
Defected $(40\bar{4}1)$	1	0.44	0.25	0.20	0.96	-
Stoichiometric $(40\bar{4}1)$	1	0.30	0.24	0.17	-	-
Zn(0001)	1	1.49 1.42 2.1	3.36	-	2.85 7.12	1.00

NOTES: 1. All of the peaks have been normalised to the CD_3OD spectrum.

2. For the polar plane, three peaks occurred for CO and D_2 at 533, 633 and 723K, and the product ratios are given for each.

TABLE 5.8

Temperatures of Peak Maxima in the TPD Experiment to Monitor CD_3OD Decomposition over Zinc Oxide

(taken from Ref. 21)

Surface	CD_3OD	CO_2	CO	D_2	CD_4	CD_2O
$(40\bar{4}1)$ $(50\bar{5}1)$ $(10\bar{1}0)$	423	673	653	653	423	-
Polar	423	753	533	533	-	-
			633	633	-	633
			723	723		

TABLE 5.9

Amount of Methanol Adsorbed on Different Surfaces

(taken from Ref.21)

Surface	Total Coverage (molecules/cm^2)
$(10\bar{1}0)$	4.86×10^{12}
$(50\bar{5}1)$	4.92×10^{12}
(0001)	6.72×10^{12}

NOTE: These values represent the total coverage of methanol calculated from the TPD peak areas of methanol and the decomposition products. (The sample was not facing the mass spectrometer during these experiments and the dosing procedure was : 2×10^{-9} torr for 15s.)

On inspection of Table 5.7, it would appear that the extent of methanol decomposition increases in the order: stoichiometric $(10\bar{1}0)$, defected $(10\bar{1}0)$, defected $(50\bar{5}1)$, defected $(40\bar{4}1)$, with the polar plane exhibiting the maximum decomposition of the surfaces studied. For the prism planes (flat and stepped) this could be attributed to an increased concentration of anion vacancies, because a step in the surface is effectively a row of such vacancies. However, the fact that stoichiometric and defected $(40\bar{4}1)$ planes yield approximately the same extent of decomposition (unlike the stoichiometric and defected $(10\bar{1}0)$ surfaces) suggests that the stepped sites are particularly active, and that if present, their effect will predominate over that of oxygen vacancies alone.

Steps in the polar plane (created by annealing the crystal in vacuo at 658K, as opposed to 773K or 873K, had little effect on the extent of the decomposition reaction.

The ratios between the decomposition products were fairly constant on all of the prism planes studied (both stepped and flat), which leads to the conclusion that the decomposition reaction occurs by the same mechanism on these surfaces. The polar plane however, yields different values and must suggest an alternative mechanism. Desorption from the prism planes yields methane amongst the decomposition products, but no formaldehyde, methyl formate or dimethyl ether. By contrast, desorption from the polar plane does produce formaldehyde but no methane. Cheng et al propose

the following mechanisms:

On the prism plane, methanol decomposes to methane and oxygen at 423K then at higher temperatures the formate species is produced (accompanied by surface reduction) and decomposes into CO, CO_2, H_2, and H_2O at ca.653K.

On the polar planes, decomposition occurs via a formaldehyde intermediate, which is either dehydrogenated to CO or oxidised to the formate (again utilising zinc oxide's lattice oxygen) and decomposes above 673K.

5.3.5 Resumé

It is interesting to compare the results presented in Sections 5.2.1 and 5.2.3. with those of Cheng et al[21,22] (see Section 5.3.4). There are similarities between them and also striking contrasts.

Both studies on the zinc oxide prism plane using stoichiometric and defected surfaces, indicate that whilst oxygen vacancies may enhance the methanol decomposition activity slightly, steps (or other special sites) on the crystal surface have a more profound effect. The thermal desorption spectra for CH_3O-/CD_3O- (mass 31/34) appear at ca.433K, and are of comparable coverage (9.78×10^{12} and 4.86×10^{12} molecules/cm^2). The results diverge greatly, however, in the extent of methanol decomposition on the prism plane. In this work, a very high value has been reported on the defected $(10\bar{1}0)$ plane - 90% decomposition - but Cheng et al only observed 13-47% decomposition (on defected $(10\bar{1}0)$ and defected $(40\bar{4}1)$ respectively), at 100K higher temperatures. This discrepancy could only arise due to differences in experimental procedure - since the method of analysis for both sets of results appear equally rigorous.

The most fundamental difference between this work and that of Cheng et al is the sample size. Results have been presented in this thesis on long thin needles of zinc oxide (ca.10μm diameter, 5mm long) which expose mainly the prism plane. Cheng et al used a single crystal (6mm x $6mm^2$),

which is notably more difficult to clean. Green and Lauks[31] have shown that diffusion of impurities from the bulk to the surface in a crystal of small surface area to volume ratio, leads to continual surface recontamination. Whilst Cheng and Kung adopted a rigorous initial cleaning programme it is still possible that during the TPD experiments the samples were recontaminated. Carbon, sulphur and potassium were not detected by auger electron spectroscopy, after weeks of experimentation, but other impurities, such as calcium were not mentioned[22]. The lower coverage values for methanol reported in Table 5.9 could be a reflection of this - although Cheng et al used a different dosing procedure (2×10^{-9}torr for 15 secs., pump out time 120 secs.) but claim[22] that the dose pressure near the sample is "probably ten to a hundred times higher". Similarly, the discrepancy in the temperature of desorption of the decomposition products, may be further evidence for a very limited number of active centres on this sample.

By contrast, on the zinc polar plane, Cheng et al report considerable decomposition (90%). However, from their six fold symmetric LEED pattern this surface has double layer steps (see also Chapter 1), which could be responsible for the decomposition activity.

The results presented in Section 5.2.3, suggest that methanol decomposition increases as the percentage of polar planes increases. This deduction may be too simplistic - for as the percentage of polar planes increases, so do their

associated steps and defects.

The results as a whole seem to indicate that the crystal plane of zinc oxide is not as important as the surface irregularities on it. Until experimental techniques improve sufficiently for all surface lattice imperfections to be produced or eliminated "to order", this will remain a very uncertain or unquantifiable area of surface science.

Clearly, the debate surrounding the active planes and active sites, of the zinc oxide component of the methanol synthesis catalyst, is not closed. Klier et al[15,18] report needle-like crystallites of zinc oxide in catalysts containing $\leq$30% Cu, and hexagonal platelets of zinc oxide in catalysts containing >30% Cu - both of which are active - although the proximity of copper is of paramount importance in their work and has not been investigated here. The I.C.I. catalyst would therefore consist of predominantly polar planes.

With regard to reaction mechanism, the results presented for the prism plane are consistent with the theories invoking a formate and formyl intermediates.

1. G. NATTA

Catalysis Vol.3 Ed.P.H.Emmett (1955) Reinhold NY.

2. H.H. KUNG

Catal.Rev.- Sci.Eng 22(2), 235, 1980

3. K. KLIER

Adv.Catal. 31, 243, 1982

4. M. BOWKER

Vacuum 33(10/12), 669, 1983

5. E.K. POELS AND V.PONEC

RSC Spec.Per.Rep. Catalysis Vol.6 Chap.7 1983

6. M. BOWKER, H. HOUGHTON, K.C. WAUGH

J.C.S. Far.Trans.I 77(12), 3023, 1981

7. M. BOWKER AND R.J. MADIX

Surface Science 95, 190, 1980

8. A. UENO, T. ONISHI AND K. TAMARU

Trans.Far.Soc. 66, 756 1970

9. A. UENO, T. ONISHI AND K. TAMARU

Trans. Far. Soc. 67, 3585, 1971

10. T. VAN HERWIJNEN, R.T. GUCZALSKI AND W.A. DE JONG

J.Catal. 63, 94, 1980

11. A. DELUZARCHE, R. KIEFFER AND A. MUTH

Tetrahedron Letters 38, 3357, 1977

12. J. SAUSSEY, J.C. LAVALLEY, J. LAMOTTE AND T. RAIS

J.C.S.Chem.Comm. (1982) P.278

13. K. KLIER, V. CHATIKAVANIJ, R.G. HERMAN AND G.W. SIMMONS

J.Catal. 74, 343, 1982

14. J.C. LAVALLEY, J. SAUSSEY and T. RAIS

J.Molec.Catal. 17, 289, 1982

15. R.G. HERMAN, K. KLIER, G.W. SIMMONS, B.P. FINN, J.B. BULKO AND T.P. KOBYLINSKY
J.Catal. 56, 407, 1979

16. Y. OKOMOTO, K. FUKINO, T.IMANAKA AND S.TERANISHI
J.C.S. Chem.Comm. (1982) P.1405

17. O. RUGGERI, F. TRIFIRO AND A. VACCARI
J.Sol.St.Chem. 42, 120, 1982

18. S. MEHTA, G.W. SIMMONS, K. KLIER AND R.G. HERMAN
J.Catal. 57, 339, 1979

19. K.L. D'AMICO, M. TRENARY, N.D. SHINN, E.I. SOLOMON AND F.R. McFEELY
J.A.C.S. 104(19), 5102, 1982

20. R.R.GAY, M.H. NODINE, V.E. HENRICH, H.J. ZEIGLER AND E.I. SOLOMON
J.A.C.S. 102(22), 6752, 1980

21. W.H. CHENG, S. AKHTER AND H.H. KUNG
J.Catal. 82, 341, 1983

22. S. AKHTER, W.H. CHENG, K. LUI AND H.H. KUNG
J.Catal. 85, 437, 1984

23. W. GOPEL AND U. LAMPE
Phys.Rev.B (22)12, 6447, 1980

24. W. HOTAN, W. GOPEL AND R. HAUL
Surface Science 83, 162, 1979

25. M. BOWKER, H. HOUGHTON, K.C. WAUGH, T. GIDDINGS AND M. GREEN
J.Catal. 84, 252, 1983

26. W. HIRSCHWALD AND D. HOFMANN
Surface Science 140, 415, 1984

27. S.R. MORRISON

The Chemical Physics of Surfaces (1977) Plenum Press N.Y.

28. J.M. THOMAS AND W.J. THOMAS

Introduction to the Principles of Heterogeneous Catalysis (1967) Academic Press

29. CRC HANDBOOK OF CHEMISTRY AND PHYSICS

30. G.C. BOND

Heterogeneous Catalysis : Principles and Applications Oxford Chemistry Series (1974) Clarendon Press

31. M. GREEN AND I.R. LAUKS

Surface Science 71, 735, 1978

32. J. SAUSSEY, J.C. LAVALLEY, T. RAIS, A. CHAKOR-ALAMI, J.P. HINDERMANN AND A. KIENNEMANN

J.Molec.Catal. 26, 159, 1984

33. J.F. EDWARDS AND G.L. SCHRADER

J. Phys. Chem. 89(5), 782, 1985

CHAPTER 6

ADSORPTION OF OXYGEN, CARBON DIOXIDE AND NITROUS OXIDE ON ZINC OXIDE

A brief review of the literature for most gas-semiconductor systems is sufficient to ascertain that adsorption studies generally are rather inconclusive. Different research groups report widely varying and conflicting results. Many, are performed on powdered samples of unknown morphology, yet quite detailed mechanisms have been invoked in order to explain the various results. Only recently (last eight years or so) have single crystal studies been possible, and hence research has intensified on prototype surfaces, such as zinc oxide, in order to investigate these systems more thoroughly. It is the purpose of this work to establish whether oxygen vacancies at the surface of the $(10\bar{1}0)$ prism plane of zinc oxide enhance the adsorption of the molecules listed above, and so test the hypothetical mechanisms and few primitive calculations which have been done, suggesting that charge transfer adsorption might just occur. In Section 6.1 a resumé of charge transfer adsorption will be presented which will lead on to consideration of specific systems.

6.1 Charge Transfer Adsorption

The theory of charge transfer adsorption was devised independently by Weisz, Aigran and Dugas, Hauffe, and Wolkenstein over thirty years ago and is reviewed thoroughly

in Ref. 1. Basically, this theory describes the chemisorption process as, the transfer of a de-localised electron (or hole) from the surface of a semiconductor adsorbent to become associated with an adsorbed species, thus giving a localised surface state. Fig 6.1a shows the formation of a surface state. In the simple theory the binding energy for a negative species can be represented, at zero coverage (ΔE_o), as the difference between the work function (ϕ) of the adsorbent and the electron affinity (E.A.) of the adsorbate . On an n-type semiconductor, such as zinc oxide, as adsorption continues the work function increases, a depletion layer is formed, and once the space charge potential difference(ΔV) becomes equal to (ϕ - E.A.), adsorption ceases (see Fig. 6.1b).

From the equilibria: $X = X_{(ads)}$, $K_P = \frac{[X_{(ads)}]}{P(X)}$

The amount adsorbed is given by:

$$[X_{(ads)}] = P(X)\ K_P \exp -\frac{(\Delta E_o - q\Delta V)}{RT}$$

The level of doping in the semiconductor governs ΔV. Defects in the lattice - which are essentially localised charges - provide an additional interaction energy which is predicted to facilitate this adsorption process.

It is necessary to consider the adsorption interaction on a more atomic level, in order to attempt to calculate the binding energy theoretically.

Ionic adsorption represents an extreme form of

FIG. 6.1a

Energy Band Diagram Showing the Formation of a Surface State

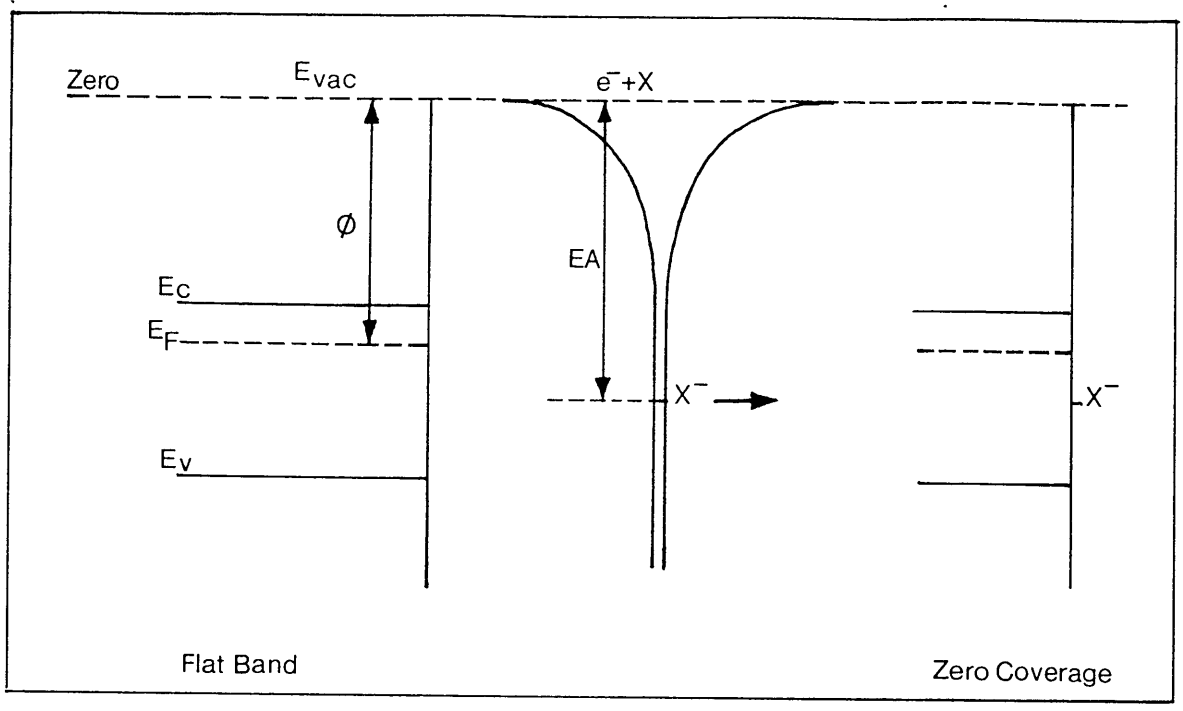

ϕ = Work Function of Solid, $E_{vac} - E_F$

E.A. = Electron Affinity of Adsorbate

FIG. 6.1b

Energy Band Diagram Showing the Formation of a Depletion Layer

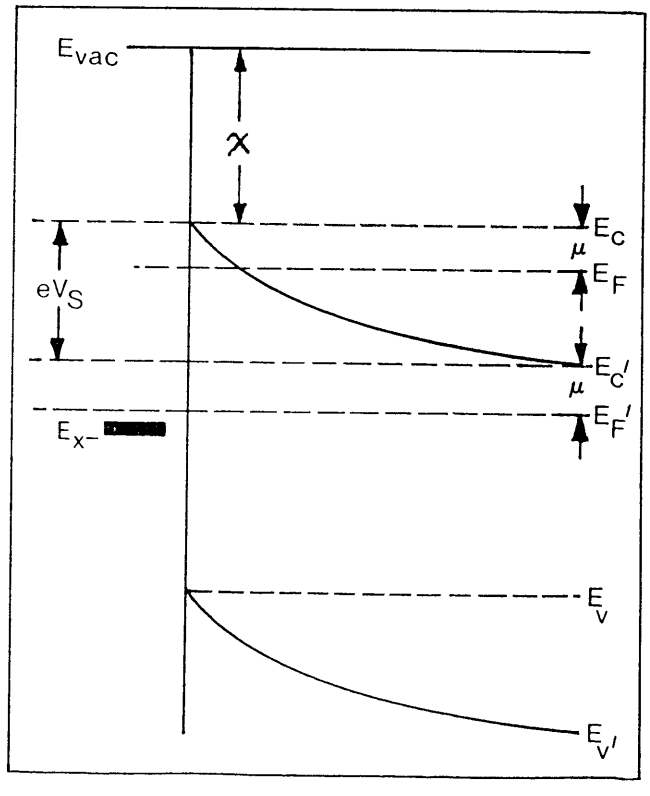

$\phi = \mu + eV_S + \chi$

$\mu = E_C - E_F$

$\chi = E_{vac} - E_C$

chemisorption, where a species X^- exists on the surface. Obviously more intermediate forms of bonding exist, such as homopolar bonding - but this work has been confined to systems which have been predicted (or presumed) to exemplify ionic adsorption.

Green and Lee[2], developed calculations to determine the energy change associated with ionic adsorption (charge transfer adsorption), based on the energy cycle shown in Fig. 6.2. The energy of adsorption for a species X^-($\Delta E_{(X^-)}$) is given by :

$$\Delta E_{(X^-)} = \phi + E.A. + E_{int} \qquad (6.1)$$

The work function of many adsorbents, and the electron affinity of many adsorbates, have been determined experimentally, and are documented in the literature. The binding energy, E_{int} however, is more difficult to measure. Temperature programmed desorption studies are used to evaluate this parameter for particular systems, (although one has to assume : that the binding energy and desorption energy are equivalent and that space charge effects can be ignored). Detailed theoretical analysis of the interaction between gases and solids however is lacking or incomplete.

FIG. 6.2

Energy Cycle for Charge Transfer Adsorption

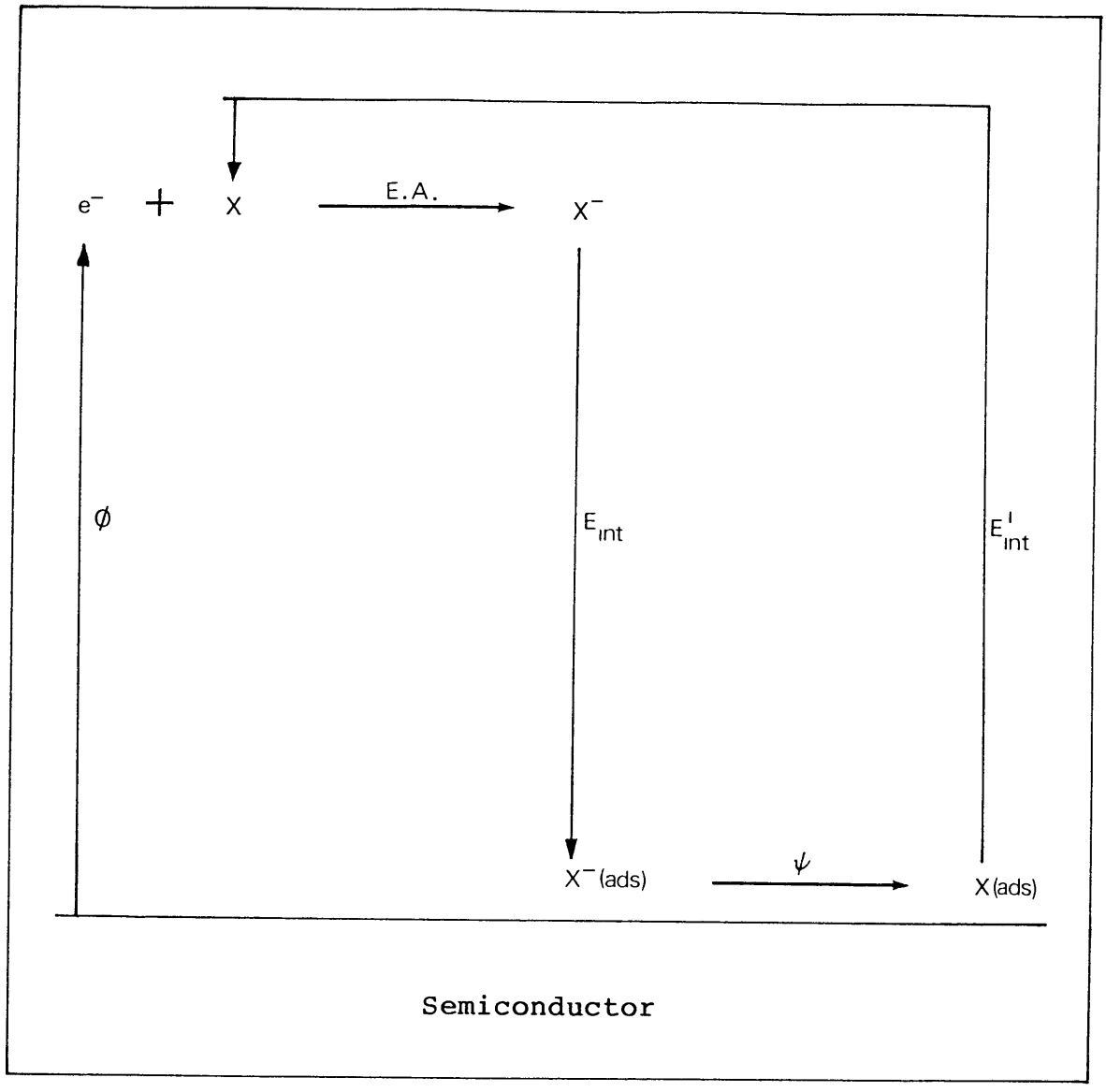

Where, ϕ = work function of semiconductor

E.A. = electron affinity of adsorbate X

E_{int} = energy change as X^- is brought up to the surface (binding energy of X^-)

ψ = energy difference between surface state and Fermi level

E_{int}' = binding energy of neutral species

Basically, the adsorption of an atom (or molecule) on the surface of a solid can be described by three types of interaction : dispersion, induction and electrostatic. These will be outlined below.

6.1.1 Dispersion Interaction.

As a molecule approaches a surface, it experiences weak Van de Waal's (or dispersion) forces, caused by attractions and repulsions of transient fluctuating dipoles of the atoms of the solid and the molecule. The pair-wise interaction can be characterised by the Lennard Jones 6-12 potential:

$$U_{disp} = - Cr^{-6} + Br^{-12} \qquad (6.2)$$

where r = distance between the centre of the adsorbate species and the surface plane (running through the centres of the surface atoms of the adsorbent)

and C and B are constants, for a particular gas/solid system.

Several authors have derived expressions for the constant C, in terms of ionisation energies, polarisabilities and magnetic susceptibilities, and these are reviewed in Ref.5. The order of magnitude of C is 10^{-77} Jm^6.

$$C/B = r_c^{-6} = 2r_e^{-6}$$

r_c = collision radius (at $U_{disp} = 0$)

r_e = Van de Waal's radius (at $U_{disp} = U_{max}$)

These parameters are defined in Fig. 6.3. For covalent species the collision radius can be calculated from the equation[2]: $r_c = 2(\rho + 0.8)$

where ρ = covalent radius

For a negative ion, r_c = ionic radius

For a positive ion, r_c = ionic radius + 0.8

The combining rule gives the collision radius for two dissimilar species, a and b :

$$r_c = \tfrac{1}{2} [r_c(a) + r_c(b)]$$

Green and Seiwatz[3] discuss methods of summation for an adsorbate/adsorbent system using Fourier series and cylindrical co-ordinates.

FIG. 6.3

Lennard Jones 6-12 Potential

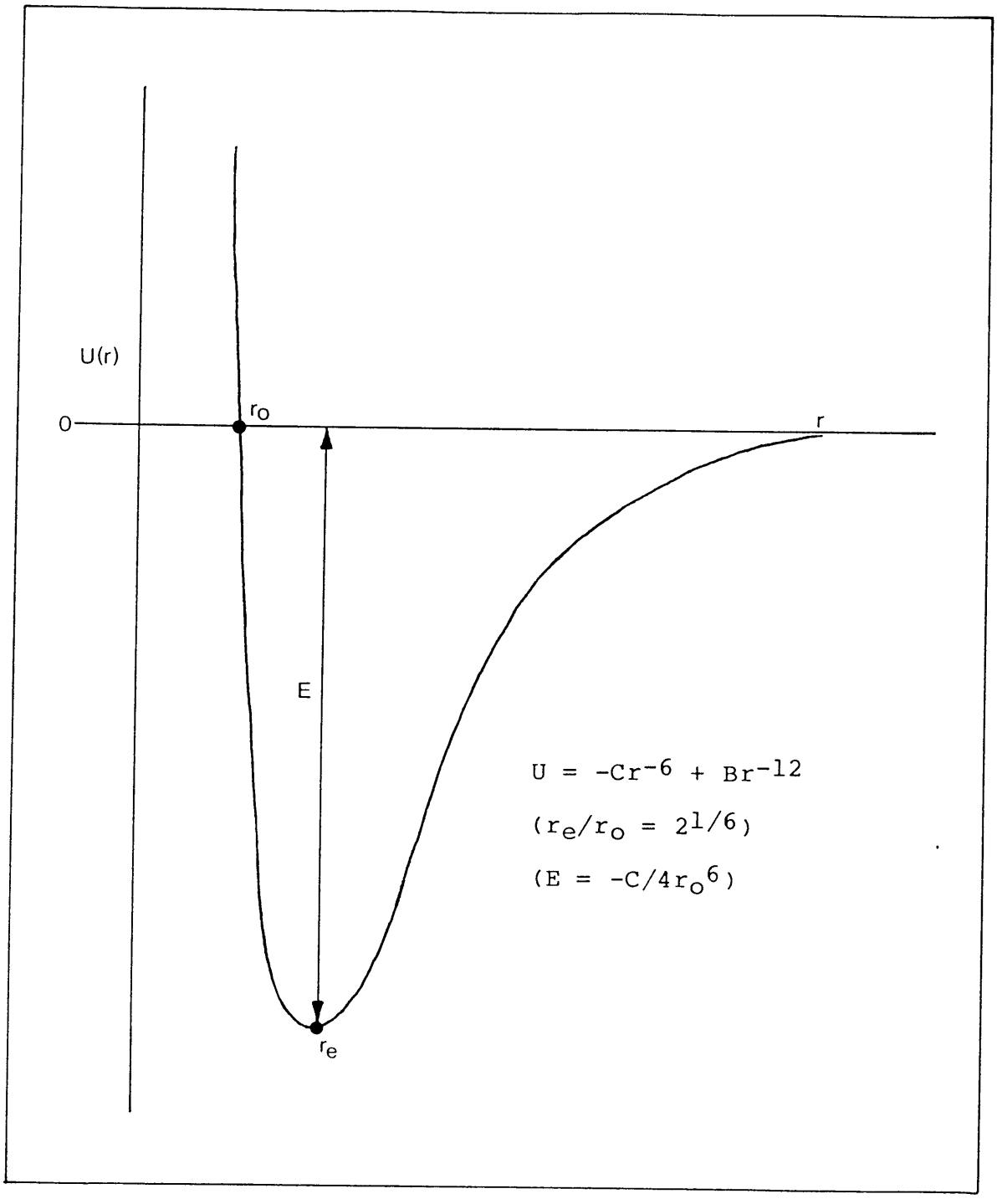

6.1.2 Inductive Interaction

If the adsorbate is ionic and/or the adsorbate molecules possess a permanent dipole moment, extra considerations have to be made for the inductive interactions. As an ion approaches the surface of a dielectric a charge distribution is induced in the solid, which can interact with the ion, according to the equation[2]:

$$U_{ind\ 1} = \frac{e^2 q_{ion}^2}{16\pi\varepsilon_o r} \cdot \frac{K-1}{K+1} \qquad (6.3)$$

where q = number of charges on ion adsorbed (in this work $q_{ion} = 1$)

e = electronic charge (1.6×10^{-19} C)

r = distance of centre of ion from surface plane (defined above) (m)

K = dielectric constant of solid (relative permittivity)

ε_o = permittivity of free space ($8.85 \times 10^{-12} Fm^{-1}$)

A similar effect would arise for a dipolar molecular adsorbate, although it would be a much weaker dipole-dipole interaction.

Conversely, an ionic solid could induce a dipole moment in a neutral adsorbate , leading to inductive interactions of the form[4]:

$$U_{ind\ 2} = -2\pi\varepsilon_o \alpha E^2 \qquad (6.4)$$

where E = electric field due to the solid at a suitable reference point (Vm^{-1})

α = polarisability of molecule (Fm^2)

6.1.3. Electrostatic Interaction

The coulombic or electrostatic interaction is the predominant component of the binding energy and can be expressed as:

$$U_{e.s.} = \frac{Z\, q_{ion}\, e^2\, A}{4\pi\varepsilon_o\, r} \qquad (6.5)$$

where Z = effective ionic charge on lattice ions (0.5 for ZnO)

q_{ion} = charge on adsorbed ion

A = Madelung constant for the lattice (see below)

r = perpendicular distance of ion from the surface plane (m)

The Madelung constant is calculated using the equation:

$A_{virtual\ lattice\ site} = A_{bulk} - A_{surface}$

where $A_{surface}/A_{bulk} = \Gamma = 0.79$, for the $(10\bar{1}0)$ plane of Wurtzite lattice (see Ref. 12)

Using this value, one is restricting the adsorbate to a virtual lattice position at a distance from the surface of the interplanar spacing. Obviously A increases if the adsorbate is brought nearer the surface.

The magnitudes of these interactions for a realistic set of parameters are tabulated below. The interplanar spacing for the prism planes in the hexagonal Wurtzite lattice is only 1.41Å. A more realistic value for r however, would be 2-3Å (using the ionic radius of Zn^+ and the ionic radius of various negative ions used here - see Sec. 6.2.

TABLE 6.1

Summary of Gas-Solid Interactions

Interaction	Magnitude ($kJ\ mol^{-1}$)		Ref.
Dispersion	<< 0	Using, $C = 10^{-77} Jm^6$ $r = 2.5 \times 10^{-10} m$	5,2
Induction (ion adsorbed on dielectric)	108	Using, $K = 8.15$ $r = 2.5 \times 10^{-10} m$	13
Induction (molecule in electric field	0.08	Using, $\alpha = 2.65 \times 10^{-24} cm^3$ $E = 10^9 Vm^{-1}$	30,2
Electrostatic	166	Using $A = 0.3147$ $Z = 0.5, q = 1$ $r = 2.5 \times 10^{-10} m$	12, 31

From equations (6.3) and (6.5) one can see that the electrostatic interaction and the inductive interaction between an ion and the dielectric, are comparable. The adsorbates used in this work (O_2, CO_2 and N_2O) are not ions initially (in the gas phase), and the purpose of these experiments/calculations has been to ascertain whether ions might form on the surface of zinc oxide, thus exemplifying charge transfer adsorption.

6.2 Application of the Theory

The work function of zinc oxide (bulk Fermi level at conduction band edge) has been determined on several crystal planes by Heiland et al[6], and the results are tabulated below.

TABLE 6.2

Work Function of Zinc Oxide Crystal Planes

Crystal Plane	Work Function (eV)
$(000\bar{1})$Zn	4.25
$(10\bar{1}0)$	4.64
$(000\bar{1})$O	4.95

Electron affinities are well documented in the literature, and particularly useful references are : Rosenstock et al[7], Lowe[8] and Chen and Wentworth[9]. Table 6.3 gives the electron affinities of molecules used in this study and Table 6.4 gives details of ionic and molecular structure.

TABLE 6.3

Selected Values of the Electron Affinity

Molecule	Electron Affinity (eV)
O_2	0.44
N_2O	0.27
CO_2	-0.9

NOTE: A positive electron affinity means that:

$A + e^- \rightarrow A^-$ is exothermic.

On inspection of the work function and electron affinity values tabulated above, it is clear that in order to obtain a favourable (exothermic) adsorption energy, the interaction

TABLE 6.4

DIMENSIONS OF GASEOUS ADSORBATES

Neutral Molecule		Bond Lengths		Negative Ion		Bond Lengths/Angles		Ref.
O_2	O = O	O = O	1.21Å	O_2^-		O = O	1.26	11, 11
CO_2	O = C = O	C = O	1.161Å	CO_2^-	$\left[\begin{matrix} & O & \\ C & & \\ & O & \end{matrix} \right]^-$	C = O O-C-O	1.249 Å 134.9°	14, 15
N_2O	N - N = O	N - N N = O	1.126Å 1.186Å	N_2O^-	$\left[\begin{matrix} & O & \\ N & & \\ & N & \end{matrix} \right]^-$	N = O N - N N-N-O	1.375Å 1.222Å 132.7°	11, 29

The molecular diameters of the neutral adsorbates are :

O_2(2.92Å), CO_2(3.23Å) and N_2O(4.7Å) (see Refs. 11 and 33)

The ionic radii of the negative ions are :

O_2^-(1.23Å), *CO_2^-(2.228Å) and *N_2O^-(2.219Å) .

* Calculated from the radius of the orthocircle (geom.) plus 0.6Å (the covalent radius for oxygen.)

energy, E_{int}, must be strong. (See Eqn. 6.1). At this level, discussions of space charge potential energy are unimportant because they are relatively small.

For oxygen adsorption, on $(10\bar{1}0)$ zinc oxide, to occur, the interaction energy must be well in excess of 4.2eV (4.64 - 0.44eV). In order for this interaction energy to be attained an adsorbate must approach the surface within a minimum distance, which will be calculated below

From section 6.1. we see that this interaction energy would be made up of an electrostatic and inductive interaction. Using equations (6.3) and (6.5) the minimum perpendicular surface distance, r_{min}, required between the adsorbate and the surface plane, to counterbalance the work function and electron affinity, can be calculted:

$$E_{int} = \frac{0.5 \times e^2 \times 0.3147}{4\pi\varepsilon_o r} + \frac{e^2 \times 7.15}{16\pi\varepsilon_o r \times 9.15} \qquad (6.6)$$

$$= \frac{e^2}{16\pi\varepsilon_o r \times 9.15} \qquad [(0.5 \times 0.3147 \times 9.15 \times 4) + 7.15]$$

$$= \frac{8.113 \times 10^{-29}}{r}$$

$$r_{min} = 1.21\text{Å}$$

More generally, $r_{min} = \frac{5.07 \times 10^{-10}}{\phi(eV) - E.A.(eV)}$ (6.7)

Table 6.5 shows the value of the minimum distance calculated using Eqn. (6.7) for each of the adsorbates used in this work, and also, the distance required to achieve significant binding energy (1 eV).

TABLE 6.5

Minimum Distance Between Adsorbate and Surface Plane to Achieve Adsorption

Adsorbate	Ionic Radius (Å)	Minimum Distance (Å)	Distance to Achieve Binding Energy leV (Å)
O_2^-	1.23	1.208	0.975
N_2O^-	2.22	1.161	0.945
CO_2^-	2.23	0.916	0.776

Clearly, none of these species would appear to be able to approach the surface within the minimum radii.

For CO_2 and N_2O energy is required to bend the linear molecule to form the bent ion. The activation barrier for electron attachment to the neutral molecule is ca. 0.76 eV for carbon dioxide[32] and ca. 2.28 eV for nitrous oxide[29]. These additional energy requirements could further prohibit charge transfer adsorption.

The $(10\bar{1}0)$ prism plane of zinc oxide consists of channels 1.41Å deep, 3.215Å wide at the top and 1.992Å wide at the bottom (see Fig.6.4) with 0.45Å surface relaxation in the cation lattice and 0.05Å relaxation in the anion lattice (see Chapter 1). The possibility of adsorption in these channels was considered - but rejected - as the ionic radii of the zinc and oxygen ions in the $(10\bar{1}0)$ surface plane could not accommodate even the O_2^- ion. (From Ref. 11, the

FIG. 6.4

Channels on the $(10\bar{1}0)$ Prism Plane of Zinc Oxide

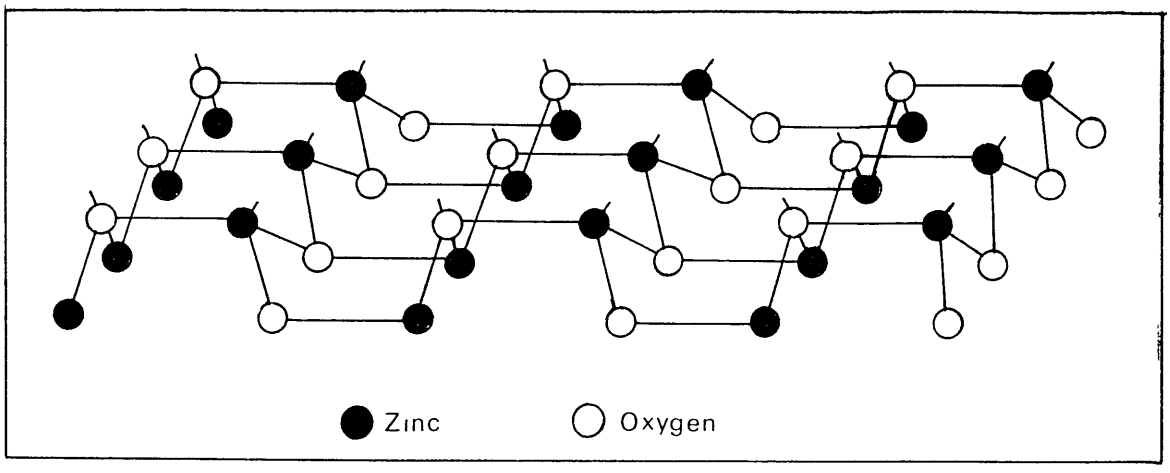

ionic radii for O^- and Zn^+ are: 1.76Å and 0.88Å respectively. Obviously for ionic charge less than unity, $O^{\delta-}$ will be slightly smaller and $Zn^{\delta+}$ slightly larger.) Hence, charge transfer adsorption was not expected for stoichiometric surfaces.

It would seem possible to improve the likelihood of adsorption by increasing the charge on the zinc oxide surface, either with impurities (such as Ga^{3+}) or by generating oxygen vacancies in the surface plane of the crystal which effectively adds a further positive charge. Another electrostatic term has therefore to be introduced into Eqn. (6.6) viz.

$$\frac{e^2 Z' q_{ion}}{4\pi\varepsilon_o r}$$

where Z' = number of charges on impurity or vacancy

NOTE: Since the impurity replaces a lattice ion, which has already been included in the Madelung constant, the electrostatic interaction from this ion has to be subtracted.

The effect of this is shown in Table 6.6.

TABLE 6.6

Minimum Distance Between Adsorbate and Surface Plane to Achieve Adsorption with Impurities or Vacancies Present

Adsorbate	Ionic Radius (Å)	Minimum Distance (Å)	Distance to Achieve Binding Energy leV (Å)
O_2^-	1.23	2.92	2.36
N_2O^-	2.22	2.81 (1.84)	2.28 (1.60)
CO_2^-	2.23	2.21 (1.95)	1.88 (1.68)

NOTE: The number in brackets () in columns 3 and 4 represents the value of the minimum distance when the energy to bend the ion is taken into consideration.

Clearly, the additional electrostatic interaction of an impurity/vacancy has a dramatic effect on all of the r_{min} values. Charge transfer adsorption over oxygen vacancies now seems likely for O_2^-, but not really feasible for N_2O^- or CO_2^- (remembering that the ionic radii of the Zn^+ cation is 0.88Å, which has to be added to the ionic radii of the adsorbate).

Despite these calculations, charge transfer adsorption has been invoked in the literature for all of these systems, (to explain conductivity changes in particular).

The experiments to be presented in the following sections describe adsorption studies on both stoichiometric and defected surfaces, in order to assess the validity of the theory above.

6.3.1 Adsorption of Oxygen on the $(10\bar{1}0)$ Prism Plane of Zinc Oxide at Room Temperature

Stoichiometric and defected $(10\bar{1}0)$ prism planes of zinc oxide were prepared as described in Chapter 4 Section 4.2. The adsorption experiment procedure was similar to that for methanol adsorption. The gas admission chamber, V_A, was filled with oxygen to 0.228 torr. Then LV_2 was closed and LV_1 was opened, to allow the oxygen and zinc oxide to equilibrate for ca. 1hr. Subsequent evacuation for 200-300s prior to temperature programming should remove any adsorbed species of binding energy < 88 kJ mol^{-1} (assuming a pre-exponential factor of $10^{13}s^{-1}$ in the rate equation). Because of conversion of oxygen (to CO and CO_2) in the mass spectrometer, particularly at low pressure, it was considered necessary to monitor all three gases during the TPD experiment. This was done by scanning between mass 28 and 44, every 30 secs., and using the peak height to represent the average for that time interval. The initial oxygen coverage was evaluated, using the summation of the oxygen equivalents of these species (namely O_2, $\frac{1}{2}CO$, CO_2).

The resulting TPD spectra are shown in Fig. 6.5 and are identical for stoichiometric and defected surfaces. The coverages and desorption energies are tabulated in Table 6.7

The experiment was repeated several times in order to check its reproducibility.

FIG. 6.5

TPD Spectra of Oxygen Adsorption on Stoichiometric and Defected $(10\bar{1}0)$ Prism Planes of Zinc Oxide at Room Temperature

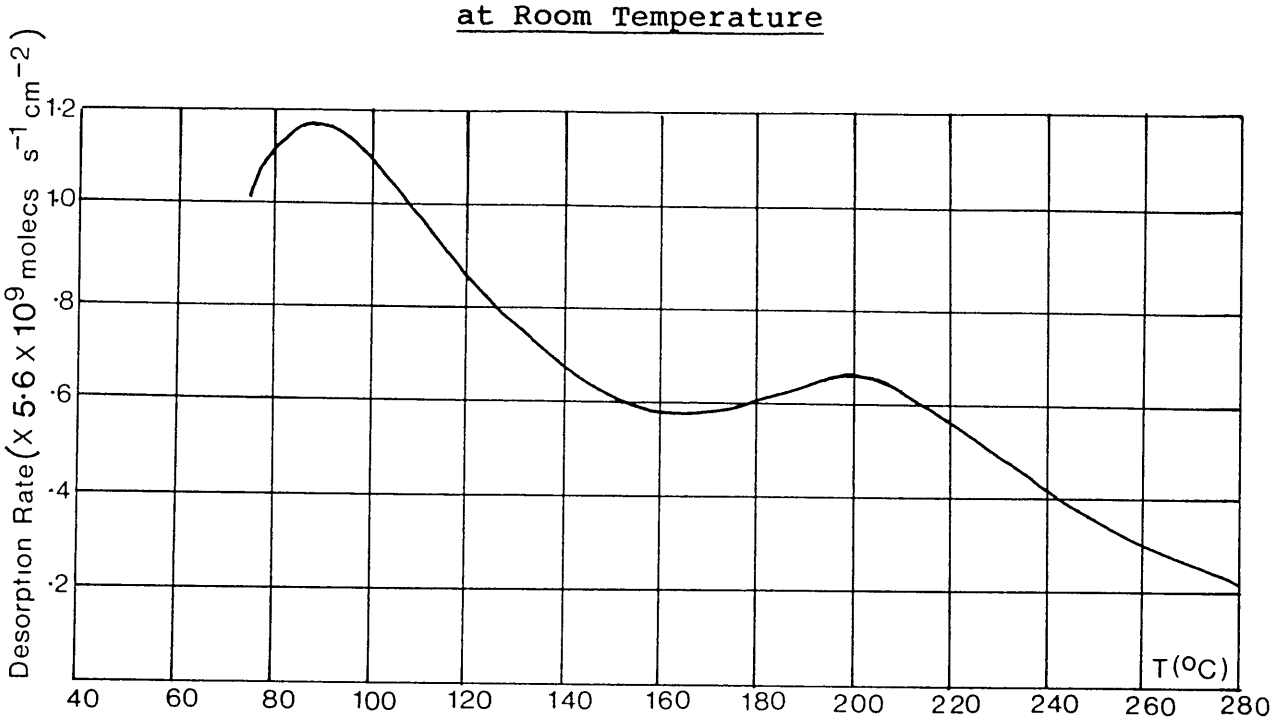

TABLE 6.7

Adsorption of Oxygen on Stoichiometric and Defected $(10\bar{1}0)$ Prism Planes of Zinc Oxide at Room Temperature

Temperature of Peak Maximum (K)	Desorption Energy (kJ mol^{-1})	Coverage on Stoichiometric Surface (molecs cm^{-2})	Coverage on Defected Surface (molecs cm^{-2})
343	94	3.5×10^{11}	1.7×10^{11}
463	128	2.3×10^{11}	1.1×10^{11}

NOTE: 1. The desorption energy was calculated using the Redhead equation (Chapter 2 Section 2.2.2) assuming $\nu = 10^{13} s^{-1}$

2. Because the two peaks were not very well resolved the coverages reported are subject to errors associated with the manual deconvolution process, which cannot easily be estimated. In addition, the error associated with the ion gauge readings ($\pm$ 7%) still applies. Hence, an estimate of the overall error is $\pm$ 15%.

It was not possible to use the "Baratron" gauge reading to verify the total amount adsorbed (compare methanol adsorption, Chapter 5), because of insufficient sensitivity.

6.3.2 Adsorption of Oxygen on the $(10\bar{1}0)$ Prism Plane of Zinc Oxide at Low Temperatures

The oxygen adsorption experiments on stoichiometric and defected $(10\bar{1}0)$ prism planes described in Section 6.3.1 were repeated at 175K. The experimental arrangements for cooling the zinc oxide sample and for temperature monitoring and control, have been detailed in Chapter 3, Section 3.1.2. After equilibration of the sample with 0.223 torr oxygen for ca. 1hr. at 175K the 200-300s evacuation removed any adsorbed species of binding energy < 51kJ mol^{-1} (assuming $\nu = 10^{13} s^{-1}$).

Masses 28-44 were scanned as before and the resulting peak maxima, binding energies and coverages are shown in Table 6.8. The TPD spectra are shown in Fig 6.6 and are identical for stoichiometric and defected surfaces. The results were reproducible to within $\pm$ 14%.

TABLE 6.8

Adsorption of Oxygen on Stoichiometric and Defected $(10\bar{1}0)$ Prism Planes of Zinc Oxide at 175K

Temperature of Peak Maximum (K)	Desorption Energy (kJ mol^{-1})	Coverage on Stoichiometric Surface (molecs cm^{-2})	Coverage on Defected Surface (molecs cm^{-2})
241	65.5	9.3×10^{9}	5.1×10^{10}
343	94	1.7×10^{11}	4.9×10^{11}
423	116.6		

NOTE: 1. The peak at 423K appears as a shoulder to the high

temperature side of the 343K peak. This indicates a second adsorption state (as for room temperature adsorption) but since the peak is not so well defined, deconvolution was not attempted.

2. The desorption energy was calculated using the Redhead equation (see Chapter 2 Section 2.2.2) using $\nu = 10^{13} s^{-1}$.
3. The accuracy of the coverage values is $\pm$ 7-14%.

FIG. 6.6

TPD Spectra for Oxygen Adsorption on Stoichiometric and Defected $(10\bar{1}0)$ Prism Planes of Zinc Oxide at 175K

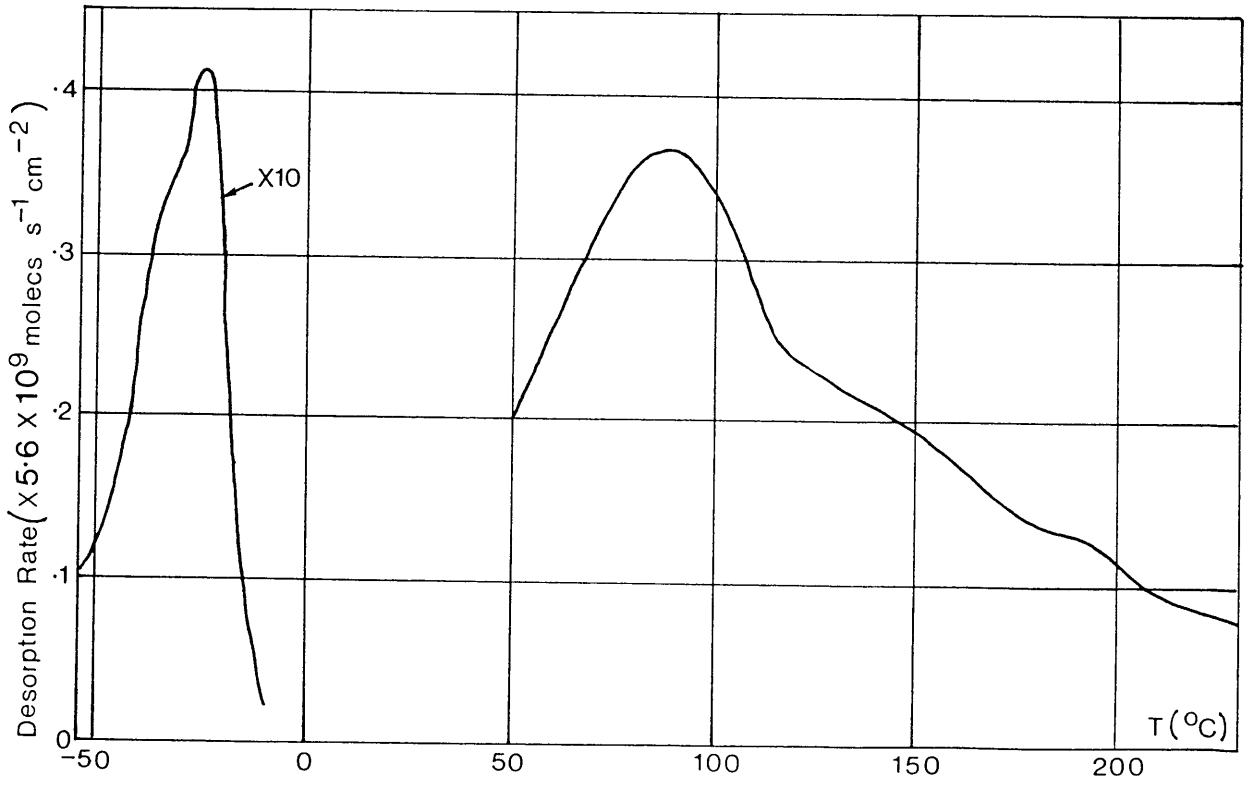

6.3.3 Discussion

It is apparent from Tables 6.7 and 6.8 that oxygen adsorption on the $(10\bar{1}0)$ prism plane of zinc oxide is very low - irrespective of whether a stoichiometric or defected surface is being studied. The apparently greater coverage (however slight) on the stoichiometric surface at room temperature, and vice versa at 175K is considered to be an experimental artefact. Discrepancies in evacuation time are probably responsible. The fact that oxygen vacancies do not have a significant effect on the adsorption of oxygen on zinc oxide, certainly challenges some of the basic theory of charge transfer adsorption. From Section 6.2, adsorption of oxygen over oxygen vacancies, was expected, as the additional electrostatic interaction should increase the binding energy sufficiently for ionic adsorption to occur. Admittedly these experiments could not detect species of binding energy < ca. 51 kJ mol^{-1}.

This discrepancy could be due to the fact that the theory, was derived for low surface vacancy concentrations (probably < 0.1%), and so, repulsions arising from the negative space charge were ignored. The experiments however, were conducted on surfaces with ca. 4% vacancy concentration. In this situation, a degenerate space charge exists which may screen out the positive charge due to the vacancy (see Fig. 6.7).

FIG. 6.7

Screened and Unscreened Local Surface Charge

Low Vacancy Concentration

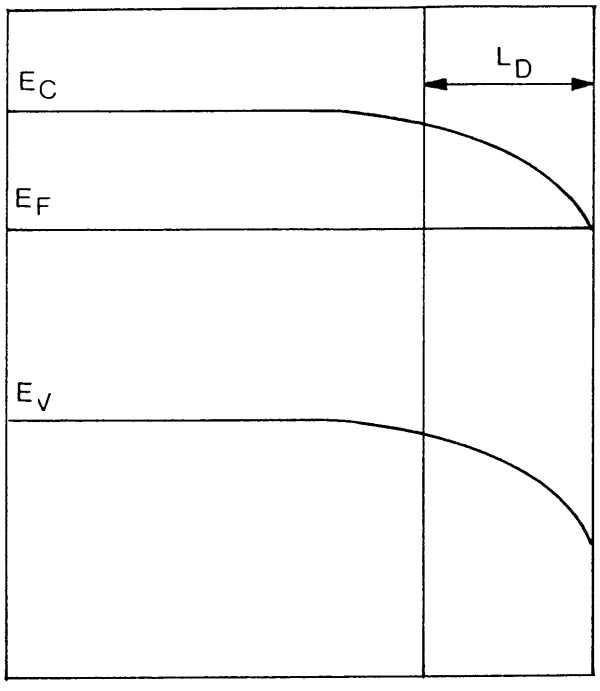

Small surface density of +ve charge centres and therefore long Debye length

Hence no screening of surface charge

High Vacancy Concentration

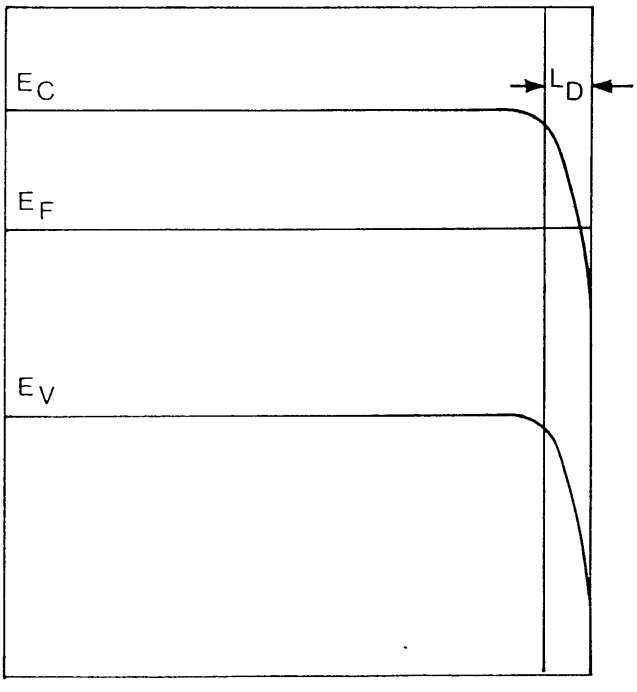

Large surface density of +ve charge centres and therefore short Debye length

Hence strong screening of surface charge

The adsorption that is detected would therefore appear to be associated either with particularly active sites on the prism plane, or perhaps the polar planes at the extremities of each crystal. "Active sites" such as steps or kinks in the surface effectively increase the electrostatic interaction due to the large Madelung constant - presumably having a value intermediate between that of the surface plane (1.1838) and the value for a virtual plane above the surface (0.3147).

From the dimensions given in Chapter 3 Section 3.2 (c), the ratio of polar to prism planes is about 1:1000. The order of magnitude of the coverages reported is ca. 10^{11} molecs cm^{-2}, hence it is a possibility that adsorption is occurring on the polar plane only. From UPS and ELS experiments, Luth et al observed that oxygen is adsorbed on the oxygen polar and stoichiometric prism planes ($\theta < 10^{-2}$) but more extensively (monolayer coverage) on the zinc polar plane (see review by Heiland and Luth[34]). Without estimating the concentration of the step sites they cannot be eliminated from the inquiry however.

Green and Lauks[35] estimated the concentration of step sites (or wide channels) on the $(10\bar{1}0)$ surface to be ca.28%. This was derived using a vacancy-pair mechanism, with parallel zinc loss, to produce oxygen vacancies on the surface to a concentration of 4%. A heterogeneous surface model was invoked to explain the variation of T_p with vacancy concentration, which is quite feasibly manifested as

step sites.

This proportion of step sites is much higher than the coverages obtained, which implies that either the polar planes are indeed responsible for the adsorption or that steeper, more jagged step sites are required, than those envisaged by Green and Lauks. LEED data for the $(10\bar{1}0)$ prism plane however, do not suggest step formation[16,18] at temperatures up to 1050K.

As explained in Chapter 2, the peak shape cannot reliably be used to obtain quantitative information about the surface heterogeneity/reaction order etc., but, inspection of Figs. 6.5 and 6.6 does support the idea of a heterogeneous surface, rather than adsorption on an ideal polar plane. Obviously the latter may contain step sites - but the amount adsorbed would then be two orders of magnitude lower.

Other research groups have been conducting experiments on large single crystals of zinc oxide, to try to ascertain the nature of the adsorption site.

Kung et al[16] obtained similarly low coverages for oxygen, after adsorption at room temperature on defected $(10\bar{1}0)$ and defected $(50\bar{5}1)$ surfaces, treated in 10^{-6} torr oxygen for 2 mins. followed by 2 mins. of evacuation. The peak maxima in their experiments[16] was 458K. A second peak occurred at 513K after adsorption on an oxidised surface (cooled in oxygen to 673-473K and then in vacuo). The previous

year[17], their comparative study of $(10\bar{1}0)$ and $(40\bar{4}1)$ surfaces produced peak maxima at 553 and 373K for the $(40\bar{4}1)$ surface in the ratio 4:1, and just at 373K for the $(10\bar{1}0)$ surface. These findings are not inconsistent with those presented here, as step sites are the predominant adsorption centre on $(40\bar{4}1)$ and $(50\bar{5}1)$ surfaces.

Gopel et al[18,19] also observed low coverages of oxygen after adsorption on the $(10\bar{1}0)$ prism plane at room temperature ($\theta < 2.5 \times 10^{-4}$). Their desorption peak maximum occurred at 410K. Stoichiometric and defected surfaces gave similar results in the temperature range 300-650K (although isotopic exchange reactions occurred at T > 750K over defected surfaces).

Other experimental techniques have been employed to investigate this system, namely conductivity and work function changes on adsorption. Electron transfer is manifested by a decrease in the former and an increase in the latter. Gopel et al[18,19] reported a change (decrease) in conductivity during oxygen adsorption, on a stoichiometric $(10\bar{1}0)$ surface at room temperature, of 0.5×10^{-5} AV^{-1}, which corresponds to a coverage of $\Theta < 2.5 \times 10^{-4}$ (in close agreement with his TPD results). On a defected surface (ca. 0.1% defect concentration), the coverage increases to $\Theta = 2 \times 10^{-3}$. Previous authors[34] only observed the decrease in conductivity after formation of an accumulation layer by hydrogen pretreatment.

The data presented in this thesis however, do not support the idea of enhanced charge transfer over oxygen vacancies, and implies that the additional electrostatic interaction contributed by the oxygen vacancy to E_{int} is still not sufficient to give measurable adsorption.

The low coverages reported here at room temperature and below are therefore attributed to adsorption on active sites only, such as steps. Gopel et al's low temperature work[21] can be interpreted as indicating significant energetic heterogeneity which is characteristic of irregularities in the surface (for T_{ads} 95-241K, T_p ranged from 150-250K). This supports the idea of adsorption on active sites .

6.4.1 Adsorption of Carbon Dioxide on the $(10\bar{1}0)$ Prism Plane of Zinc Oxide at Room Temperature

The experimental procedure was similar to that for the oxygen adsorption experiments described in Section 6.3.1 : equilibration for ca. 1hr. in 0.223 torr carbon dioxide; subsequent evacuation for 200-300 secs., followed by temperature programmed desorption at $0.4Ks^{-1}$ monitoring mass 44. The experiment was repeated several times in order to check its reproducibility.

The peak maximum temperatures and their corresponding binding energies are shown in Table 6.9. The second "peak" at ca. 433K appears as a shoulder on the first peak and the two cannot easily be resolved. Consequently only the total coverage is shown in Table 6.9.

TABLE 6.9

Adsorption of Carbon Dioxide on Stoichiometric and Defected $(10\bar{1}0)$ Prism Planes of Zinc Oxide at Room Temperature

Temperature of Peak Maximum (K)	Desorption Energy ($kJ\ mol^{-1}$)	Coverage on Stoichiometric Surface (molecs cm^{-2})	Coverage on Defected Surface (molecs cm^{-2})
363	99.5	3.7×10^{11}	6.8×10^{11}
433	119.5		

NOTE: 1. The desorption energies were calculated using $\nu = 10^{13}s^{-1}$ in the Redhead equation (see

Chapter 2 Sec. 2.2.2).

2. The coverages reported are total values for main peak plus shoulder.
3. The accuracy of the coverage values is ± 7-14%.

6.4.2 Adsorption of Carbon Dioxide on Polycrystalline Powdered Zinc Oxide at Several Temperatures

The Johnson Matthey, "Puratronic" grade zinc oxide, was cleaned and pre-treated as described in Chapter 4 Section 4.1 then taken to, and held at, the required temperature for adsorption (T_{ads}).

The gas admission chamber was filled with carbon dioxide to 0.228 torr then expanded into V_R and allowed to equilibrate for 15 mins. Subsequent evacuation at T_{ads} for 200 secs. removed any adsorbed species of binding energy < 0.2929 x T_{ads} kJ mol^{-1}. Leak valve 1 was then closed, and leak valve 2 opened ready to commence temperature programming. The heating rate was 0.4Ks^{-1}. The results were reproducible to within ± 7-14%.

Temperatures of peak maxima, binding energies and coverages are shown in Table 6.10. The experiment at room temperature was repeated using 2.28 torr and 0.023 torr carbon dioxide, and the resulting coverages were 1.14 x 10^{15} and 1.08 x 10^{15} molecules cm^{-2}. It would seem therefore that saturation of the surface by CO_2 occurs quite readily.

TABLE 6.10

Adsorption of Carbon Dioxide on "Puratronic" Zinc Oxide at Various Temperatures

T_{ads} (K)	T_p (K)	Desorption Energy (kJ mol^{-1})	Total Coverage (molecs cm^{-2})	Temperature TPD Commenced (K)
298	418 (373)	116	1.28×10^{15}	298
488	523 (673)	146	3.92×10^{14}	373
523	573 (673) (623)	160	3.18×10^{14}	523
541	563 (673)	157	3.69×10^{14}	473
541	573 (693)	160	4.17×10^{14}	393
575	623 (673)	175	2.91×10^{14}	471
628	673	183	1.81×10^{14}	478
688	698	197	1.14×10^{14}	568

NOTE: 1. The value of T_p in brackets () corresponds to the temperature at which a shoulder on the main peak appears, indicating a second or even third binding state.

2. The desorption energies were calculated using the Redhead equation (Chapter 2 Sec. 2.2.2) assuming

$\nu = 10^{13} s^{-1}$.

3. The accuracy of the coverage values is $\pm$ 7-14%.

6.4.3. Discussion

From the preceding Sections (6.4.1 and 6.4.2) it is clear that adsorption of carbon dioxide on the prism plane of zinc oxide is negligible on either stoichiometric or defected surfaces. The slightly greater coverage on the defected surface is attributed to variations in evacuation time - not the influence of oxygen vacancies. In fact the coverages reported are two orders of magnitude lower than the concentration of oxygen vacancies and hence suggests that adsorption occurs only on particularly "active sites", or on the polar planes. For reasons analogous to those given in Section 6.3.3 for oxygen adsorption, active sites (steps, kinks) are the most likely adsorption centres.

A line defect (step) would probably be able to influence the electrostatic (Madelung) interaction enough to promote adsorption by complete charge transfer. The binding states would be weak on fairly well defined surfaces, or those simply with point defects, but line defects would have a stronger effect.

An alternative explanation could be, partial charge transfer. Obviously weaker binding states (< 88 kJ mol^{-1}) could not be detected here.

By contrast, on the powdered sample, carbon dioxide readily

saturates the surface at room temperature. This implies, therefore, that extensive adsorption occurs on the polar planes of zinc oxide. Unfortunately details of the surface topography are not available (see Chapter 3 Section 3.2) - scanning electron microscopy only reveals large conglomerates of material.

The experiments on the powdered sample, at higher temperatures, indicate that carbon dioxide can form very strong bonds to the surface, giving almost a monolayer coverage also, despite the unfavourable electron affinity, -0.9eV (see Sec. 6.2.). This suggests that a chemical reaction is occurring and that a carbonate is formed. The heat of formation of $ZnCO_3$ is[11] -816kJ/g mol. Hence an increase in temperature would be unfavourable, as observed.

Other reseach groups have been investigating the CO_2/ZnO system - but results, even from one author, are frequently inconsistent. Some of the more relevant work will be outlined below.

Cheng et al[16] have studied CO_2 adsorption on several prism planes - $(10\bar{1}0)$, $(50\bar{5}1)$ and $(40\bar{4}1)$, and also on the zinc polar plane. (See Chapter 5 Sec. 5.3.4 for further details of sample preparation/characterisation, although the annealing temperatures here were only 773 and 923K). After room temperature adsorption (10^{-7} torr for 2 mins., then 2 mins. evacuation), three TPD peaks were observed. The prism planes all give the main (α) peak at 398K with a

secondary shoulder (β peak) at 463K. The β peak increases, as the time between cleaning (high temperature treatment) and CO_2 exposure increases, and is also more prominent on the stepped surfaces. On the polar plane, the α and β peaks are small, but a third peak at 673K is present.

They deduced that the α and β peaks require a Zn-O pair, and the β peak may be associated with a step site. The reason for a stronger γ state on the polar plane is uncertain. It could be due to a greater density of step sites on the polar plane.

The coverages reported by Cheng et al were greater than in this work, namely (1.4, 1.2 and 0.6) x 10^{-2} on the $(10\bar{1}0)$, $(50\bar{5}1)$ and (0001) surfaces respectively. As with their oxygen data, discrepancies arise in an earlier publication[17], concerning adsorption of CO_2 on $(10\bar{1}0)$ and $(40\bar{4}1)$ surfaces. There, adsorption of CO_2 was inhibited by the presence of the steps.

Gopel et al[22] observed weak reversible adsorption of CO_2 at room temperature on the $(10\bar{1}0)$ prism plane. Using the variation of T_p with B, the desorption energy is calculated to be 90kJ mol^{-1} with a pre-exponential factor of 1.6 x $10^{14} s^{-1}$ (T_p = 350K). A decrease in conductivity and increase in work function was observed on both stoichiometric and defected $(10\bar{1}0)$ surfaces (identical in each case), and partial charge transfer adsorption with

associated surface reconstruction was invoked to explain these results. From work on powdered samples[23] however, (ostensibly using stoichiometric and defected surfaces), Gopel found T_P at 380, 510 and 690K, the peak at 510K increasing with the vacancy concentration. Two adsorption species were proposed: CO_2 (or more correctly $[ZnCO_2^-]$) associated with an oxygen vacancy with charge transfer, and formation of a carbonate-like species, also on the prism plane. Surprisingly, Gopel and Runge attributed the adsorption activity of these powders, to the prism plane only.

Bowker et al[20] advocated CO_2 adsorption over surface defects (possibly oxygen vacancies) from TPD experiments on Analar zinc oxide, and also formation of a carbonate (positions/planes unspecified).

Finally, Lavalley et al[24], using infra red spectroscopy on a powdered sample (prepared under oxidising conditions) suggests that CO_2 adsorbed on zinc oxide at room temperature exists as a linear species and also as a bidentate carbonate which are probably associated with non polar edge sites on the polar plane.

Some of these findings can easily be reconciled with the data presented in this thesis: activity of step sites, for CO_2 adsorption[16], and formation of a carbonate[20,23,24]. However, the formation[20,23] of $[V_O]^+[CO_2]^-$ or $[ZnCO_2^-]$ seems dubious.

6.5.1 Adsorption of Nitrous Oxide on the $(10\bar{1}0)$ Prism Plane of Zinc Oxide at Low Temperature

The experimental procedure was similar to that for the oxygen adsorption study, described in Sections 6.3.1. and 6.3.2. Nitrous oxide (0.223 torr) and the zinc oxide sample were equilibrated at 180K for 1 hr. After evacuation for 200-300 secs. (which removed any adsorbed species of binding energy < 53kJ mol^{-1}), temperature programming was commenced, scanning between masses 28-44, every 30 seconds as before, and processing the data in the same way. The experiment was repeated several times in order to check its reproducibility.

The resulting coverages and binding energies are given in Table 6.11.

TABLE 6.11

Adsorption of Nitrous Oxide on Stoichiometric and Defected $(10\bar{1}0)$ Prism Planes of Zinc Oxide at 180K

Temperature of Peak Maximum (K)	Desorption Energy (kJ mol^{-1})	Coverage on Stoichiometric Surface (molecs cm^{-2})	Coverage on Defected Surface (molecs cm^{-2})
243	66	1.45×10^{11} (44)	1.21×10^{11} (44)
ca.357	98	1.36×10^{11} (28)	1.62×10^{10} (28)

NOTES: 1. Desorption energies calculated using $\nu = 10^{13} s^{-1}$ in the Redhead equation.

2. The number in brackets under each value of the coverage indicates the predominant peak.

3. Accuracy of coverage values is $\pm$ 7-14%.

Adsorption at room temperature gives the same peak at ca.357K (9 x 10^{10} molecs cm^{-2}) with another at 531K (shoulder).

6.5.2 Discussion

From the preceding section it is clear that nitrous oxide does not adsorb to a significant extent on either stoichiometric or defected $(10\bar{1}0)$ prism planes of zinc oxide. This is in accord with calculations in Section 6.2, which showed that a prohibitive energy expenditure would be required to form the bent N_2O^- ion, which could not be compensated for, even by an additional positive charge at the surface, in the form of an oxygen vacancy.

The N_2O^- species however has been postulated as an intermediate in the overall decomposition reaction:

$N_2O \dashrightarrow N_2 + \frac{1}{2}O_2$, at room temperature[28] and above[25,36], over zinc oxide.

Lauks[25] proposed a mechanism, for the decomposition of nitrous oxide over zinc oxide, in which oxygen vacancies activated the N_2O molecules:

$$V_O^+ + e^- + N_2O(g) = V_O^+ \ldots N_2O^-$$

followed by:

$$V_O^+ \ldots N_2O^- \dashrightarrow V_O^+ \ldots O^- + N_2(g)$$

The bond energy $(N_2\text{-}O)^-$ is 0.43eV[29].

The resulting O^- species ($V_O^+...O^-$) can either fill the vacancy or desorb. At high temperatures (> 773K) the latter is likely. The temperature range in which decomposition occurs to a significant extent[25,36] is ca.773-1020K.

The N_2O decomposition reaction has been used for many years as an indication of the availability of electrons at the surface of a semiconductor[28] and hence a measure of catalytic activity. Several research groups have studied this system.

Cunningham et al[28] reported a decrease in conductivity during N_2O adsorption on zinc oxide powder at room temperature. The effect was reduced for samples doped with lithium or pretreated in oxygen (less adsorption/decomposition) and enhanced for samples doped with indium. These results are predicted by charge transfer adsorption theory. Caralp et al[26] however, observed no difference in nitrous oxide decomposition over zinc oxide powder at 200-300°C of varying stoichiometry. Neither did Angletti et al[27] at 300-500°C.

The work presented in Section 6.5.1 indicates that if N_2O^- is formed over stoichiometric and defected zinc oxide, its existence is very transient. A weaker interaction seems more likely, which assists in the decomposition reaction by weakening the N_2-O bond. The fact that the p-type oxides catalyse the decomposition reaction at lower temperatures (470-570K) is attributed to the greater tendency to adsorb negative species (accumulative adsorption as opposed to depletive chemisorption).

6.6 Resumé

From the preceding presentation it is clear that the three molecules used in these experiments O_2, CO_2 and N_2O do not adsorb to a significant extent on the prism plane of zinc oxide - on either stoichiometric or defected surfaces. From the calculations in Section 6.2, strong adsorption using charge transfer on stoichiometric surfaces was not really expected - however, an additional effective charge in the form of an oxygen vacancy was predicted to change the situation for O_2 (at low vacancy densities).

The limited amount of adsorption detected for all three molecules studied seems likely to occur at particularly active step sites on the prism plane. (The work functions for the zinc and oxygen polar planes are 4.25 and 4.95eV respectively - not significantly different from the prism plane (4.65eV) - hence it seems unlikely that the polar planes are responsible for the adsorption here.

This adsorption at step sites may involve charge transfer, but clearly, ionic adsorption does not occur easily for these systems and cannot be induced by point defects alone. This experiment simply seems to indicate the degree of heterogeneity in the surface.

One can only conclude that a significant amount of charge transfer adsorption does not happen for these systems.

Molecules with a more positive electron affinities viz: NO_2^-(3.1eV), S^-(2.1eV), Cl^-(3.61eV) and tetracyanoethylene(3.05eV) - may comply with the theory, but that is left to future study.

1. K. HAUFFE

Adv. Catal. 7, 213, 1955

2. M. GREEN AND M.J. LEE

Solid State Surface Science Vol.1 Chap.3

Marcel Dekker, N.Y., 1969

3. M. GREEN AND R. SEIWATZ

J.Chem. Phys. 35(3), 915, 1961

4. E.A. MOELWYN HUGHES

Physical Chemistry (2nd Ed.) p.309 Pergammon (1961)

5. M. GREEN

Sensors and Actuators 1, 379, 1981

6. H. MOORMAN, D. KOHL AND G. HEILAND

Surface Science 80, 261, 1979

7. H.M. ROSENSTOCK, K. DRAXL, B.W. STEINER AND J.T. HERRON

J. Phys. Chem. Ref. Data Vol.6 Suppl.1, 1, 1977

8. J.P. LOWE

J.A.C.S. 99(17), 5557, 1977

9. E.C.M. CHEN AND W.E. WENTWORTH

J. Phys. Chem. 87(1), 45, 1983

10. H.S.W. MASSEY

Negative Ions (3rd Ed.)

Cambridge Monographs on Physics 1976

11. C.R.C. Handbook of Chemistry and Physics

12. P. MARK

J. Phys. Chem. Sol. 29, 689, 1968

13. R.J. COLLINS AND D.A. KLEINMAN

J. Phys. Chem. Sol. 11, 190. 1959

14. W.J. MOORE

Physical Chemistry (5th Ed.) p.785

Longman 1972

15. A.R. ROSSI

J. Chem. Phys. 70(9), 4422, 1979

16. W.H. CHENG AND H.H. KUNG

Surface Science 122, 21, 1982

17. W.H. CHENG AND H.H. KUNG

Surface Science 102, L21, 1981

18. W. GOPEL

J. Vac. Sci. Tech. 15(4), 1298, 1978

19. W. GOPEL

Surface Science 62, 165, 1977

20. M. BOWKER, H. HOUGHTON AND K.C. WAUGH

J.C.S. Far. Trans. 1, 77, 3023, 1981

21. P. ESSER AND W. GOPEL

Surface Science 97, 309, 1980

22. W. HOTAN, W. GOPEL AND R. HAUL

Surface Science 83, 162, 1979

23. F. RUNGE AND W. GOPEL

Z. Phys. Chem. Neue. Folge 123, 173, 1980

24. J. SAUSSEY, J.C. LAVALLEY AND C. BOVET

J.C.S. Far. Trans. 1 78, 1457, 1982

25. I.R. LAUKS

Ph.D. Thesis, University of London (1977)

26. N. DUPONT PAVLOVSKY AND F. CARALP

J. Catal. 46, 426, 1977

27. C. ANGLETTI, A. CIMINO, V. INDOVINO, F. PEPE AND
M. SCHIAVELLO
Z. Phys. Chem. Neue. Folge. 122, 237, 1980

28. J. CUNNINGHAM, J.J. KELLY AND A.A. PENNY
J. Phys. Chem. 74(9), 1992, 1972

29. D.G. HOPPER, A.C. WAHL, R.L.C. WU AND T.O. TIEMAN
J. Chem. Phys. 65(12), 5474, 1976

30. P.W. ATKINS
Physical Chemistry, Oxford Univeristy Press (1978) P.752

31. C.S. JOHN
Chem. Soc. Spec. Per. Rep. 1980
Catalysis Vol. 3 p.169

32. J. PACANSKY, U. WAHLGREN AND P.S. BAGUS
J. Chem. Phys. 62(7), 2740, 1975

33. J.F. O'HANLON
A User's Guide to Vacuum Technology
John Wiley 1980

34. G. HEILAND AND H. LUTH
The Chemical Physics of Solid Surfaces and Heterogeneous Catalysis Vol. 3, Elsevier 1984
Ed. D.A. King and D.P. Woodruff

35. M. GREEN AND I.R. LAUKS
J.C.S. Far. Trans. II 74, 2724, 1978

36. J. HARDY
Ph.D. Thesis, University of Bradford (1971)

APPENDIX A

COMPUTER PROGRAM TO DETERMINE THE DESORPTION ENERGY USING THE REDHEAD EQUATION

```
100  PRINT "NEWTON'S APPROXIMATION"
200  PRINT
250  R = 8.314
300  PRINT "FIRST ORDER REACTION"
350  INPUT V
375  PRINT "PRE-EXPONENTIAL ="; V;"SECS-1"
400  INPUT B
450  PRINT "HEATING RATE ="; B; "DEGS K/S"
500  INPUT E
550  PRINT "TRIAL VALUE ="; E; "J/MOL"
600  T = 70
650  I = 1
700  F = E/(R x T^2) - (V/B) x EXP[-E/(R x T)]
800  F1 = 1/(R  x T^2) + (V/[B x R x T]) x EXP[-E/(R x T)]
900  Z = F/F1
950  IF ABS (Z/E) < 10^-6 THEN 1500
1000 E = E - Z
1050 I = I + 1
1100 GO TO 700
1500 PRINT "ACTIVATION ENERGY ="; E; "J/MOL": TAB (36);
     "TEMPERATURE = "; T; "DEGS"; TAB (64); "I ="; I
1660 T = T + 10
1670 IF T > 1073 THEN STOP
1680 GO TO 650
1700 END
```

APPENDIX B

APPARATUS USED AT I.C.I. NEW SCIENCE GROUP

A diagram of the apparatus is shown in Fig. AB.
The metal vacuum system was in two sections, both evacuated by a combination of rotary/oil diffusion pumps, and separated by a gate valve (Vacuum Generators). A base pressure of ca. 10^{-7} torr. was attainable without baking the system.

Zinc oxide powder was contained in a silica sample tube, inside a platinum-rhodium heating coil. Gas was admitted to the chamber (from a pyrex gas admission line) via an MD6 leak valve (Vacuum Generators). Temperature control was achieved using a Stanton Redcroft temperature programmer, and the desorbed species were monitored on a QX200 Quadrupole Mass Spectrometer (Vacuum Generators).

FIG AB.

APPARATUS USED AT I.C.I. NEW SCIENCE GROUP

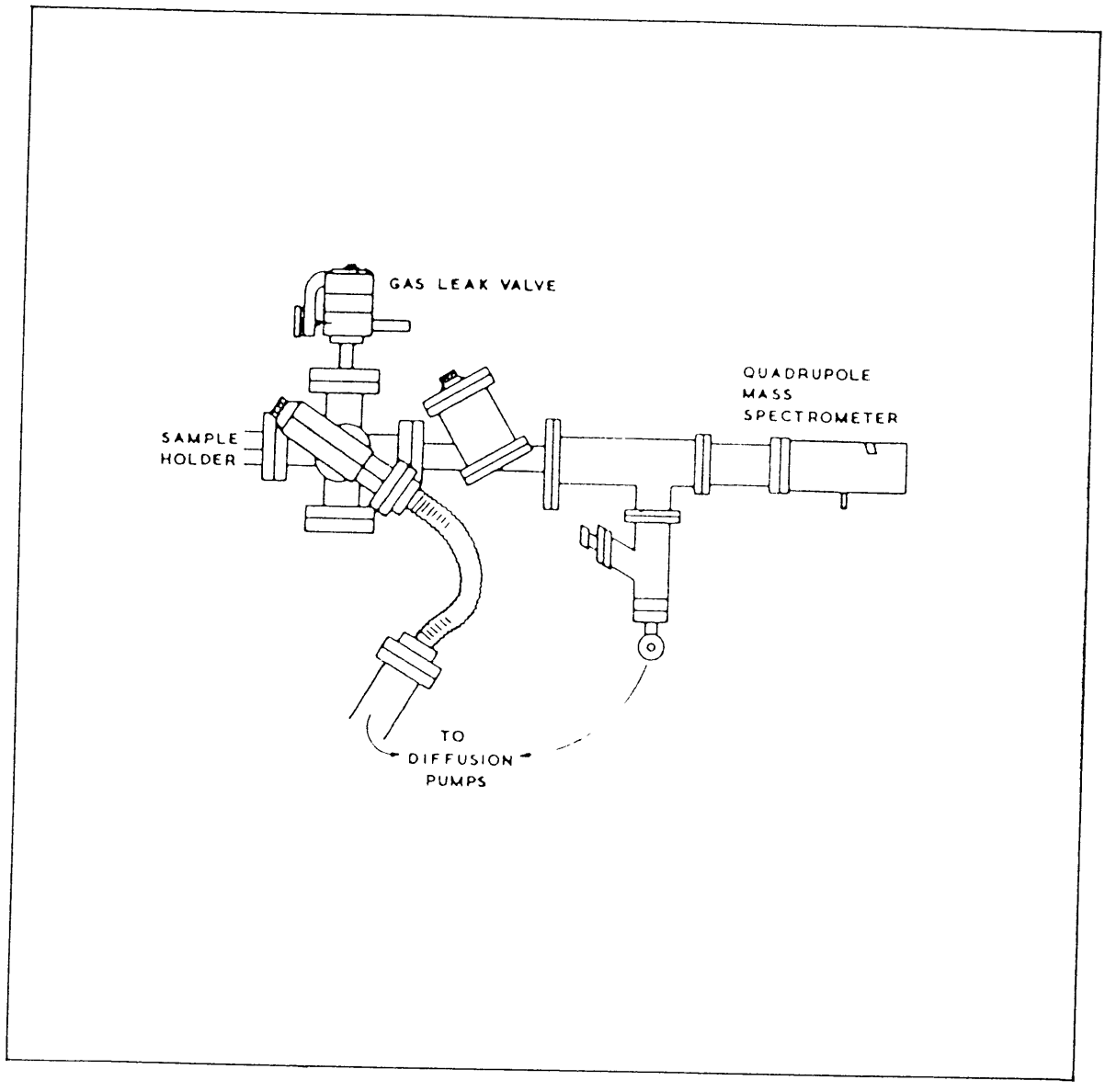

APPENDIX C

DETERMINATION OF SURFACE AREA USING THE BET EQUATION

The surface area of an adsorbent can be determined using the theory derived by Brunauer, Emmett and Teller for multilayer physical adsorption. Their famous equation can be written as :

$$\frac{1}{V(1-x)} = \frac{1}{V_m} + \frac{1}{V_m C}.\frac{(1-x)}{x}$$

where, V = volume adsorbed (cm^3 stp)

V_m = volume of adsorbate to complete a monolayer coverage (cm^3 stp)

x = P/P_o

P = final equilibrium pressure (torr)

P_o = standard vapour pressure of adsorbate

$$C = \text{constant} = \exp\left[-\frac{(\Delta G_1^o - \Delta G_2^o)}{RT}\right]$$

ΔG_1^o = standard free energy of condensation on bare surface

ΔG_2^o = standard free energy of condensation of the vapour on 1st, 2nd, layers

Clearly, a plot of $1/V(1-x)$ vs $(1-x)/x$ should yield a straight line, of intercept $1/V_m$, from which the surface area of the adsorbent can be calculated (knowing the cross sectional area of the adsorbate molecule - namely 19.5Å^2 for Kr - see Ref. 5).

After completing all the TPD experiments, the reaction chamber, V_R (see Chapter 3), was transferred to another

apparatus in order to measure the surface area of the zinc oxide needles (see Fig. AC). The surface area was expected to be in the region of 1,500 cm^2. Consequently Krypton was used as the adsorbate, because its P_o value is 1.753 torr at (l)N_2 temperature[1], and according to BET theory, P/P_o should lie in the range 0.05-0.3 torr[5]

The experimental procedure is outlined in Refs. 2 and 3. Successive doses were allowed to equilibrate for 10-15 mins. Each equilibrium pressure was corrected for thermal transpiration according to the equation of Bennett and Tompkins[4] :

$$\frac{P_{true}}{P_{measured}} = \frac{\alpha_{He}(f\phi_g X)^2 + \beta_{He}(f\phi_g X) + R_m}{\alpha_{He}(f\phi_g X)^2 + \beta_{He}(f\phi_g X) + 1}$$

$f = 1$ for tubing i.d. < 1cm

$f = 1.22$ for tubing i.d. > 1cm

$X = P_2 d$

$R_m = \sqrt{T_1/T_2}$

$\alpha_{He} = 3.7\ (1.7 - 2.6 \times 10^{-3} \Delta T)^{-2}$

$\beta_{He} = 7.88\ (1 - R_m)$ for $R_m < 1$

$\phi_{Kr} = 3.9$

Unfortunately, the experiment gave similar results with or without the zinc oxide present - namely ca. 500cm^2 and 600cm^2 respectively. The error in each of these values from the intercept alone is at least $\pm$ 200cm^2. This could suggest that Krypton does not adsorb on zinc oxide but does on glass. However, from the dimensions of the apparatus, the value of 600cm^2 is rather high. Krypton adsorption on

zinc oxide has been reported in the literature[6]. Consequently is seems more appropriate to consider the experiment invalid, on grounds of insufficient sensitivity.

1. J.M. HAYNES
J. Phys. Chem. 66, 182, 1962

2. S.ROSS AND J.P. OLIVIER
On Physical Adsorption, Interscience, 1964

3. Findlays Practical Physical Chemistry
B.P. Levitt (Ed.), Longman, 1973

4. M.J. BENNETT AND F.C. TOMPKINS
Trans. Far. Soc. 53, 185, 1957

5. J.M. THOMAS AND W.J. THOMAS
Introduction to the Principles of Heterogeneous Catalysis, Academic Press, 1967.

6. K. MORISHIGE, S. KITTAKA AND T. MORIMOTO
J. Col. and Int. Sci. 89(1), 86, 1982

FIG. AC

APPARATUS USED TO MEASURE THE SURFACE AREA OF ZINC OXIDE NEEDLES

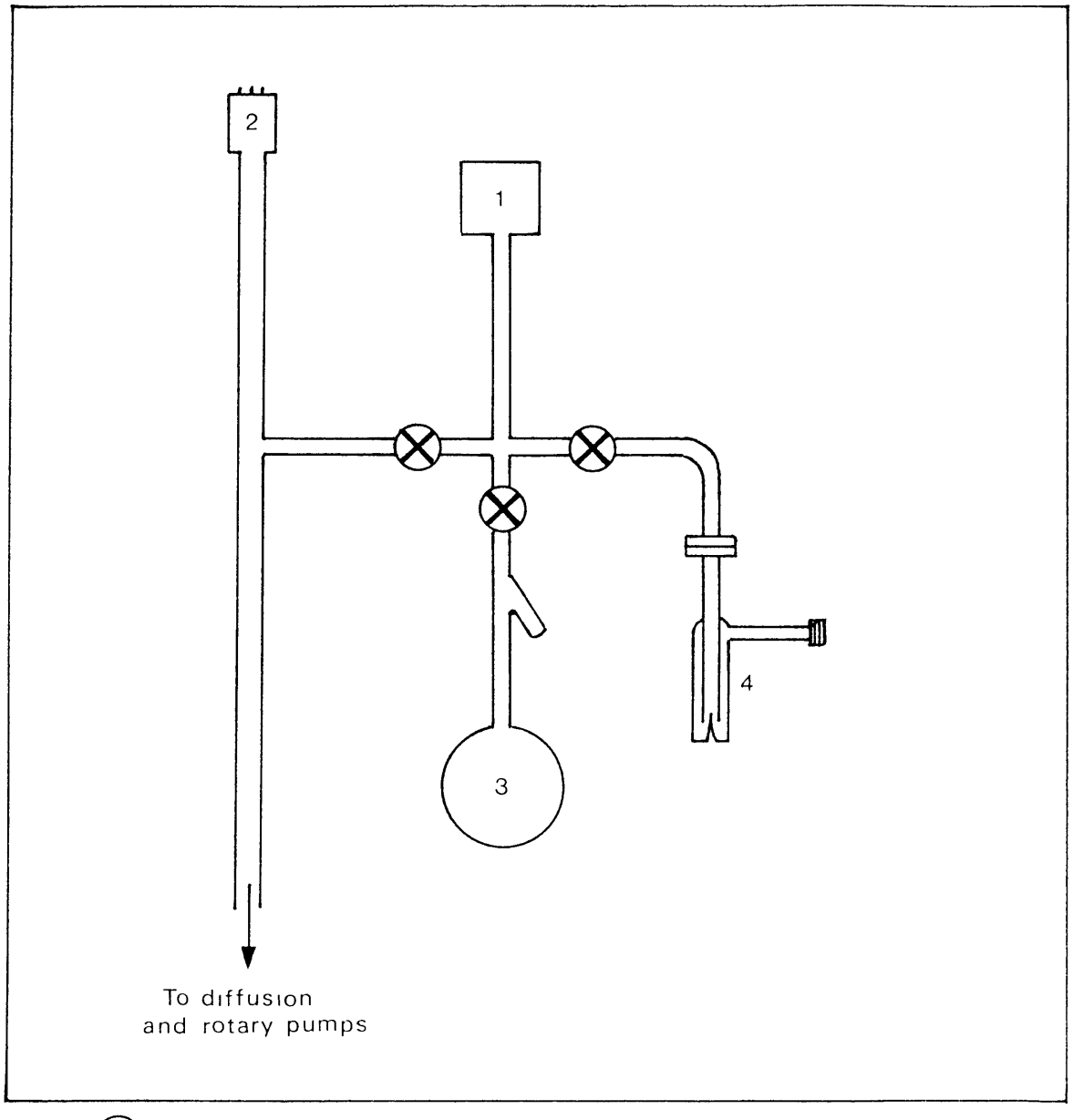

KEY : ⊗ Glass Tap

1. MKS "Baratron" Gauge, Type 222A
2. Ionisation Gauge (ITL)
3. 1 litre flask, research grade Krypton (BOC)
4. Sample Holder

APPENDIX D

MASS SPECTRAL CRACKING PATTERNS OBTAINED ON A QX200 QUADRUPOLE MASS SPECTROMETER (VACUUM GENERATORS) AT 10^{-6}TORR

CO_2

Mass	Relative Peak Ht.	% Total
44	1	67.37
28	0.314	21.13
16	0.122	8.2
12	0.049	3.29

O_2

Mass	Relative Peak Ht.	% Total
32	1	71.55
28	0.164	11.72
2	0.103	7.36
18	0.042	3.01
44	0.012	0.84
16	0.077	5.52

N_2O

Mass	Relative Peak Ht.	% Total
44	1	29.75
30	0.368	10.94
28	1.742	51.82
14	0.177	5.28
16	0.074	2.21

CH_3OH

Mass	Relative Peak Ht.	% Total
2	1.798	29.55
15	0.417	6.87
18	0.082	1.35
28	1.148	18.92
29	0.634	10.45
30	0.145	2.39
31	1	16.47
32	0.731	12.05
12	0.037	0.6
16	0.082	1.35

N_2

Mass	Relative Peak Ht.	% Total
28	1	78.39
20	0.08	6.31
14	0.059	4.64
40	0.012	0.93
4	0.101	7.88
2	0.024	1.86